

Photocatalytic Degradation of a Dye in Wastewater by Quantum Dot-Modified Microgels

by

Jingzhu Liu

A thesis submitted in partial fulfillment of the requirements for the degree of

Master of Science

Department of Chemistry

University of Alberta

© Jingzhu Liu, 2016

# Abstract

Organic contaminants found in water, and leaching into the environment, are a major concern worldwide. In this thesis, we investigate the utility of using quantum dot-doped poly (N-isopropylacrylamide) (pNIPAm) microgels to photocatalytically degrade an organic dye in water. We use an aqueous-phase process to synthesize the hybrid CdS-modified microgels. To study the structure and properties of the hybrid microgels, we use scanning electron microscopy and transmission electron microscopy. Furthermore, we showed that these microgels can photocatalytically degrade Rhodamine B upon irradiation with UV light and the nano-CdS would be steadily immobilized within in the outer surface of the spherical beads, which is dominant for efficient degradation of RhB and for repeated use the catalysts. The results showed that 95% of the Rhodamine B could be decomposed within one hour, in addition to other organics. The approach presented in this study is low-cost and provides wide application prospects in the field of photocatalysis.

# Acknowledgements

First of all, I would like to acknowledge and thank my supervisor, Dr. Michael Serpe and Serpe group for their continuous support during my program. Dr. Michael Serpe has been a tremendous mentor and supervisor. He provided guidance and direction for me throughout my research. It was a pleasure to work in his research group.

I want to thank my group members for their scientific input and contributions during my research. I am also very appreciative for the time and guidance from my committee members.

Last but not the least, I am immensely grateful for the love and support of my family and friends during my life.

Chapter 1 - Wastewater Treatment Background.....	1
1.1 Introduction.....	1
1.1.1 Status of World Water Resources.....	1
1.1.2 Water Resources Quality and Contaminants.....	2
1.1.2.1 Water Resource Quality.....	3
1.1.2.2 General Classes of Water Contaminants.....	3
1.1.3 Wastewater Treatment Methods.....	6
1.1.3.1 Adsorption Method.....	6
1.1.3.2 Membrane Separation Technology.....	7
1.1.3.3 Fenton Method.....	8
1.1.3.4 Photocatalytic Oxidation Method.....	9
1.1.3.5 Electrochemical Oxidation Method.....	10
1.1.3.6 Ultrasonic Degradation Technology.....	11
1.1.3.7 Biochemical Method.....	11
1.2 Characteristics of the Polymer/Nanocrystal Systems for Wastewater Treatment.....	12
1.2.1 Synthesis of Hybrid pNIPAm/Nanocrystal.....	14
1.2.1.1 Blend Polymerization.....	14

1.2.1.2 In-Situ Copolymerization.....	15
1.3 Introduction to Stimuli Responsive Polymers.....	15
1.3.1 Introduction.....	15
1.3.2 Thermoresponsive Polymers.....	18
1.3.3 pH Responsive Polymers.....	19
1.3.4 Other Responsive Polymers.....	21
1.3.4.1 Photoresponsive Polymers.....	21
1.3.4.2 Enzyme Responsive Polymers.....	22
1.3.5 Stimuli Responsive Hydrogels.....	23
1.3.6 Poly (N-Isopropylacrylamide) Microgels.....	24
1.3.7 Synthesis of pNIPAm Microgels.....	25
1.3.8 pNIPAm Microgel Applications.....	27
1.3.8.1 Microgels as Microreactors.....	27
1.3.8.2 Microgels for Drug Delivery.....	28
1.3.8.3 Microgels as Photonic Crystals.....	29
1.4 Introduction of Semiconductor Nanocrystals.....	30
1.4.1 Quantum Dots.....	31

1.4.1.1 Effect of Size.....	31
1.4.1.2 Effect of Surface.....	32
1.4.1.3 Dielectric Confinement Effect.....	33
1.4.1.4 Other Physical Effects.....	33
1.4.2 Quantum Dots Preparation.....	35
1.4.2.1 Chemical Precipitation Method.....	37
1.4.2.2 Thermal Decomposition Method.....	37
1.4.2.3 Hydrothermal Method and Solvothermal Method.....	39
1.4.2.4 Liquid-Solid-Solution Interface Phase Transfer and Phase Separation.....	39
1.4.3 Application of Quantum Dots.....	40
Chapter 2- Polymerization and Modification of pNIPAm/CdS Composite Microgel.....	42
2.1 Introduction.....	42
2.2 Materials & Methods.....	44
2.2.1 Transmission Electron Microscopy.....	45
2.2.2 X-ray Photoelectron Spectroscopy .....	46
2.2.3 Raman Spectroscopy.....	47
2.2.4 X-ray Diffraction.....	47

2.2.5 Electron Diffraction.....	48
2.2.6 Fluorescence Spectroscopy.....	48
2.3 Polymerization of pNIPAm-co-AAc Microgel.....	49
2.4 Preparation of pNIPAm Based Microgel@CdS Composites by In-situ Synthesis Method.....	50
2.4.1 Attempted Cd Coupling to pNIPAm-co-20% AAc Microgel.....	52
2.4.2 Preparation of CdS Quantum Dots Coupled pNIPAm-co-20% AAc Microgel.....	53
2.5 The Performance Detection of Nanodisperse pNIPAm Based Microgel@CdS.....	54
2.5.1 Transmission Electron Microscope (TEM) Results of the Microgel@CdS.....	54
2.5.2 Elemental Analysis of Microgel with CdS by XPS (X-ray Photoelectron Spectroscopy).....	58
2.5.3 The Crystallinity of CdS Nanoparticles within pNIPAm-co-20%AAc Microgel.....	61
2.5.3.1 Raman Spectroscopy.....	61
2.5.3.2 X-ray Diffraction.....	62
2.5.3.4 Electron Diffraction.....	63
2.5.4 Fluorescence Spectroscopy.....	64
2.5.5 Summary.....	64

Chapter 3 - Remediation Performance.....	66
3.1 Introduction.....	66
3.2 Materials & Methods.....	67
3.2.1 Ultraviolet–visible Spectroscopy (UV-Vis Spectroscopy).....	68
3.2.2 Mass Spectrometry.....	69
3.3 Photocatalytic Property of pNIPAm-co-20%AAc Microgel@CdS Tests.....	69
3.3.1 Photocatalytic Degradation Mechanism.....	69
3.3.2 Temperature Influence for the Photocatalytic Efficiency of Rhodamine B....	72
3.3.2.1 Kinetics at Low Temperature.....	73
3.3.2.2 Kinetics at High Temperature.....	76
3.3.2.3 The Comparison of Photocatalytic Efficiency of Hybrid Microgel at Different Temperatures.....	79
3.3.3 Photocatalytic Data for Various Amount of pNIPAm-co-20%AAc Microgel@CdS.....	80
3.3.4 Photocatalytic Data For Using pNIPAm-co-20%AAc Microgel@CdS Recyclable.....	82
3.3.5 The XPS Data of Atomic Concentration for Cd and S Before and After Photocatalytic Operation.....	84

3.3.6 Data of Working pH Range for pNIPAm-co-20%AAc Microgel@CdS.....	86
3.3.7 Stability of Hybrid Microgel with CdS Nanoparticles.....	88
3.3.8 Analyzing the Product of RhB After Photocatalytic Operation by Mass Spectroscopy.....	89
3.3.9 Photocatalytic Data of Other Organic Dgmye (Sulphur Blue).....	92
3.4 Summary.....	92
Conclusions.....	93
Future Work.....	94
References.....	97
Appendix.....	131

# List of Figure

Figure 1-1. a) Dye released wastewater and b) dead aquatic life.....	5
Figure 1-2. Schematic representation of dimensional changes in polymeric solutions, at surfaces and interfaces, in polymeric gels, and polymer solids resulting from physical or chemical stimuli. Reprinted with permission. <sup>48</sup> Copyright 2004, Elsevier.....	16
Figure 1-3. Chemical structure of pH-sensitive polyanions and polycationic polymers. a) polyacidic polymers, b) polycationic polymers.....	21
Figure 1-4. The classification of enzyme responsive materials based on their structural design elements. <sup>144</sup> .....	23
Figure 1-5. Precipitation polymerization. After initiation the oligoradical grows to a critical length before collapsing on itself to form a precursor particle. The precursor particle continues to grow either by aggregating with other precursor particles or with growing oligomers, and eventually the microgel particle precipitates out of solution.....	26
Figure 1-6. A synthetic route used for in-situ synthesis of semiconductor, metal or magnetic nanoparticles in the interior of poly(N-isopropyl acrylamide-acrylic acid-2-hydroxyethyl acrylate) microgels. Reprinted with permission. <sup>45</sup> Copyright 2004, American Chemical Society.....	28
Figure 1-7. Representation of the simple synthetic apparatus employed in the preparation of monodisperse QDs samples. Reprinted with permission <sup>190</sup> Copyright 2013, Hindawi Publishing Corporation.....	36

Figure 2-1. The synthesis of a pNIPAM-based microgels using an APS initiator. The functional group AAc in the comonomer with a double bond can involve radical polymerization in an aqueous solution <sup>166</sup> .....	49
Figure 2-2. Structure of composite pNIPAm-co-AAc microgel with CdS quantum dots	51
Figure 2-3. Reaction procedures.....	52
Figure 2-4. TEM image of one composite pNIPAm-co-20 % AAc microgel with CdS quantum dots particle.....	55
Figure 2-5. TEM image of several composite pNIPAm-co-20 % AAc microgel with CdS quantum dots particle.....	56
Figure 2-6. TEM image of the composite pNIPAm-co-20 % AAc microgel with CdS quantum dots particle.....	57
Figure 2-7. Characteristic peaks for Cd by X-ray photoelectron spectroscopy. Sample 2 is composite microgel with CdS, sample 4&5 were prepared in Chapter 3 and will be explained in Chapter 3.....	59
Figure 2-8. Characteristic peaks for S.....	60
Figure 2-9. Raman spectrum of composite pNIPAm-co-20 % AAc microgel (left) and pNIPAm-co-20 % AAc microgel (right) with CdS quantum dots with the excitation by the 514 line of an argon laser.....	61
Figure 2-10. X-ray Diffraction of composite pNIPAm-co-20 % AAc microgel with CdS quantum dots(left) and pNIPAm-co-20 % AAc microgel(right).....	62

Figure 2-11. Electron diffraction pattern of the composite pNIPAm-co-20 % AAc microgel with CdS quantum dots particle..... 63

Figure 3-1. The degradation kinetics of RhB in terms of removal efficiency (percent) at various time intervals (hour) in 10 °C. MG@CdS+UV: 0.4g MG@CdS+15mL 10mg/L RhB+UV; MG@CdS+Dark : 0.4g MG@CdS+15mL 10mg/L RhB+Dark; No Gel+UV: no Gel+15mL 10mg/L RhB+UV; MG no CdS+UV: 0.4g MG no CdS+15mL 10mg/L RhB+UV..... 75

Figure 3-2. The degradation kinetics of RhB in terms of removal efficiency (percent) at various time intervals (hour) in 45 °C. MG@CdS+UV: 0.4g MG@CdS+15mL 10mg/L RhB+UV; MG@CdS+Dark : 0.4g MG@CdS+15mL 10mg/L RhB+Dark; No Gel+UV: no Gel+15mL 10mg/L RhB+UV; MG no CdS+UV: 0.4g MG no CdS+15mL 10mg/L RhB+UV..... 78

Figure 3-3. The comparison of degradation kinetics of RhB at different temperatures at: 0.4g MG@CdS+15mL 10mg/L RhB+UV..... 79

Figure 3-4. The comparison of degradation kinetics of RhB at different amount (0.6g, 0.4g, 0.2g) of hybrid microgel with CdS..... 81

Figure 3-5. The degradation kinetics of RhB in terms of removal efficiency (percent) at various time intervals (hour) in 45 °C..... 83

Figure 3-6. Working pH range for the hybrid microgel with CdS..... 87

Figure 3-7. TEM of hybrid microgel before (left) and after (right) photocatalytic operations..... 88

Figure 3-8. TEM of hybrid microgel before (left) and after (right) half a year..... 88

Figure 3-9. Possible degradation intrmediates of RhB during the photocatalytic process.90

Figure 3-10. Mass spectra of RhB before irradiation (blue) and after 5 h irradiation (red).91

# List of Tables

Table2-1. pNIPAm-co- 10%AAc Microgel.....	1116
Table2-2. pNIPAm-co-15%AAc Microgel.....	1166
Table2-3. pNIPAm-co-20%AAc Microgel.....	1166
Table2-4. pNIPAm-co-30%AAc Microgel.....	117
Table2-5. pNIPAm-co-40%AAc Microgel.....	117
Table2-6. pNIPAm-co-50%AAc Microgel.....	117

# Chapter 1 - Wastewater Treatment Background

## 1.1 Introduction

Water is essential for maintaining the health and well being of all human life, although it is also important for various energy applications, and for maintaining food supplies. In addition to the environmental, economic, and social impacts of poor water supply and sanitation,<sup>1,2</sup> contaminated water has a disproportional impact on children, the elderly, and the poor.<sup>3</sup> It is estimated that 10-20 million people die every year due to the waterborne and nonfatal infection of more than 200 million people every year.<sup>4</sup> Every day about 5000-6000 children die due to the side effects of drinking contaminated water.<sup>5</sup> There are currently more than 780 million people around the world who do not have access to safe water resources,<sup>6</sup> resulting in major health problems.

### 1.1.1 Status of World Water Resources

Although 72% of the earth's surface area is covered by water, fresh water only accounts for ~0.75% of all water resources. Nearly 70% of this fresh water is fixed in the Antarctic and Greenland ice.<sup>4</sup> Most of the rest of the fresh water is trapped in soil or exists as deep groundwater supplies and cannot be accessed easily by everyday people and resources. Global freshwater resources are not only limited, but also exist in imbalanced distribution. Around 1.5 billion people from 80 countries and regions in the world lack fresh water. In this number, 26 countries containing 300 million people suffer an extreme lack of water. In Canada, the water level in the Great Lakes continues to decline and parts of the freshwater

supply have been polluted. In Canada, the most serious Escherichia coli (E. coli) water contamination occurred in Walkerton, Ontario 15 years ago.<sup>7</sup> The population of this town was only 5000, but the number of the infected was 2300 and seven people died because of this lethal pollution. Other provinces have improved their drinking water protection policy to increase the water quality.

According to the main study from Health Canada about national water quality, 35% of drinking water samples are polluted by drugs excreted from the human body, including drugs used to treat mental illnesses and heart disease, anti-inflammatory drugs and pain relievers, etc.<sup>5</sup> Researchers have pointed out that the use of drugs also increases as the baby boomers age in North America, and the environmental problems caused by drug emissions pollutant are expected to become more and more serious.

### **1.1.2 Water Resources Quality and Contaminants**

Urban sewage could achieve the national standard for drinking water after purification, in order to solve the water shortage issue, the source of urban sewage recycling is increasingly serious and there are many advantages of comparing with other water source development. First of all, the quantity of urban sewage is huge and stable. Secondly, the reclaimed water could be produced as long as the urban sewage is produced. The scale of sewage recycling is flexible and could be focused on the edge of a city to construct not only large-scale recycling waterworks, but also small-scale recycling waterworks or integration of processing equipment in various neighbourhoods and public buildings. The size is changeable and can adjust measures to local conditions.

### **1.1.2.1 Water Resource Quality**

According to statistics, 70% of reclaimed water could be recycled after treatment from the wastewater. This means the amount of available water to a city could be increased greatly by wastewater recycling. Countries around the world all attach importance to the use of reclaimed water, and reclaimed water as a legitimate alternative water source is becoming more and more widely used as an important part of urban water resources.<sup>6</sup>

Reasonable use of reclaimed water not only benefits cities economically but also socially and ecologically. First of all, it can reduce the costs of reclaimed water and recycling water. Secondly, reasonable use of recycled water could maintain the ecological balance and effectively protect water resources by changing the traditional mode of "mining - use - drainage" to achieve the virtuous circle of the water resources with long-term social benefits and a positive role in a relaxation effect on the city water resources shortage; Thirdly, the ecological benefit of rational utilization of reclaimed water not only embodies clear adverse impacts on effluent sewage on the urban environment but also further purifies the environment and beautifies.

### **1.1.2.2 General Classes of Water Contaminants**

The safe drinking water act defines the term "contaminant" as meaning any physical, chemical, biological, or radiological substance or matter in water. Therefore, the law defines "contaminant" very broadly as being anything other than water molecules. Drinking water may reasonably be expected to contain at least small amounts of some contaminants. Some drinking water contaminants may be harmful if consumed at certain levels in drinking water while others may be harmless. The presence of contaminants does not necessarily indicate

that the water poses a health risk. The following are general categories of water contaminants and examples of each.

Physical contaminants primarily impact the physical appearance or other physical properties of water. Examples of physical contaminants are sediment or organic material suspended in the water of lakes, rivers and streams from soil erosion. Chemical contaminants are elements (heavy metals) or compounds (organics). These contaminants may be naturally occurring or man-made. Examples of chemical contaminants include nitrogen, bleach, salts, pesticides, metals, toxins produced by bacteria, and human or animal drugs. Biological contaminants are organisms in water. They are also referred to as microbes or microbiological contaminants. Examples of biological or microbial contaminants include bacteria, viruses, protozoan, and parasites. Radiological contaminants are chemical elements with an unbalanced number of protons and neutrons resulting in unstable atoms that can emit ionizing radiation. Examples of radiological contaminants include cesium, plutonium, and uranium. The main problem caused by water pollution is that it negatively impacts the health of the life that depends on these water bodies, which can lead to death. Dead fish, crabs, birds and sea gulls, dolphins, and many other animals often wind up on beaches as shown in Figure 1-1. Pollution disrupts the natural food chain as well. Tiny animals eat pollutants such as lead and Cd. Later, fish and shellfish consume these animals, and the food chain continues to be disrupted at all higher levels. The health effects of drinking contaminated water can range from no physical impact to severe illness or even death. Eventually, this process affects humans as well. People can get diseases such as hepatitis by eating seafood that has been poisoned. In many poor nations, there are outbreaks of cholera and diseases as a result of poor drinking water treatment from contaminated waters.



**Figure 1-1.** a) Dye released wastewater and b) dead aquatic life.

In recent decades, the availability of clean water is a major concern in both developed and developing countries for use in domestic and industrial applications. It is estimated that 1.1 billion people in the world lack access to improved water supply and 2.6 billion people lack adequate sanitation.<sup>8</sup> The water consumption estimates range from 1,382 km<sup>3</sup>/year in 1950 to 5,235 km<sup>3</sup>/year in 2025. Moreover, the water availability in 2025 will be about 872 m<sup>3</sup>/capita/year, well underneath the limit of 1,000 m<sup>3</sup>/capita/year, which defines the people who live in water scarce regions.<sup>9</sup> The increase in water scarcity is one of the most critical environmental problems facing many parts of the world. It has been predicted that in the year 2025, about 3.5 billion people, i.e. 48% of the world population, will have an inadequate water supply.<sup>10</sup> With an increase in the population growth rate, the amount of fresh water availability is expected to reduce with time, negatively affecting the socio-economic development in many countries. Therefore wastewater reuse can be one of the possible strategies to increase water resources if it can be safely managed.<sup>11</sup>

### **1.1.3 Wastewater Treatment Methods**

Population explosion and expansion of urban areas increased the adverse impacts on water resources, particularly in regions where natural resources are still limited. Currently, water use and reuse have become a major concern. With the development of the dyeing and printing industries, its wastewater production has become one of the most important sources of water pollution. This kind of wastewater has deep color, complicated composition, huge emissions, wide distribution of surface, and the characteristics of refractory, as well as other aspects to consider. Direct emissions would bring serious harm to the ecological environment without treatment. Population growth leads to significant increases in default volumes of wastewater, there by making it imperative to develop effective and affordable technologies for wastewater treatment. Here I introduce new technologies and new methods in the treatment of dye wastewater on the basis of the literature.

#### **1.1.3.1 Adsorption Method**

Adsorption is one of the most widely used water remediation techniques. Adsorption methods concentrate and remove the pollutant on the surface by using the activity on the surface of the adsorbent. In recent years, the activated carbon<sup>12,13</sup> has been used for pollutant adsorption in wastewater treatment and has obtained certain achievement. Combining ClO<sub>2</sub> oxidation with activated carbon adsorption in printing and dyeing wastewater treatment greatly improved both the removal rate of the chemical oxygen demand (COD) and the decolourizing rate compared with the single use ClO<sub>2</sub> oxidation or the activated carbon adsorption process. Since coal ash is widely available and the price is low, it has great potential in terms of the printing and dyeing wastewater treatment. Wang and co-

investigators<sup>14</sup> studied the adsorption decolourizing ability of coal ash in reactive dyes, acid dye, and cationic dye in wastewater. Sun and other researchers<sup>15</sup> used fly ash to deal with reactive dye wastewater and the result is promising. Dealing with dye wastewater by the adsorption method treatment has the advantages of less investment, short cycle, and suitability for smaller companies. However, we must also focus on the adsorbent regeneration after the adsorption of dye and the post-processing of waste adsorbent in order to reduce secondary pollution.

### **1.1.3.2 Membrane Separation Technology**

Membrane filtration is a process used to separate dissolved substances and fine particles from solutions. Membranes act as a semipermeable and selective barrier that separate particles based on molecular or physical size. Membrane separation technology used in printing and dyeing wastewater has low energy consumption, is a simple process, and produces no pollution. Feng and coworkers<sup>16</sup> deal with printing and dyeing wastewater by chitosan ultrafiltration membrane. The COD removal rate can reach 80% and the decolourization rate could be more than 95%. Wu and coworkers<sup>17</sup> found that by using an ultrafiltration method in processing waste water containing indigo, the concentrated dye solution could be recycled directly and the permeate could be used as a neutral water to reuse. Su and coworkers<sup>18</sup> made a cellulose acetate (CA) nanofiltration membrane, the membrane was used for printing and dyeing wastewater treatment and dye recycling. Jiang and coworkers<sup>19</sup> proposed a facile approach for constructing tuneable hydrophilic or amphiphilic antifouling membrane surfaces for combating different surface foulants during the water treatment. The membrane with an amphiphilic surface exhibited over 99.5% retention ratio of

COD without appreciable membrane fouling. But there are many disadvantages of the membrane separation technology, such as the concentration polarization, membrane fouling, expense of the membrane, and the expensive processing, which severely hampered the larger-scale industrial application of membrane separation technology.

### **1.1.3.3 Fenton Method**

Fenton and related reactions encompass reactions of peroxides (usually hydrogen peroxide ( $\text{H}_2\text{O}_2$ )) with iron ions to form active oxygen species that oxidize organic or inorganic compounds. The Fenton reaction was discovered by H.J.H. Fenton in 1894 and he reported that  $\text{H}_2\text{O}_2$  could be activated by ferrous ( $\text{Fe}^{2+}$ ) salts to oxidize tartaric acid.<sup>20</sup> In the last few decades, the importance of radical reactions has been recognized and rate constants for over 1700 OH radical reactions with organic and inorganic compounds in aqueous solution have been tabulated.<sup>21</sup> In the recent past, the Fenton reaction was efficiently utilized in the wastewater treatment process for the removal of many hazardous organics.<sup>22</sup> The Fenton process can be carried out at room temperature and atmospheric pressure. In addition, required reagents are readily available, easy to store and handle, safe, and environmentally friendly.<sup>23</sup> Ma and coworkers<sup>24</sup> showed that degradation was enhanced and degradation time shortened when using a small amount of ultraviolet visible light to irradiate. They evaluated the influence of low-molecular-weight organic acids (LMWOAs), such as malonic acid, ethylenediaminetetraacetic acid, and oxalic acid, on the Fenton degradation of organic pollutants under visible irradiation. With the Fenton reagent as a strong oxidizer to deal with the organic pollutants in water, reaction condition is mild and only simple equipment is needed, but processing costs too much to be used daily.

#### 1.1.3.4 Photocatalytic Oxidation Method

There has been a growing interest in the use of semiconductors as photosensitizers for the complete oxidative mineralization of pollutants by oxygen.<sup>25,26</sup> The purification of water by semiconductor photocatalysis is attracting a great deal of interest, not only from research workers but also from water purification companies. This interest arises because (i) the by-product is harmless to the environment, (ii) the process of photomineralization can be turned on or off simply by tuning on/off the light source, and (iii) there is a real possibility that it could be readily incorporated into existing UV water purification systems.<sup>25</sup>

There are various semiconductor materials to choose from, which are readily available, but only a few are suitable for sensitizing the photomineralization of a wide range of organic pollutants. A sensitizer for reaction must be (i) photoactive, (ii) capable of utilising visible and/or near UV light, (iii) biologically and chemically inert, (iv) photostable, and (v) cheap. In many cases, the semiconductor is labile to oxidative decomposition by the photogenerated hole. It is generally found that only n-type semiconductor oxides are stable towards photoanodic corrosion. CdS is an example of a highly active semiconductor photosensitizer that not only has bandgaps sufficiently large that the semiconductors absorb only UV light, but also has the highly desirable feature that it can be activated using visible light. Another commonly used catalyst is titanium dioxide (TiO<sub>2</sub>). Ohtani and co-researchers<sup>27</sup> present a detailed mechanism for the photooxidation of alcohols on TiO<sub>2</sub> that requires the reductive and oxidative trapping of pairs of photoexcited electrons and holes by surface-adsorbed substrates. Zhang and coworkers<sup>28</sup> prepared spherical TiO<sub>2</sub> catalysts, which were composed

of nanocrystal grain by reversed suspension polymerization and a sol-gel method with a porous structure to degrade KN-R dye in a suspension form.

### **1.1.3.5 Electrochemical Oxidation Method**

Electrochemical processes have gained increasing interest in recent years for the treatment of polluted waters.<sup>29-31</sup> They are considered to be versatile and capable of degrading a wide range of contaminants. Electrochemical systems offer several advantages over other approaches, such as operation at ambient temperature and pressure as well as robust performance and capability to adjust to variations in the influent composition and flow rate. They generally require no auxiliary chemicals and do not produce waste. Electrochemical processes can be adapted to various applications, and can be easily combined with other technologies. Researchers use the electrochemical method to deal with salt dye wastewater. From the study they found that the generation of residual chlorine in the process of electrolysis has a decisive role in the COD removal. The COD removal rate are very high during electrolytic process. Using activated carbon and iron hydroxide composite catalyst to deal with dye wastewater by electric catalytic method, Zhang and coworkers<sup>33</sup> deal with dye wastewater by internal electrolysis-catalytic oxidation-oxidation pond method. As a result, the removal rate of COD and the chromaticity are all above 95%. Qi and coworkers<sup>34</sup> adopted a micro electrolysis-catalytic oxidation- combination of a fly ash adsorption process to deal with reactive dye production wastewater. As a result, the COD removal rate could be above 95% and the decolorization rate could be 99.9%. The key for electric catalytic oxidation technology moving towards practical application is developing electrode material with efficient catalytic performance, improving the catalytic performance of electrode

materials, and improving current efficiency. Lowering polarization in order to reduce the energy consumption is the main research direction in the future. Combining electrocatalysis and pulse power to change electrode structure would be the new direction to implement electric catalytic oxidation into industrial application.

#### **1.1.3.6 Ultrasonic Degradation Technology**

Ultrasonic refers to sound waves with a frequency above 20 KHz. When the higher frequency with certain intensity goes through the media, it produces a series of physical and chemical effects, resulting in the breaking up of the dye. Degradation of organic pollutants by ultrasonic means in water is a new, simple and effective wastewater treatment technology.

#### **1.1.3.7 Biochemical Method**

The biochemical method has a low running cost and is therefore widely used in dye wastewater treatment. Researchers extensively studied anaerobic - aerobic, deep aeration, pure oxygen aeration, and other biochemical methods in recent years and applied this technology to engineering. Breeding and producing a variety of excellent decolorizing bacteria strains is an important development for the biochemical method. A microorganism has certain challenges for nutrients, pH, and temperature conditions when using the biochemical method to remove the dye wastewater, such as the difficulty to adapt to the dyestuff wastewater quality fluctuation, the characteristics of variety, and high toxicity.

The development of cost-effective and stable materials and methods for providing fresh water in adequate amounts is desperately needed. Traditional water/wastewater treatment technologies remain ineffective for providing adequate safe water due to increasing demand

of water coupled with stringent health guidelines and emerging contaminants. The photocatalysis system<sup>26,35-37</sup> has great advantages by using a clean light resource as energy for wastewater treatment compared to other methods. Otherwise, polymer-based multifunctional and highly efficient processes are providing affordable solutions to water/wastewater treatments that do not rely on large infrastructures or centralized systems. So combining polymer with semiconductor nanocrystals is an increasingly promoted method in the application of environmental wastewater treatment.

## **1.2 Characteristics of Polymer/Nanocrystal Systems for Wastewater Treatment**

Composite materials of polymer and semiconductor nanocrystals materials not only combine the advantages of organic polymer and inorganic nanocrystals, but also possess many new and unique properties.<sup>38</sup> There are many advantages to using polymer-based materials, such as optical transparency, physical and chemical stability, and easy workability; they also provide a good carrier for stabilizing nanoparticles to preserve their function. The presence of nanocrystals enhances the function of the polymer material and also strengthens the polymer in the physical view, like mechanical property. More importantly, they can bring photocatalytic properties to the polymer materials.<sup>39</sup> Due to the superior performance of polymer-nanocrystalline composites under light, it is more and more widely used in electrical, magnetic, industry, agriculture, medical, aerospace, and other cutting-edge technology. Thus, polymer nanocrystalline composite material has attracted extensive attention in the research community. Colvin and coworkers<sup>38</sup> prepared CdSe@Poly(p-phenylene vinylene) compound multilayer film by using CdSe nanocrystals and polymer Poly(p-phenylene vinylene). This

composite material has a change in the light emission spectrum from red to green as the electric voltage is changed from high to low. The color of the polymer layer is red to yellow when the voltage is 4V and the color of the polymer layer is green when the voltage is higher. Thus, it could be used to make light emitting diode (LED) and other electroluminescent materials. Zhang and co-investigators<sup>39,40</sup> prepared different sizes of CdTe nanocrystals and introduced unsaturated surfactant on the surface to make it copolymerize with the styrene and methyl methacrylate. The resulting material is a nanocrystal-polymer composite with different colours and could potentially be used as a display device. Weng and coworkers<sup>41</sup> used a single molecule targeted drug delivery system and connected the CdSe-ZnS core-shell nanocrystals to the cancer antibody with a PEG polymer chain. The biological test results confirmed that nanocrystals produced fluorescence imaging in the live mice tumor site.

The ultimate integration of nanocrystals into future devices can largely benefit from the availability of precisely engineered designer nanocomposites with stimulus responsive polymers. A frequently used stimulus responsive polymer is poly (N-isopropylacrylamide) (pNIPAm), which exhibits a lower critical-solution temperature (LCST) in water around 32 °C (in the region of interest for biological applications) where an abrupt chain collapse and phase separation occur. Thus, several inherent disadvantages of suspension catalysts could be overcome, e.g., photocatalysts with nanoparticles tend to result in their aggregation into larger particles and some photocatalysts would be subjected to undesirable photocorrosion, both of which result in a decrease in the photoreaction efficiency. pNIPAm-based microgels were selected due to the high porosity/surface area for absorption/adsorption of contaminants. The pNIPAm-based microgels could help restrain the aggregation of nanoparticles. Furthermore, the pNIPAm-based microgels are thermoresponsive. Discussing the volume

change of microgels from a swollen (hydrophilic) state to a compact (relatively hydrophobic) state in the photocatalytic effect of the semiconductor nanocrystals has an important value in the research of wastewater treatment.

### **1.2.1 Synthesis of Hybrid pNIPAm/Nanocrystal**

In the synthesis of polymeric nanocomposite photocatalyst nanocrystal/pNIPAm microgel, it is important that the semiconductor nanocrystals are doped in pNIPAm-based microgels with homogeneously dispersity. In general, there are two polymerization methods to synthesize polymeric nanocomposite photocatalyst nanocrystal/pNIPAm: (1) blend polymerization and (2) in-situ copolymerization.

#### **1.2.1.1 Blend Polymerization**

In blend polymerization, the monomer, the initiator, and the semiconductor nanocrystals are directly mixed together in a suitable solvent to form nanocomposite photocatalyst nanocrystal/pNIPAm. The polymeric nanocomposite is fabricated by impregnating semiconductor nanocrystals within pNIPAm-based microgels. Blend polymerization is a relatively simple and straightforward approach, but the semiconductor nanoparticles without modification can easily aggregate in the reaction system. Thus, nanocrystals in a composite gel system are not stable and inhomogeneous. Using the surfactants to modify the surface of nanocrystals can make nanocrystals more monodispersed in the reaction system, increasing stability, and therefore the nanocrystals would exist in the composite microgel stably without aggregation. It can reflect the common excellent properties of nanocrystals and microgel. Previously, this simple and convenient method attracted the attention of the researchers.

### **1.2.1.2 In-Situ Copolymerization**

As for the in situ polymerization method, the semiconductor nanocrystals are formed by the surface modification of pNIPAm-based microgels. The in-situ polymerization system is relatively complicated, but the semiconductor nanocrystals within the polymeric nanocomposite are not only distributed evenly in the polymer matrix but also more stable. Through this method, nanocrystals can be grown inside a polymer and the polymer acts as the protective shell for nanocrystals in an aqueous solution. For example, PAMAM dendrimer<sup>42</sup> and PMMA polymeric microsphere<sup>43,44</sup> were used to fabricate highly luminescent PAMAM/CdS and PMMA/CdS hybrid materials. Zhang and coworkers<sup>45</sup> reported the approach employs polymer microgels (pNIPAm) as templates for the synthesis of semiconductor, metal or magnetic nanoparticles. The generated pNIPAm/ nanocrystals retain both stimulus-responsive behavior of the polymer and the optical property of nanocrystals.

## **1.3 Introduction to Stimuli Responsive Polymers**

### **1.3.1 Introduction**

Stimuli responsive polymers and systems,<sup>46-48</sup> which are also called smart materials, are novel materials capable of responding to external stimuli.<sup>49</sup> The definition of response of a polymer is highly dependent on the restrictions of the polymeric segments' mobility. Which means the polymer chain always have higher dimensional change than a polymer gel, since there is restricted network in the gel. The response is exhibited in a variety of ways, such as changes in size, secondary structure, color, solubility, or the degree of intermolecular

association changes. External stimuli can be either chemical or physical signals,<sup>50-53</sup> or also multiple responsive systems.<sup>54,55</sup> Physical signals such as light,<sup>56-58</sup> temperature,<sup>51,52,59-61</sup> electric potential,<sup>62</sup> and pressure<sup>63,64</sup> modify the energies of chain dynamics and molecular interactions. Chemical signals, such as pH,<sup>65-67</sup> ionic species,<sup>67</sup> or metabolites,<sup>68</sup> interfere with the molecular interactions between polymeric chains and solutes. For multiple responsive systems, combining physical and chemical stimulus in one material component or systems has been applied. Ionic interactions and hydrogen bonding or hydrophobic interactions of polymeric systems can be modified by the external stimuli, causing changes in the physical state of the system. The removal of the stimulus should result in a reversion to the original physical state. The examples of responses are depicted in Figure 1-2.

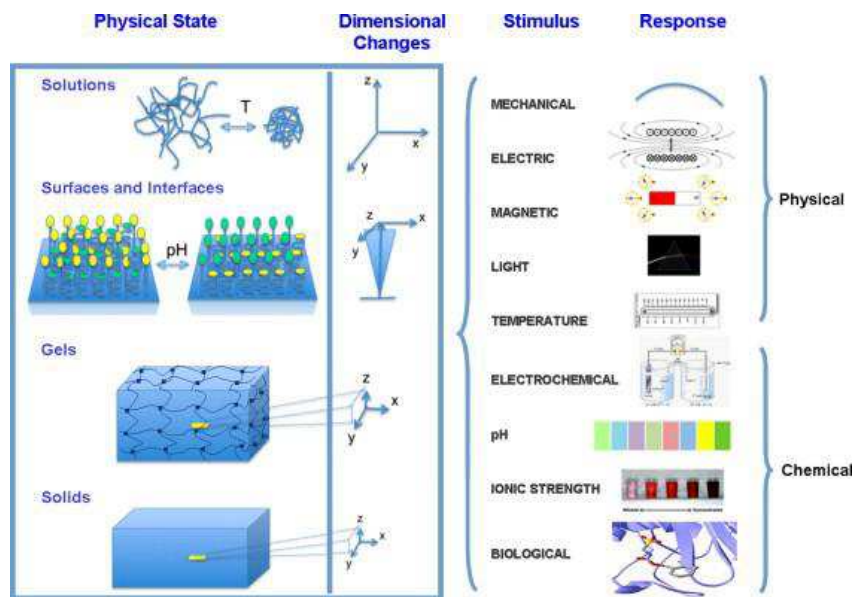


**Figure 1-2.** Schematic representation of dimensional changes in polymeric solutions, at surfaces and interfaces, in polymeric gels, and polymer solids resulting from physical or chemical stimuli. Reprinted with permission.<sup>48</sup> Copyright 2002, Elsevier.

Physical stimuli responses include those brought on by temperature and light. Temperature responsive polymers<sup>50,51,59,69</sup> have been among the most studied stimuli-responsive materials for several decades due to their ability to change features such as solubility and conformation, and they are convenient to operate, thereby having a potential for a variety of applications. Polymers that undergo hydrophilic–hydrophobic phase transitions are of great interest for researchers who have taken advantage of these transitions to promote the formation, transformation, or deformation of aggregates in response to variations in temperature. PNIPAm<sup>52,70-72</sup> is one of the most popular polymers among these smart materials. Poly [2-(dimethylamino) ethyl methacrylate] (PDMAEMA)<sup>73-77</sup> is another very frequently used temperature responsive polymer that undergoes a hydrophilic-to-hydrophobic phase transition at its LCST, which is between 40-50 °C. In chemically responsive polymers,<sup>67,78-80</sup> frequently used stimuli are pH and redox. One of the important reason for using pH responsive polymers in the medical area is that the local pH values of human tissues and cellular environment vary significantly, and thus provides great potential application of these kinds of polymers in biomedical areas, such as controlled drug delivery. Combining physical and chemical stimuli is an important advance in designing responsive polymer systems often aimed at taking advantage of the key features in both internal and external stimuli. The combination of the two stimuli greatly improves the flexibility to trigger the stimuli-responsive polymers temporally and spatially and therefore has the capability to achieve the desired properties on demand. Other stimuli, like biochemical stimuli,<sup>81-84</sup> can find use in many applications including drug and gene delivery, imaging, sensing, and so on. The advantage of incorporating biochemical stimuli responses to a system is that they have the potential to be specific for a biomedical function, particularly when combined with a

second cooperative physical or chemical stimulus. Multiple stimuli responsive materials are those that are responsive to three or more stimuli and are fundamentally interesting but less explored. For example, a pH sugar and temperature responsive polymer<sup>85</sup> was synthesized by a polymerization of boronic acid acrylamide monomer (APBA) with NIPAm monomer by atom-transfer radical-polymerization (ATRP) or reversible addition-fragmentation chain transfer (RAFT) polymerization. Recently, there are several very unique multi-responsive polymer systems developed by different groups<sup>86-91</sup> to enrich the stimuli responsive polymer family.

### **1.3.2 Thermoresponsive Polymers**

Thermoresponsive polymers are one of the most extensively studied smart materials. There are two main types of thermoresponsive polymers involved in most of the studies. One is the polymer with a lower critical solution temperature (LCST) while the other one presents an upper critical solution temperature (UCST).<sup>92-94</sup> LCST and UCST are the respective critical temperature points below and above which the polymer and solvent are completely miscible.<sup>95</sup> Thus, for example, a polymer solution below the LCST is a clear, homogeneous solution, while a polymer solution above the LCST appears cloudy. The cloudiness appears because of the increased light scattering from the denser, collapsed species. It is noteworthy that LCST is an entropically driven effect, while UCST is an enthalpically driven effect.<sup>96,97</sup> Most of the studies use polymers that present an LCST.<sup>98</sup> The most common of these is poly (N-isopropylacrylamide) (pNIPAm). pNIPAm has a lower critical solution temperature (LCST) of around 32 °C, a very useful temperature for biomedical applications since it is close to the body temperature (37 °C). Adjustment of the LCST of pNIPAm has been

achieved by copolymerizing with hydrophilic or hydrophobic monomers<sup>99,100</sup> rendering the overall hydrophilicity of the polymer higher or lower, respectively. Other polymers with thermoresponsive properties include poly(N-vinylcaprolactam) (PVCL)<sup>101-103</sup> with an LCST between 25 and 35 °C and PDMAEMA<sup>104</sup> with an LCST of around 50 °C. However, it is important to note that the LCST of a polymer is dependent on molecular weight and architecture.<sup>105</sup>

The LCST of pNIPAm is an entropically driven transition. Heskins and Guillet<sup>52</sup> first proposed the thermodynamic origin of the LCST. The Gibbs free energy of the system is given by the following equation:

$$\Delta G_m = \Delta H_m - T\Delta S_m$$

Where  $\Delta G_m$  is free energy of mixing,  $\Delta H_m$  is the enthalpy change of mixing,  $T$  is temperature in Kelvin, and  $\Delta S_m$  is the entropy change on mixing. At low temperatures, formation of hydrogen bonds between NIPAm and water reduce the free energy of mixing ( $\Delta G_m$ ) as the enthalpic contribution ( $\Delta H_m$ ) is negative. Structured water around the pNIPAm leads to a loss in entropy (negative  $\Delta S_m$  term) and a positive entropic contribution. As  $T$  increases, the positive entropic contribution to the free energy grows. When the positive entropic contribution dominates over the enthalpic contribution, phase separation begins.

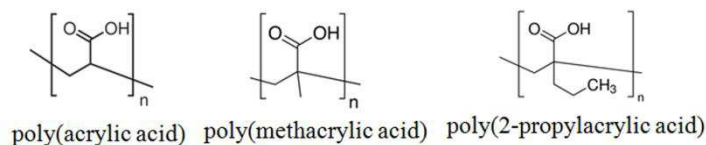
### 1.3.3 pH Responsive Polymers

pH-sensitive polymers are polyelectrolytes composed of weak acidic or basic groups that either accept or release protons in response to changes in environmental pH. Polyanions and polycationic<sup>106-108</sup> are the most used pH-sensitive polymers, which are characterized by a large number of ionizable functional groups such as carboxylic or amine groups. In the case

of pH-sensitive polymers, the key element of the system is the presence of ionizable weak acidic or basic moieties attached to a hydrophobic backbone. Upon ionization, the coiled chains extend dramatically responding to the electrostatic repulsions of the generated charges (anions or cations).<sup>66,109-111</sup> The pH at which the pendant acidic groups become ionized depends on the  $pK_a$  (the log value of the acid dissociation constant,  $K_a$ ) of the polymer, which in turn depends on the polymer's composition and molecular weight. However, complete ionization on polyelectrolytes is more difficult due to electrostatic effects exerted by other adjacent ionized groups. It makes the apparent  $K_a$  different from that of the corresponding monoacid or monobasic.

Polyacidic polymers will be unswollen at low pH, since the acidic groups will be protonated and unionized. When increasing the pH, a negatively charged polymer will swell. The opposite behaviour is found in polybasic polymers, since the ionization of the basic groups will increase when decreasing the pH. Typical examples of pH sensitive polymers with anionic groups are poly (carboxylic acids) as poly(acrylic acid) (PAA)<sup>112,113</sup> or poly(methacrylic acid) (PMAA).<sup>114,115</sup> A few examples of cationic polyelectrolytes are poly(*N,N*-diakyl aminoethyl methacrylates),<sup>116</sup> poly(lysine) (PL),<sup>117</sup> poly(ethylenimine) (PEI),<sup>118</sup> and chitosan.<sup>119-121</sup> The examples of pH responsive polymers are listed in Figure 1-3.

### a) Polyacidic polymers



### b) Polycationic polymers

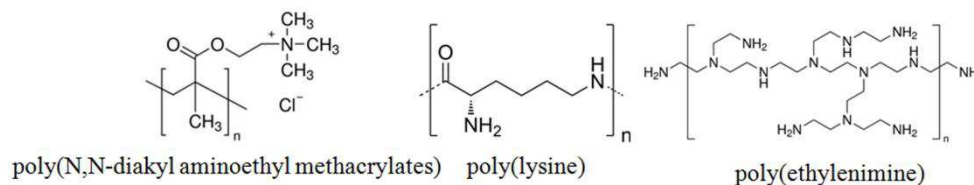


**Figure 1-3.** Chemical structure of pH-sensitive polyanions and polycationic polymers. a) polyacidic polymers, b) polycationic polymers. Reprinted with permission.<sup>112</sup> Copyright 2002, American Chemical Society.

## 1.3.4 Other Responsive Polymers

### 1.3.4.1 Photoresponsive Polymers

Photoresponsive polymeric systems<sup>50,122-125</sup> are polymers with photo-sensitive moieties on the backbone or side chain, and have been widely studied in many areas, such as photonic materials,<sup>126,127</sup> photo-mechanical systems,<sup>128</sup> display<sup>129</sup> and micropatterning.<sup>130</sup> These systems are important because light is non-destructive, can be localized, as well as remotely activated. Thus delivering energy to systems results in photo-triggered sensing, actuating, and transporting. Photoresponsive polymers exhibit conformational changes in response to light with different wavelengths. Such polymers can be constructed by incorporating

chromophores that can translate light energy into a change in conformation. Photochromism is defined as a reversible transformation of chemical species between two states having observable light absorptions in different regions. In photoresponsive functionalities, the response may be associated with chemical processes involving either isomerization or cleavage of chemical bonds. The main chemical processes involved in photochromism are *cis-trans* isomerization (azo compounds),<sup>56</sup> pericyclic reactions (spiropyrans)<sup>131</sup>, dissociation reactions (triphenylmethane leuco derivatives),<sup>132</sup> electron transfer (viologens),<sup>133</sup> and so on.

#### **1.3.4.2 Enzyme Responsive Polymers**

enzyme-responsive materials undergo reversible macroscopic transitions that are triggered by selective enzyme catalysis. Enzyme reactions<sup>134-137</sup> are highly selective and efficient toward specific substrates under mild conditions, such as aqueous media, typically neutral or slightly acidic and alkaline pH. They are involved in all biological and metabolic processes, serving as the prime protagonists in the chemistry of living organisms at a molecular level. The integration of enzyme reactions with responsive polymers can further broaden the design flexibility and scope of applications with enhanced triggering specificity and selectivity. Enzyme-responsive polymeric systems typically possess enzyme-reactive moieties in the form of labile linkages along the polymer main chain or side groups. In addition, they can also produce effects in an indirect manner by utilizing enzyme reaction products or intermediates as the triggering signal input,<sup>138,139</sup> which can in principle be integrated with the design of conventional responsive polymers and polymeric assemblies.<sup>140</sup> It is worth noting that these enzyme-triggered structural transformation or transition processes are relevant to the practical applications of responsive polymers concerning

functions of drug delivery and controlled release, imaging, and diagnostics. For example, the Ulijn group<sup>141</sup> fabricates an enzyme-responsive peptide-based material and uses this material to form small molecule assemblies to apply in the controlled release of dextran. This group has developed a variety of enzyme-responsive materials exhibiting relevant functions in the fields of regenerative medicine, diagnostics, and controlled release nanovehicles.<sup>136,142,143</sup> The classification of enzyme responsive materials is shown in Figure 1-4.

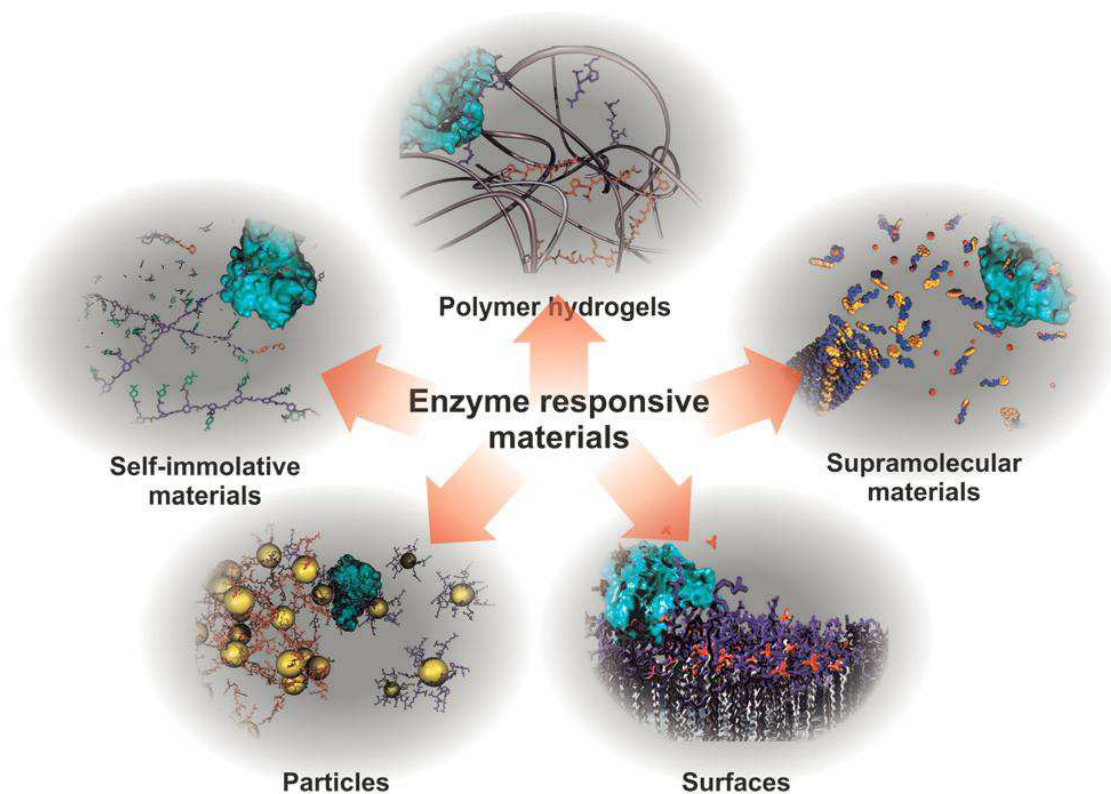


**Figure 1-4.** The classification of enzyme responsive materials based on their structural design elements.<sup>144</sup>Reprinted with permission. Copyright 2014, American Chemical Society.

### 1.3.5 Stimuli Responsive Hydrogels

Hydrogels, by definition, are three-dimensional cross-linked polymeric networks that can imbibe large amounts of water.<sup>145-149</sup> Stimuli responsive hydrogels are classified as a

responsive polymer network and can have conformation change by applying external stimuli. Extensive efforts in the field of responsive hydrogels have been focused on the design of structures that respond to specific stimuli.<sup>150</sup> One of the pioneering works comes from the Tanaka group,<sup>151,152</sup> which shows that thermoresponsive ionic gels exhibit a discontinuous transition in contrast to a continuous transition exhibited by non-ionic gels. In addition to this contribution, Yan and Hoffman<sup>153</sup> reported that polymerization of NIPAm gels at higher temperatures than the LCST of the polymer results in formation of the gels that have a large pore size. Under this methodology, the pNIPAm gels with faster swelling rate were successfully synthesized. Early responsive hydrogel studies were focused on the development of new materials that responded to various stimuli such as pH, temperature, light, and electric field that eventually cause the phase separation of the polymeric materials. For instance, when gels are formed by polymerizing the thermoresponsive main monomer, NIPAm, and the light-sensitive chromophore chlorophyllin, in the presence of a cross-link agent, the phase transition of the gels is induced by illumination.<sup>154</sup> Another interesting study on responsive gels was performed by applying electric fields to polyacrylamide gels.<sup>125</sup> In this study, some portion of the acrylamide group was converted into an acrylic acid group by hydrolysis, and then the volume phase transition of the ionic gels was induced under electric fields, which provide pH gradient and Coulombic interaction between electrodes.

### **1.3.6 Poly (N-Isopropylacrylamide) Microgels**

Microgel networks, just like hydrogels, are extremely solvent swellable (approximately 95 % by volume) in their hydrated state and contain approximately 20 % solvent in their deswollen state.<sup>52,155-157</sup> Colloidal microgels constructed from pNIPAm range from 50 nm to

5  $\mu\text{m}$  in size and exhibit similar temperature responsive properties to their hydrogel. That is, they undergo a volume phase transition at the LCST of pNIPAm. The LCST of the microgels is affected by cross-linking density, solvent nature and composition, and the nature of the functional groups in the copolymer.<sup>158-160</sup> Microgels possess several advantages over bulk hydrogels: small size and volume, high surface area, faster response to stimuli and high diffusivity. Most of the recent researchers focus on the incorporation of functional moieties within pNIPAm based microgel materials that alter the hydrophilic/hydrophobic balance as well as the swelling capacity, while exploring the application of pNIPAm microgels. One of the examples is copolymerization of acrylic acid monomer into the system to incorporate a charged species into pNIPAm-based microgels, which found employment in the controlled uptake and release of various model drug compounds.<sup>158,161-163</sup>

### **1.3.7 Synthesis of pNIPAm Microgels**

Microgel particles composed primarily of pNIPAm can be synthesized using a variety of techniques including emulsion polymerization<sup>164</sup> and thermally induced free radical precipitation polymerization.<sup>165</sup> In all of the syntheses performed, NIPAm served as the main monomer. Two different types of cross-linkers were normally explored in the polymerization. The first was N,N'-Methylenebisacrylamide (BIS), a relatively short and rigid cross-linker, while the second was a more flexible oligomeric cross-linker, Poly(ethylene glycol) diacrylate (PEGDA). Microgels are formed by homogenous nucleation. Figure 1-5 illustrates the mechanism of precipitation polymerization. There are two reasons for the polymerization to be carried out at high temperature: one is formation of sulfate radicals, which initiate the polymerization. The second is, after initiation the NIPAm monomer polymerizes and the

chain starts to grow. Once the chain length reaches a certain critical length, it collapses on itself, producing precursor particles. The chain collapses because the polymerization temperature is higher than the LCST of the polymer and hence it phase separates. The precursor particles grow by two mechanisms: they either aggregate with the other precursor particles or are captured by existing colloiddally stable particles. The charge imparted by the initiator stabilizes the microgels. To synthesize small microgels, the precursor particles have to be stabilized earlier in the reaction. Since there is not enough charge available to stabilize the small precursor particles, surfactant is used, which stabilizes the small precursor particles, so a lower surfactant concentration will generate larger microgels particles. Depending on the application of the microgels, they can be modified by post polymerization modification.<sup>166</sup>

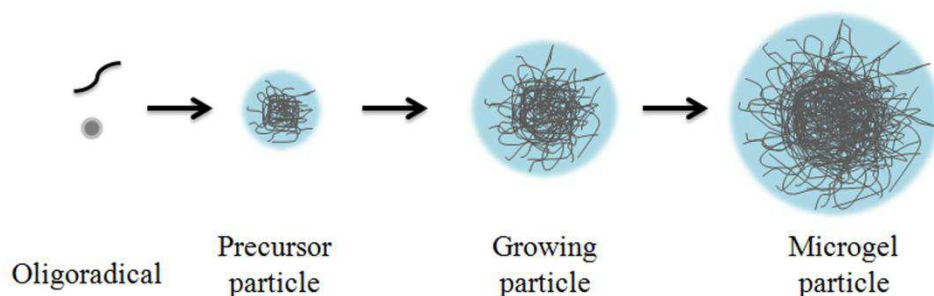


**Figure 1-5.** Precipitation polymerization. After initiation the oligoradical grows to a critical length before collapsing on itself to form a precursor particle. The precursor particle continues to grow either by aggregating with other precursor particles or with growing oligomers, and eventually the microgel particle precipitates out of solution. Reprinted with permission.<sup>48</sup> Copyright 2004, Elsevier.

### **1.3.8 pNIPAm Microgel Applications**

Over the past few decades, several new applications of microgels have arisen due to their stimulus-responsive nature. These include their uses as microreactors for the synthesis of inorganic nanoparticles with predetermined properties, as carriers for targeted drug delivery, as tunable optical lenses and as building blocks of photonic crystals. The section below will briefly chart the functional roles and properties of microgels in the context of these applications.

#### **1.3.8.1 Microgels as Microreactors**

Nanoparticles (NPs) have been synthesized by template, such as dendrimers, block copolymer micelles, and polyelectrolyte multilayers. In comparison with other polymer template systems, microgels serve as ideal microreactors for NPs formation due to their simple synthesis, easy functionalization, and relatively large size comparable to the wavelength of visible light. Zhang et al.<sup>45</sup> used poly(N-isopropylacrylamide-acrylic acid-2-hydroxyethyl acrylate) [poly(NIPAm-co-AA-co-HEA)] microgels with a hydrodynamic diameter of 200-600 nm as templates for the synthesis of three exemplary types of NPs: semiconductor, metal, and magnetic nanoparticles.

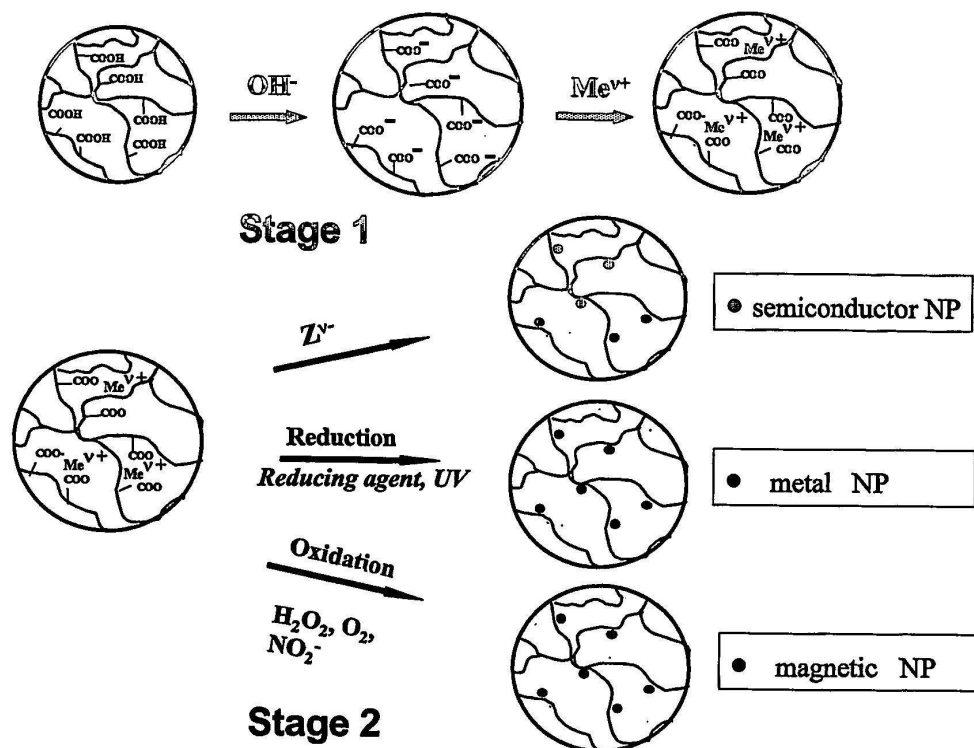


**Figure 1-6.** A synthetic route used for in-situ synthesis of semiconductor, metal or magnetic nanoparticles in the interior of poly(N-isopropyl acrylamide-acrylic acid-2-hydroxyethyl acrylate) microgels. Reprinted with permission.<sup>45</sup> Copyright 2004, American Chemical Society.

### 1.3.8.2 Microgels for Drug Delivery

One of the key areas of intensive research is the application of microgels in controlled drug delivery. The open network structure of microgels can be used to incorporate small molecules such as drugs in their interiors while their large swelling-deswelling transitions may be employed as physico-chemo-mechanical triggers to direct the release of the drugs. In addition to pH, ionic strength, or temperature-triggered volume transitions, microgels loaded with a drug can interact with biological components or events such as enzymatic processes

that would activate the release of the drug. Langer et al.<sup>167</sup> and Frechet et al.<sup>168</sup> reported pH triggered nonspecific release of a drug from submicron-sized microgel particles to the macrophages. Functionalization of microgels allows one to tune their volume transitions in physiologically relevant conditions. Furthermore, modification with other functional groups can extend the external stimuli to be applied in controlled drug delivery application. By attaching receptor-specific proteins to the microgel surface, one can achieve selective targeting ability designed to treat specific diseases or specific tumor cells. The Kumacheva group demonstrated the use of two types of biofunctionalized, pH responsive, drug-loaded microgels for targeted intracellular delivery to HeLa cancer cells<sup>169</sup> poly(NIPAm-co-AA) and the biopolymeric, chitosan-based microgels.<sup>170</sup> The Todd group has prepared magnetic responsive nanogel film for on-off drug release application.<sup>171</sup> They also developed injectable hydrogels containing entrapped microgels<sup>172</sup> for small-molecule drug delivery. Drug release could be sustained for up to 60 days from these nanocomposite hydrogels, significantly longer than that achievable using the constituent hydrogel or microgels alone (<1 week).

### **1.3.8.3 Microgels as Photonic Crystals**

Microgels are excellent examples of materials with structural hierarchy. Lyon et al.<sup>173</sup> reported color-tunable colloidal crystals formed by the assembly of thermoresponsive poly(NIPAm-AA) microgels. Upon centrifugation, the microgels assembled into a close-packed colloidal crystalline array that displayed striking iridescence. The Bragg diffraction was modulated by a change in temperature. Microgel also can be hybridized with inorganic nanoparticles to form hybrid microgels. The coupling of structure- and composition-dependent properties of both polymer microgels and inorganic nanoparticles opens new

avenues in the production of smart materials with many degrees of freedom in controlling their performance. Kumacheva et al.<sup>174</sup> circumvented these limitations by encapsulating hybrid poly(NIPAm-AA-HEA) microgels with a dense hydrophobic shell of a copolymer of methyl methacrylate, butyl acrylate, and acrylic acid (MMA-BA-AA). The narrow polydispersity, negative charge, and smooth surface of these hybrid core-shell particles carrying CdS and Ag NPs in their cores favored their self-assembly into colloid crystals.

## **1.4 Introduction of Semiconductor Nanocrystals**

Semiconductor nanocrystals (NCs) are nanometer-sized crystalline particles that exhibit size-dependent optical and electronic properties.<sup>175</sup> With typical dimensions in the range of 1-100 nm, these nanocrystals bridge the gap between small molecules and large crystals, displaying discrete electronic transitions reminiscent of isolated atoms and molecules, as well as enabling the exploitation of the useful properties. The unique size-dependent optical properties of colloidal semiconductor nanocrystals have been the subject of considerable interest in the past three decades.<sup>176</sup> Strongly luminescing II-VI semiconductor NCs have found potential applications in biological imaging and labeling,<sup>177</sup> photovoltaics,<sup>178</sup> electroluminescence devices,<sup>179</sup> optical sensors,<sup>180</sup> etc. Structural, photophysical,<sup>181</sup> photochemical,<sup>182</sup> and photoelectrochemical<sup>183</sup> properties of the semiconductor NCs have been intensively studied. The major feature of semiconductor nanomaterials is the quantum confinement effect, which is essentially due to changes in the atomic structure as a result of direct influence of ultra-small length scale on the energy band structure. It is a highly size dependent effect and influenced by the surface of the nanocrystals.

### **1.4.1 Quantum Dots**

Quantum dots (QD) are semiconductor devices that tightly confine electrons or holes in all three spatial dimensions. They can be made via several possible routes including colloidal synthesis, plasma synthesis, or mechanical fabrication. The term “quantum dot” was coined by Mark Reed in 1988;<sup>184</sup> however, they were first discovered in a glass matrix by Alexey Ekimov<sup>185,186</sup> in 1981 and in colloidal solutions by Louis E. Brus in 1985.<sup>187</sup> The electronic properties of the quantum dots fall between those of bulk semiconductors and those of discrete molecules of comparable size, and optoelectronic properties, such as band gap, can be tuned as a function of particle size and shape for a given composition. In QDs, light absorption generally leads to an electron being excited from the valence to the conduction band, leaving behind a hole. The electron and the hole can bind to each other to form an exciton. When this exciton recombines (i.e. the electron resumes its ground state), the exciton's energy can be emitted as light. This effect is called fluorescence. In a simplified model, the energy of the emitted photon can be understood as the sum of the band gap energy between the highest occupied level and the lowest unoccupied energy level, the confinement energies of the hole and the excited electron, and the bound energy of the exciton.

#### **1.4.1.1 Effect of Size**

The energy difference between the absorption and emission spectra is known as the Stokes shift. Generally, the smaller the crystal size, the larger the band gap. Therefore, the electron will require more energy to become excited, and in turn will emit light with higher energy when returning to a lower energy state. The color and emission wavelength of a QD are determined by its size and composition. QDs can emit light at wavelengths ranging from

the ultraviolet (UV) to the infrared (IR). The ability to tune the size of quantum dots is advantageous for many applications. For instance, larger quantum dots have a greater spectrum-shift towards red compared to smaller dots, and exhibit less pronounced quantum properties. Conversely, the smaller particles allow one to take advantage of more subtle quantum effects.

#### **1.4.1.2 Effect of Surface**

The surface effect of QDs is a reduction in the particle size of the quantum dots, most of the atoms located at the surface. The quantum dot surface area will increase when particle size decreases. Due to the large surface area of the nanoparticles, the number of surface atoms increases, resulting in a lack of coordination of the surface atoms, unsaturated bonds and increased dangling bonds. These surface atoms have high activity, are very unstable, and combine easily with other atoms, which creates a large surface energy and high activity. Active surface atoms not only cause surface atom transport and structural changes, but also cause a conformational change in the surface electron spin and electron energy spectrum. Surface defects lead to trap electrons or holes, which in turn will affect the luminescent properties of quantum dots, causing a nonlinear optical effect. The light reflection coefficient will decrease usually less than 1%. That is why the QDs are generally black, have smaller particle size, and display deeper color. The light absorption capability of the QDs is stronger, showing a strong absorption spectrum of wide band.

#### **1.4.1.3 Dielectric Confinement Effect**

Dielectric confinement is effective reduction of the dielectric constant due to the penetration of the electric field into a barrier medium with a small dielectric constant. Since the size of quantum dots are confined in nano space, electron transport is limited, the electron mean free path is short, localized electrons and coherence are enhanced and produce quantum confinement effect. For quantum dots, when the particle size is close or smaller than Bohr radius in the strong confinement area, it is easy to form excitons and exciton absorption bands. As the particle size decreases, the absorption coefficient of exciton band is increased, and strong exciton absorption will appear. Due to the quantum confinement effect, the lowest energy exciton movement that is blue-shifted to higher energy.

#### **1.4.1.4 Other Physical Effects**

Other physical effects such as the quantum tunneling effect and Coulomb blockade effect are also very important for application of QDs. A quantum tunneling effect occurs when particles have a finite probability of crossing an energy barrier, such as the energy needed to break a bond with another particle, even though the particle's energy is less than the energy barrier. Quantum tunneling has no counterpart in classical mechanics, in which a particle can never cross an energy barrier with a higher energy level than the particle has. The emission of alpha rays in radioactive decay is a case of quantum tunneling; though the alpha particles are strongly bound to the nucleus and don't have as much energy as the bond does, they still have a finite probability of escaping the nucleus. The design of transistors and many diodes makes use of this effect. When the sum of a quantum dot and the capacitance of all its associated electrode are small enough, only one electron can go into the quantum dot,

and the increase of electrostatic energy of the system will be far greater than the increase of electron thermal motion ability. This effect can prevent a subsequent second electrostatic electron entering the same quantum dot, which is called the Coulomb blockade effect.

Bulk semiconductors are characterized by a composition-dependent band gap energy ( $E_g$ ), which is the minimum energy required to excite an electron from the ground state valence energy band into the vacant conduction energy band. The exciton has a finite size within the crystal defined by the Bohr exciton diameter, which can vary from 1 nm to more than 100 nm depending on the material. If the size of a QDs is smaller than the size of the exciton, the charge carriers become spatially confined, which raises their energy. Therefore, the exciton size delineates the transition between the regime of bulk crystal properties and the quantum confinement regime, in which the optical and electronic properties are dependent on the QDs' size. QDs with dimensions smaller than the Bohr exciton diameter demonstrate size-dependent absorption and fluorescence spectra with discrete electronic transitions. The most important consequence of the quantum confinement effect is the size dependence of the band gap for QDs. By confining the exciton of a semiconductor, the band gap may be tuned to a precise energy depending on the dimensionality and degree of confinement.<sup>188</sup> The effect on the optical properties by the particle size is internal structure phenomenal. However, when the QDs has a small size, the density of atomic layer on the surface will increase and lead to new features optical properties. For example, reducing the diameter of a spherical sample from 1 m to 1 nm increases the surface area by a factor of  $10^9$ . Such a large change cannot be ignored, since it also induces other characteristics for the nanomaterial. This is called the surface effect of QDs. Research shows that when the diameter of a particle is smaller than 10 nm, the density of its surface atoms increase greatly, leading to higher surface energy and

enhanced activity of the QDs. Also, due to higher surface energy, particles are extremely unstable under normal conditions and are likely to aggregate. The lack of atomic coordination and high surface activity of QDs atoms could cause a lot of surface defects on the surface of the QDs.

The surface state of the nanocrystalline is the trap to capture the electrons and holes. There is a big effect for the luminescence properties of QDs. It is advantageous to coat QDs with an insulating inorganic shell in order to stabilize and maximize fluorescence. A lot of researches have been done to prevent the aggregation of QDs, such as surface modification, QDs /polymer composite, and the preparation of core-shell QDs. These researches are very important for extending the application of QDs.

#### **1.4.2 Quantum Dots Preparation**

The preparation of QDs is a popular area of research due to the wide application of the nanomaterials. The research on the preparation of QDs has made tremendous progress through the continuous efforts of chemical, physical, and material scientists. The inclusion of nano to micron sized QDs materials into glasses was first explored in 1930s. Rocksby found that the glass matrices with CdSe inside can change the hue of the glasses and then applied these materials for color filters. After several decades, Louis Brus first observed the size dependent properties of colloidal CdS QDs,<sup>189</sup> through the measurement of size dependent redox potentials. The morphology and size of QDs can be controlled by choosing appropriate reactants and suitable reaction conditions, such as the solvent component, temperature and reacting time. A typical synthesis system for colloidal QDs consists of three components: precursors, organic surfactants, and solvents. Upon heating a reaction medium to a

sufficiently high temperature, the precursors chemically transform into active atomic or molecular species (monomers); these then form QDs whose subsequent growth is greatly affected by the presence of surfactant molecules. The formation of the QDs involves two steps: nucleation of an initial ‘seed’ and growth. In the nucleation step, precursors decompose or react at a relatively high temperature to form a supersaturation of monomers followed by a burst of nucleation of QDs. These nuclei then grow by incorporating additional monomers still present in the reaction medium. The process is schematically shown in Figure 1-7.

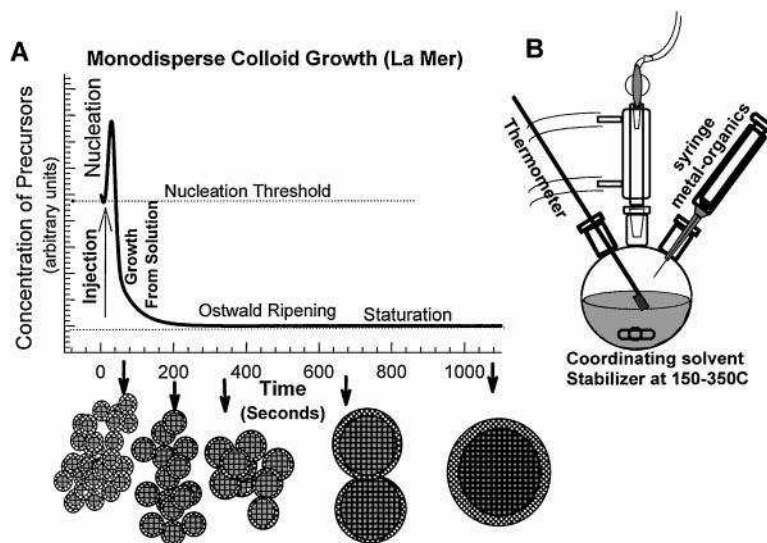


**Figure 1-7.** Representation of the simple synthetic apparatus employed in the preparation of monodisperse QDs samples. Reprinted with permission <sup>190</sup> Copyright 2013, Hindawi Publishing Corporation.

#### **1.4.2.1 Chemical Precipitation Method**

The chemical precipitation method is the formation of a separable solid substance from a solution, either by converting the substance into an insoluble form or by changing the composition of the solvent to diminish the solubility of the substance in it. The thermal decomposition is required for the synthesis of QDs or dehydration. Precipitation methods include direct precipitation, homogeneous precipitation and co-precipitation, and so on. Chemical precipitation methods are simple to operate and need only mild reaction conditions. However, the disadvantage for this method is a lack of control of the reaction process, and it is difficult to observe the growth of the QDs environment. In general, the diameter distribution of QDs made by the chemical precipitation method was relatively broad. For example, Pratima Chauhan and coworkers<sup>191</sup> synthesized CdS semiconducting quantum dots by the chemical precipitation method using thioglycerol as the capping agent. Nanocrystals of ZnS have been synthesized through a simple chemical precipitation method using thiourea as the sulphur source by Nadana and coworkers.<sup>192</sup> The synthesized products were annealed at different temperatures in the range of 200-800° C. The influence of thermal annealing on the structural, optical, and morphological features of ZnS QDs was investigated.

#### **1.4.2.2 Thermal Decomposition Method**

A very important development in nanoparticle synthesis came in the early 1990s, when Murray, Norris, and Bawendi<sup>193</sup> introduced the first non-aqueous, controlled growth process for II-VI semiconductor QDs. The keys to this synthesis were (1) to use non-aqueous solvents and capping ligands to stabilize the products against ripening, (2) to carry out the reaction at high temperature to ensure good crystallinity, and (3) to separate the steps of

particle nucleation and growth, and thereby obtain particles of uniform size. It is generally believed that the degree of crystallinity is improved under high temperature. To increase the nanocrystallinity, a high temperature and suitable environment were applied when synthesizing the QDs. Researchers have achieved the thermal synthesis of QDs by using an organic solvent, such as a high boiling solvent mixture of trioctylphosphine (TOP) and trioctylphosphine oxide (TOPO), since they can have a high boiling point. At the same time, a long-chain surfactant is added to the reaction system to prevent the aggregation of QDs. In this way, both the growth and stability of the QDs can be controlled. This method allows the reaction to occur in a relatively short time under high temperature, thus creating highly crystalline QDs. With the continuous development of a thermal decomposition method, this kind of method has become the most commonly used method to synthesize QDs. QDs with relative narrower particle size distribution could likely be synthesized by this method through continuous improvement of the reaction conditions. Zhu and coworkers<sup>194</sup> report a simple and safe synthetic system to prepare high quality AIS and AIS/ZnS QDs using thermal decomposition. The synthetic system simply involves heating a mixture of silver acetate, indium acetate, and oleic acid in dodecanethiol at 170 °C to produce AIS QDs with a 13% quantum yield (QY). Jin-Kyu Lee and coworkers<sup>195</sup> investigated the mechanism underlying amine promoted thermal decomposition of single-molecule precursors, namely, zinc alkyldithiocarbamate complexes, in order to understand the conversion of the precursor molecules into intermediates, their decomposition into nanoparticles.

### **1.4.2.3 Hydrothermal Method and Solvothermal Method**

Hydrothermal and solvothermal are methods that involve reactants at high temperature and pressure to preparing QDs. The hydrothermal method generally uses water as the solvent of the reaction system, while the solvothermal method uses organic solvent as the reaction solvent. These methods are all performed in a closed system. When the closed system is heated, evaporation of the solvent increases the pressure, so the reaction system could be in a critical state with high temperature and high pressure. Under the critical state with high temperature and high pressure, the solubility and activity of reactants are increased, and this will promote crystallization of the product from the liquid phase. Under these conditions, the hydrothermal and solvothermal methods are no longer restricted by the boiling point of solvent. Solvents with lower boiling points could also be used as a reaction medium for this method to prepare nanocrystalline at high temperature. Hydrothermal and solvothermal methods greatly expand the types of precursor materials that can be used in the synthesis of QDs. These methods are also simple and have industrial potential. Qian and co-workers<sup>196</sup> have reported a solvothermal synthesis in the solution of ethylenediamine, poly (vinyl acetate), and ethanol for preparation of CdS nanorods.

### **1.4.2.4 Liquid-Solid-Solution Interface Phase Transfer and Phase Separation**

The ability to synthesize monodisperse QDs is one of the difficulties in nanomaterials research. Yadong Li from Tsinghua University<sup>197</sup> proposed a synthesis, which is known as "liquid-solid-solution" phase transfer, to produce monodisperse QDs. This strategy partially overcomes the challenge by carefully designing the chemical reactions taking place at the interfaces of different phases.<sup>198</sup> In this approach, a water/ethanol mixed solution is used as

the main continuous solution phase. Since water is an ideal solvent for most inorganic species, and ethanol is a good solvent for most of the surfactants, including fatty acid, most of the soluble inorganic salts can be used as the starting materials. Long chain alkyl surfactants such as octadecylamine or oleic acid can be used as protecting reagents for the QDs. With these important features, this approach has been proven to be quite general in generating a huge group of monodispersed QDs with sizes in the range of 2-15 nm, which have quite different crystal structures, compositions, and properties. This method overcomes the problems of cost and environmental pollution by using organic solvents, and breaks through the limitations of the existing method to synthesize nanocrystalline, but only applies for single or limited nanocrystalline materials.

However, despite all the success that has been achieved, more precise control over the dynamic process across the synthesis remains a challenging task, which may serve as the basis for the establishment of QDs crystallography. Meanwhile, integration of monodispersed nanostructures into complex devices or superstructures is another problem that researchers face in nanoscience fields. The chemical and physical properties of surfaces and interfaces in QDs are still the first issue to consider in the development of integration strategies

### **1.4.3 Application of Quantum Dots**

QDs have been used in many research areas due to their unique optical properties, such as optical transistors, light-emitting diodes, semiconductors and photovoltaic. Those are highly relative to the quantum effect and optical properties. There are many studies and reviews on this topic,<sup>199-202</sup> and we will not go through that detail about this area. Recently, QDs have been used in biotechnology efficiently after Alivisatos et al.<sup>199</sup> and Nie et al.<sup>203</sup> showed that

QDs can be used in biotechnology. Generally, QDs are synthesized in apolar solvents such as toluene and heptanes. However, quantum dots must be water soluble to be used in bioimaging. For that reason, researchers try to make water soluble QDs with different methods, such as ligand exchange and one pot synthesis. With their excellent optical properties, QDs are used as labeling agents in bioimaging. Although organic dyes can be used as fluorophores in biological applications, QDs have overcome many of the restrictions of organic dyes, such as poor photostability, low quantum yield, and insufficient in vitro and in vivo stability in bioimaging. QDs are also emerging as a promising class of nanoscale materials for the development of artificial photocatalytic systems. The energy of excited states in these nanoparticles can be tuned continuously via nanoparticle size, which presents a unique opportunity for the design of nanostructures exhibiting a significant spatial separation of charges, an important property for a photocatalytic material.<sup>204</sup> One of the most important and emerging applications on photocatalytic property of QDs is in environmental area. It appears to be a promising technology that has a number of applications in environmental systems such as air purification, water disinfection, hazardous waste remediation, and water purification.

# Chapter 2- Polymerization and Modification of pNIPAm/CdS Composite Microgel

## 2.1 Introduction

Semiconductor nanocrystals (NCs) are well known to exhibit size-dependent optical and electronic properties.<sup>204</sup> With typical diameter in the range of 2-10 nm, these nanocrystals bridge the gap between small molecules and large crystals, displaying discrete electronic transitions reminiscent of isolated atoms and molecules, as well as enabling the exploitation of the useful properties of crystalline materials. The unique size-dependent optical properties of colloidal semiconductor nanocrystals have been the subject of considerable interest in the past two decades.<sup>205</sup> The synthesized colloidal nanocrystals are normally inorganic/organic hybrid materials where the inorganic nanocrystal core is covered by an organic ligand monolayer, such as vinyl and azide-terminated carboxylic acids. The organic ligands typically play a crucial role in controlling the size, shape, colloidal stability and solubility of the particles and for colloidal stability and solubility.<sup>205,20607</sup> Therefore, surface modification or ligand exchange is required for improving the stability of the particles for further applications.<sup>208,209</sup> Removing the nanocrystal's native ligands that originate from its synthesis can cause etching, introduce surface defects, and often leads to a significant loss in quantum yields and poor stability of the colloids in aqueous solutions. However, there is a way to prevent these side effects.<sup>210-213</sup> Polymers offer opportunities for flexible, lightweight, and mechanically stable nanocrystal composites. Most of the studies on

semiconductor nanocrystals are focused on their physical properties.<sup>214-216</sup> The incorporation of semiconductor nanocrystals into a thin polymer film has been attempted for potential application in flat panel displays with a polymer matrix, such as polyvinylcarbazole,<sup>217</sup> poly(vinyl butyral).<sup>218</sup> Recently, incorporating semiconductor nanocrystals into microgel particles have attracted interest among researchers for the development of new applications.<sup>213,219-221</sup>

The ability to control the volume and size of these microgels by changing the temperature is important for creating unique, controllable composites with CdS nanocrystals. The photocatalytic activity of CdS nanocrystals is dependent on the particle dispersity and the aggregation of nanocrystals will induce a decrease in their activity. In the case of the hybridized pNIPAm microgel with CdS nanocrystals (CdS@pNIPAm), CdS nanocrystals, which are embedded in the polymer network, are more prone to aggregation due to microgel shrinkage, and thus exhibit lower catalytic activity. Therefore, adjusting the temperature to below the LCST will allow the microgel to expand and the nanocrystals to have improved the particle distribution.

The purpose of this chapter is to discuss the in situ synthesis, modification and characterization of CdS@pNIPAm microgels. Specifically, the attachment of CdS nanoparticles to the crosslinked polymer will be discussed. Techniques used to characterize the composite materials to confirm their structure and properties include transmission electron microscope (TEM), Raman spectroscopy, X-ray diffraction (XRD), X-ray photoelectron spectroscopy, and fluorescence spectroscopy.

## 2.2 Materials & Methods

N-isopropylacrylamide was purchased from TCI (Portland, OR) and purified by recrystallization from hexanes (ACS reagent grade, purchased from EMD, Gibbstown, OR). N,N'-Methylenebisacrylamide (99%), acrylic acid (99 %), ammonium persulfate (98 %), CdCl<sub>2</sub> (99.99%) sodium hydroxide (97%) hydrogen chloride (99%) sodium sulfide (98%) and rhodamine B (95%) were purchased from Sigma-Aldrich (Oakville, ON) and were used as received. Microgel samples were lyophilized using a VirTis bench-top K-manifold freeze-dryer (Stone Ridge, New York). Deionized (DI) water with a resistivity of 18.2 MΩ·cm was obtained from a Milli-Q Plus system (located in the Biological Laboratory in the Department of Chemistry, University of Alberta) purchased from Millipore (Billerica, MA), and filtered through a 0.2 μm filter prior to use.

The size and morphology of CdS nanoparticles were determined at 60 to 120 kV accelerating voltage by a Hitachi H-7650 transmission electron microscope (TEM) from cell imaging centre (University of Alberta). The atomic concentration and valence electrons of Cd and S were determined by X-ray photoelectron spectroscopy from Nano Fab (Department of Chemistry, University of Alberta). The crystalline phases of the CdS nanoparticles were determined by X-ray diffraction (XRD) (Dr. Arthur Mar's group, Department of Chemistry, University of Alberta) Raman spectroscopy (Dr. Mark T. McDermott's group, National Institute for Nanotechnology, University of Alberta) and electron diffraction (High Resolution Transmission Electron Microscopy from cell imaging centre). The fluorescence property of CdS nanoparticles was determined by fluorescence spectroscopy (Analytical and Instrumentation Laboratory, Department of Chemistry, University of Alberta).

### 2.2.1 Transmission Electron Microscopy

Transmission electron microscopy (TEM) is a technique in which a beam of highly energetic electrons is transmitted through an ultra-thin specimen, interacting with the specimen as it passes through. An image is formed due to the interaction of electrons with the specimen. While passing through the sample, certain areas of the material will stop or deflect electrons more than other areas. The electrons are collected from below the sample onto a phosphorescent screen or through a camera. In the regions where electrons do not pass through the sample the image is dark. The image is magnified and focused onto an imaging device, such as a fluorescent screen, on a layer of photographic film, or to be detected by a sensor such as a CCD camera.

Good images of composite pNIPAm-co-AAc microgels/CdS were obtained at 60 to 120 kV accelerating voltage by a Hitachi H-7650 Transmission Electron Microscopy (TEM) from cell imaging centre (University of Alberta). During the detection, pH values of the pNIPAm-co-AAc microgel were modified from 1.00 to 14.00 by the addition of NaOH. And the  $pK_a$  of AAC is around 4.2 in pNIPAm-co-AAc microgel. When the pH is higher than 4.2, the AAC moiety will be deprotonated and associate with sodium ions. However, when the pH is lower than 4.2, the carboxylic group will be protonated. Thus, there is an optimal pH value for the synthesis of composite microgel with CdS quantum dots. Furthermore, the percentage of AAC in the microgel is also important during the synthesis. Firstly, the percentage of AAC matters in synthesizing pNIPAm-co-AAc microgel. The percentage of AAC also matters in subsequent steps to attach CdS quantum dots.

The morphology and particle size of composite pNIPAm-co-AAc microgels/CdS were also measured by transmission electron microscopy. Also, the stability of the particles was analyzed before and after one year. TEM is capable of imaging at a significantly high resolution, owing to the small de Broglie wavelength of electrons. This enables us to examine features as small as a single column of atoms.

### **2.2.2 X-ray Photoelectron Spectroscopy**

X-ray photoelectron spectroscopy (XPS) is a surface-sensitive qualitative and quantitative spectroscopic technique that measures elemental composition, chemical states, and electronic states of the elements that exist within a material. XPS spectra are obtained by irradiating a material with a beam of X-rays while simultaneously measuring the kinetic energy and number of electrons that escape from the top 0 to 10 nm of the material being analyzed.

To synthesize the composite microgel with CdS quantum dots, the elements of the composite pNIPAm based microgel doped with CdS quantum dots were analyzed using X-ray photoelectron spectroscopy from Nano Fab (Department of Chemistry, University of Alberta).

Furthermore, the amount of Cd and Na were measured within the composite microgel by X-ray photoelectron spectroscopy. In this way, the approximate capacity of CdS quantum dots doped within the pNIPAm-co-AAc microgel will be calculated. Also, X-ray photoelectron spectroscopy was used in chapter 3-Remediation Performance. More detailed will be introduced in Chapter 3.

### **2.2.3 Raman Spectroscopy**

In general, Raman analysis is based on the Raman scattering effect found by the Indian scientist C.V. Raman. Raman spectroscopy is a technique used to observe vibrational, rotational, and other low-frequency modes in a system with different incident light frequency scattering spectrum and it is commonly used in chemistry to provide a fingerprint by which molecules can be identified.

We have observed Raman scattering from both composite microgel with CdS and pNIPAm-co-AAc microgel to analyze the molecular structures. The Raman spectrum was obtained by excitation at 514 nm by an argon laser. We used the instrument from Dr. Mark T. McDermott's group, National Institute for Nanotechnology, University of Alberta, with a conventional photon-counting system.

### **2.2.4 X-ray Diffraction**

X-ray diffraction is a tool used for identifying the atomic and molecular structure of a crystal, in which the crystalline atoms cause a beam of incident X-rays to diffract into many specific directions.

X-rays are optical radiation from the transition of inner electron atoms under the bombardment of the high velocity electrons. This technique mainly includes continuous X-ray and characteristic X-ray. Crystal can be used as a X-ray grating, the interference of light effect will happen due to the coherent scattering generated by the large number of particles (atoms, ions or molecules), so that the X-ray scattering intensity increase or decrease. Due to the superposition of scattering wave from a large number of particles, the maximum intensity

of the beam produced by mutual interference is called X-ray diffraction line and could be used in Bragg's law:

$$2d\sin\theta=n\lambda \quad (1)$$

$n$  is a positive integer.  $\lambda$  is wavelength incident wavelength.  $\theta$  is the scattering angle of light.  $d$  is the interplanar distance of lattice plane. To determine the crystalline structure of the composite microgel with CdS quantum dots, the  $\theta$  angle was measured with a certain X-ray. The size and the type of crystal plane distance can be calculated by using Bragg's law.

### **2.2.5 Electron Diffraction**

Electron diffraction is most frequently used in solid-state physics and chemistry to study the crystal structure of solids. Experiments are usually performed in a transmission electron microscope (TEM), or a scanning electron microscope (SEM) as electron backscatter diffraction. This technique is similar to X-ray and neutron diffraction.

The electron diffraction pattern for the composite microgel with CdS quantum dots was also measured by a Hitachi H-7650 Transmission Electron Microscopy (TEM) from cell imaging centre to further detect the crystalline structure followed X-ray diffraction. The sample is the same as the one used in Transmission Electron Microscopy imaging. Camera lens with high resolution was used in Electron diffraction.

### **2.2.6 Fluorescence Spectroscopy**

Fluorescence spectroscopy is a type of electromagnetic spectroscopy, which analyzes fluorescence from a sample.

In general, the size of a quantum dot is usually between 1 ~ 10 nm in diameter. Because the quantum confinement of electrons and holes, the continuous band structure changes into discrete energy levels properties. Hence, quantum dots can emit fluorescence after excitation.

### 2.3 Polymerization of pNIPAm-co-AAc Microgel

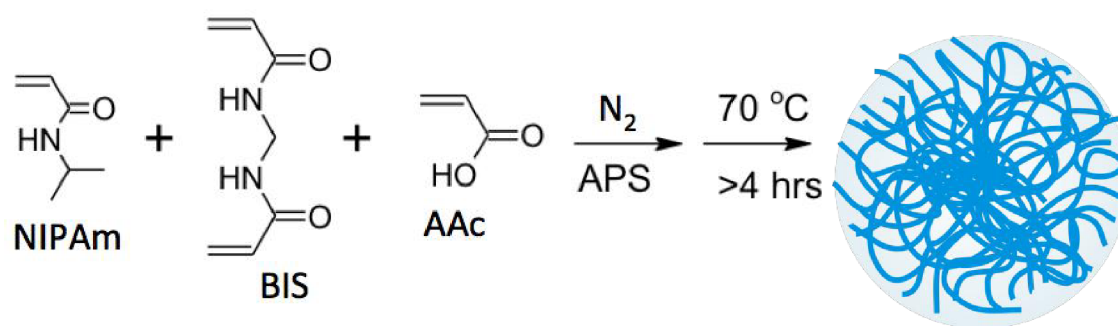


**Figure 2-1.** The synthesis of a pNIPAm-based microgels using an APS initiator. The functional group AAc in the comonomer with a double bond can involve radical polymerization in an aqueous solution<sup>166</sup>. Reprinted with permission. Copyright 2004, Elsevier.

NIPAm and BIS were added to a 500 mL beaker. Then, 99 mL of deionized (DI) water was added. The solution was stirred for 30 min and then filtered with a 0.2  $\mu\text{m}$  filter into a 500 mL 3-neck round bottom flask. The solution was heated with hot plate to 70  $^\circ\text{C}$  with stirring and degassed with  $N_2$  for around 1 hour. After that, we added another comonomer acrylic acid and initiated with APS by injection syringe. After 4 hours, the hot plate was turned off and cooled to room temperature. The mixture was then filtered through

cotton wool and centrifuged at 10000 RPM for 1 hour. The supernatant was removed and washed with deionized (DI) water. This process was repeated 6 times to purify the microgel.

As the CdS quantum dots grafting density depending on the amount of carboxylic group in microgel, the molar ratio of NIPAm to AAc was adjusted from 8.5 to 0.9. The detailed synthesis molar ratio was shown below.

For the syntheses, the AAc content was adjusted, while changing the %NIPAm in the reaction and keeping the %BIS constant as shown in tables (Appendix). Polymerized particles with different percentages of acrylic acid may affect the doped amount of CdS nanoparticles and the morphology of the composite microgel due to the carboxyl bond from acrylic acid. Theoretically, more CdS nanoparticles will be doped when the percentage of AAc is higher. However, CdS nanoparticles may aggregate because of high activity if the concentration is too high. To find the optimum condition, microgels with different proportions was tried to merge CdS nanoparticles.

## **2.4 Preparation of pNIPAm Based Microgel@CdS Composites by In-situ Synthesis Method**

A quantum dot is a nanocrystal composed of semiconductor materials that are small enough to exhibit quantum mechanical properties. Specifically, its excitons are confined in all three spatial dimensions. CdS quantum dot is one of the most promising photocatalysts because of its relatively narrow band gap.

In this thesis, CdS nanoparticles are in-situ synthesized on poly (N-isopropylacrylamide)-co-acrylic acid (pNIPAm-co-AAc) microgels. The structure of the

hybrid microgel is shown in Figure 2-2, where black spots are CdS quantum dots. They are attached to the crosslinked mesoporous structure, which is pNIPAm based microgel.

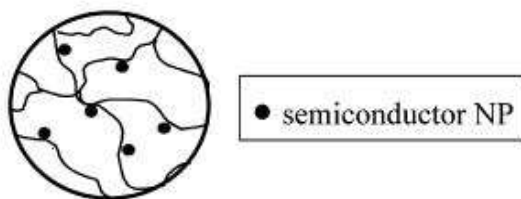


**Figure 2-2.** Structure of composite pNIPAm-co-AAc microgel with CdS quantum dots

According to this, pNIPAm based microgel act as a carrier and mircoreactor that has crosslinked mesoporous structure. At the same time, it could increase the stability of CdS nanoparticles.

Generally, the synthesis process has two steps that could be shown as in Figure 2-3. Step 1 is an ion-exchange process and step 2 is an aqueous-phase process.

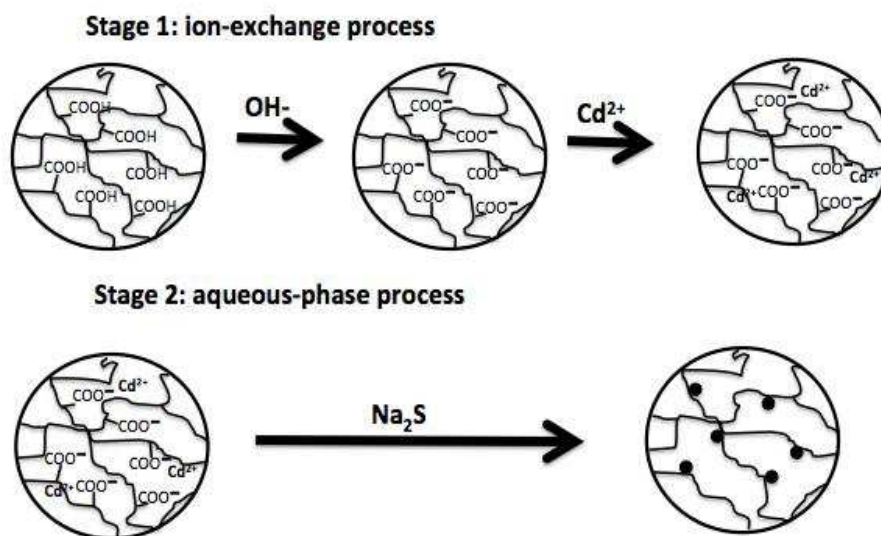


### Figure 2-3. Reaction procedures

For the ion-exchange process, if we adjust the pH value of the solution to be above the pKa of AAc (~ 4.2) to deprotonate the carboxyl groups in AAc, the hydrogen ions would be replaced with sodium ions. The AAc then becomes sodium acrylate, resulting in the dissociation of the weak acid and subsequent exchange of sodium and  $\text{Cd}^{2+}$  when  $\text{CdCl}_2$  is added. Because of the high concentration of  $\text{Cd}^{2+}$  in solution (100 times than AAc), it is possible to exchange sodium ions with  $\text{Cd}^{2+}$  into the solution, resulting in attachment of  $\text{Cd}^{2+}$  to the carboxylic groups. After attachment saturation, the excess  $\text{Cd}^{2+}$  and  $\text{Cl}^-$  must be removed.

For the aqueous-phase process, Because of the positive charge of  $\text{Cd}^{2+}$  in solution, the sulfide ions would attach to  $\text{Cd}^{2+}$  because of the negative charges. Also the concentration of sodium sulfide is 100 times that of AAc.

#### 2.4.1 Attempted Cd Coupling to pNIPAm-co-20% AAc Microgel

Based on the pNIPAm based microgel with different percentage of acrylic acid shown above, the primary hybrid pNIPAm based microgels doped with Cd were synthesized, which is step one: ion-exchange process.

After six runs of centrifugation, we tried pNIPAm-based microgels with 10%, 20% and 30% acrylic acid one by one. pNIPAm based microgel with each percentage of AAc was added to a 250 mL beaker along with 50 mL of deionized (DI) water with stirring. Firstly, sodium hydroxide (1M) and hydrogen chloride (1M) were used to adjust the pH value of the microgel solution from 1.00 to 14.00. Secondly, deionized (DI) water was used to purify the

mixture. The supernatant was decanted and centrifuged at 10000 RPM for 1 hour. It was then put inside the ultrasonic instrument for 15 min. The particles were purified using this process, which was repeated 6 times. Theoretically, the pH value should be above pKa of AAc (~ 4.2) to deprotonate the carboxyl groups in AAc. When the pH is low, the microgel is milky and opaque. As the pH is increased, the microgel becomes more and more transparent. Thirdly, the mixture was added to a 250 mL beaker along with 40 mL CdCl<sub>2</sub> (0.5 M), which was allowed to stir for 12 hours to make it completely reacted. This step and following process should be engaged in a fume hood. Fourthly, similar as above, the mixture was centrifuged at 10000 RPM for 1 hour and the supernatant was decanted and the resulting polymer mixture was washed with Deionized (DI) water. It was then put inside the ultrasonic instrument for 15 min. The particles were purified using this process, which was repeated 6 times. After this step, lots of precipitate was formed in the solutions. So those solutions with precipitate could not be used in the process below.

#### **2.4.2 Preparation of CdS Quantum Dots Coupled pNIPAm-co-20% AAc Microgel**

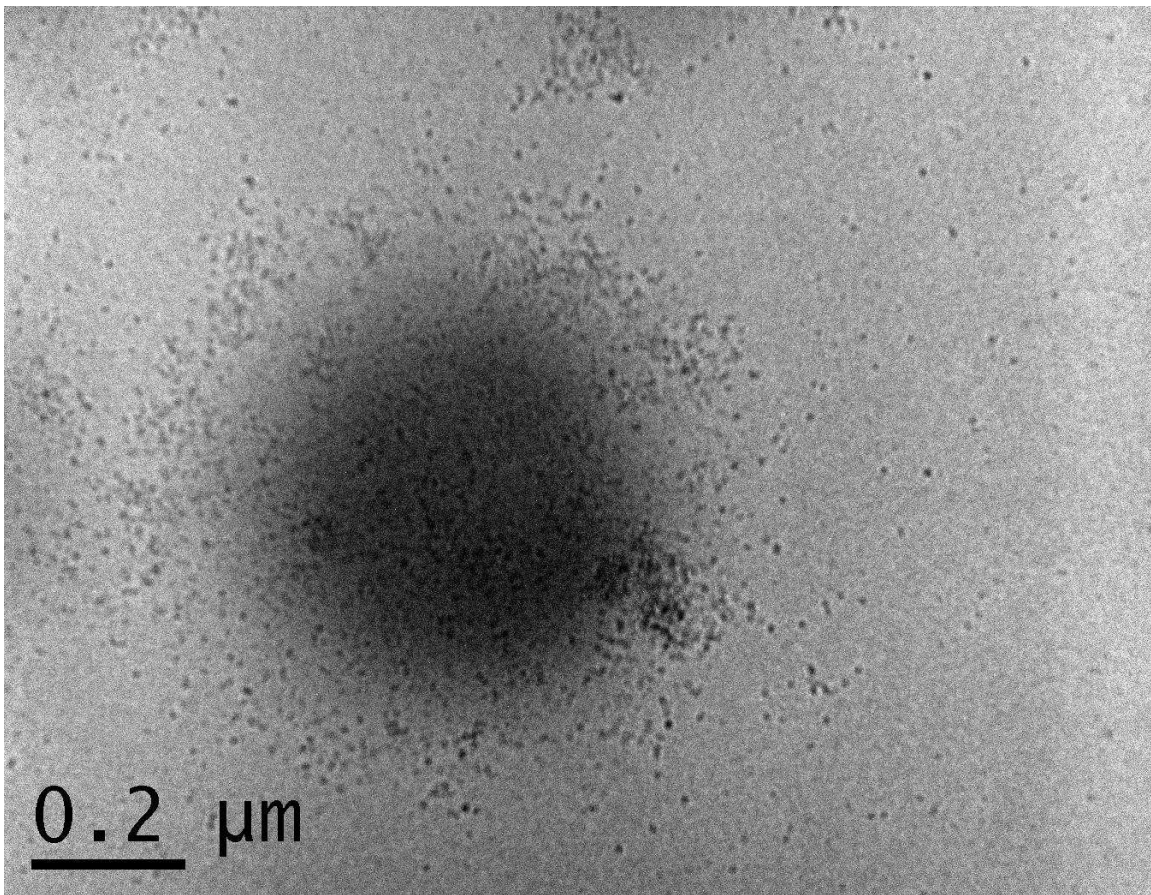
Based on the pNIPAm based microgel doped with Cd in step one, the CdS quantum dots were believed to be synthesized in situ by adding sodium sulfide in an aqueous- phase process. The synthesizer is the same as the one used for making pNIPAm based microgel. Microgel and Cd were added to a 500 mL beaker. Then, 300 mL of deionized (DI) water added. The solution was heated with hot plate to 80 °C with stirring and degassing with N<sub>2</sub> for around 1 hour. After that, we added 40mL sodium sulfide (0.5 mol/L) by injection syringe. Once the sodium sulfide solution was injected, the color of the solution suddenly changed to yellow. After 12 hours, the hot plate was turned off and cooled to room

temperature. The mixture was then filtered through cotton wool and centrifuged at 10000 RPM for 1 hour. The supernatant was removed and washed with deionized (DI) water. It was then put inside the ultrasonic instrument for 15 min. The process was repeated 6 times to purify the microgel.

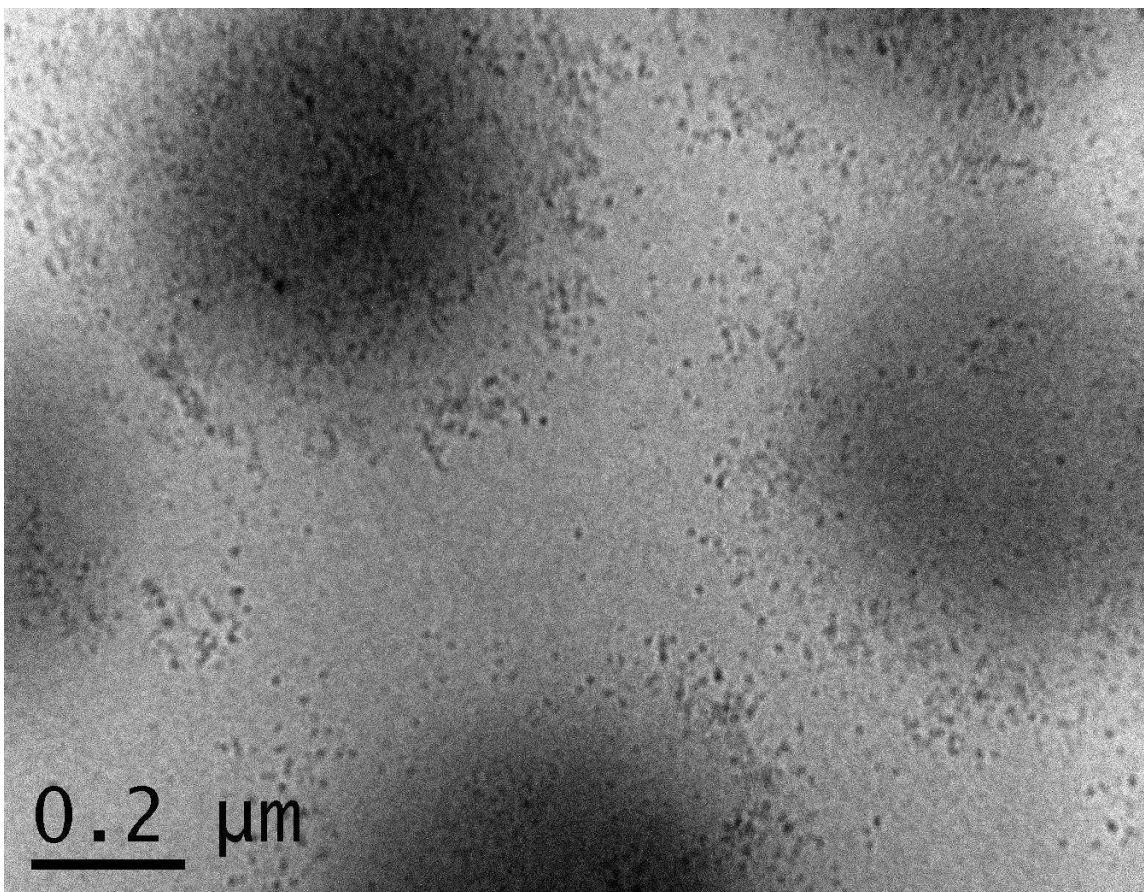
## **2.5 The Performance Detection of Nanodisperse pNIPAm Based Microgel@CdS**

### **2.5.1 Transmission Electron Microscope (TEM) Results of the Microgel@CdS**

The colour of the pNIPAm based microgel@CdS solution was yellow at the beginning. The solution was diluted with distilled water until the solution became clear and colorless. After sonication for 15 minutes, 50  $\mu$ L of the solution was dropped onto the copper grid using a 200 $\mu$ L micropipette. The morphology and microscopic structure of the composite microgel with CdS quantum dots were observed using the transmission electron microscope. The result is shown below:



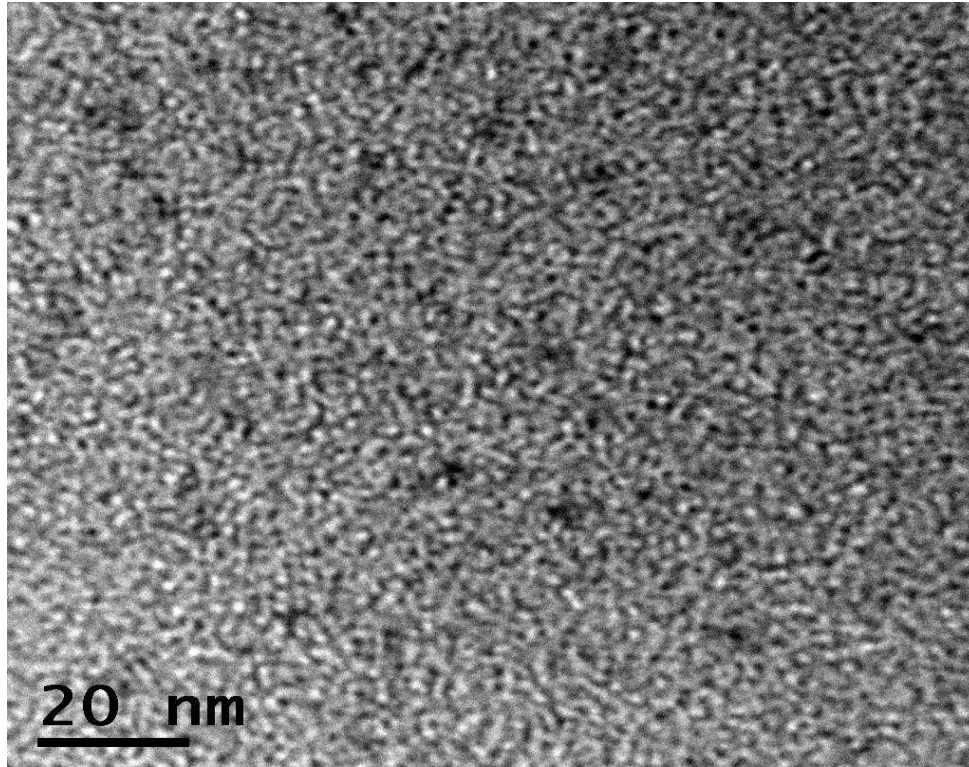
**Figure 2-4.** TEM image of one composite pNIPAm-co-20 % AAc microgel with CdS quantum dots particle



**Figure 2-5.** TEM image of several composite pNIPAm-co-20 % AAc microgel with CdS quantum dots particle

As shown before, there are several pNIPAm based microgels with different percentages of AAc and synthesized under different pH values. After analyzing each sample with TEM, the optimum conditions are determined. The percentage of AAc is 20% and the pH value of the microgel is 8.58.

From Figure 2-4 & 2-5, many black spots are homogeneously dispersed in the microgel. However, lots of small black particles aggregated in the beginning. In order to improve dispersion, the reaction was performed more slowly, especially during the injection of CdCl<sub>2</sub> and Na<sub>2</sub>S. Ultrasound treatment was also increased to 30 minutes.



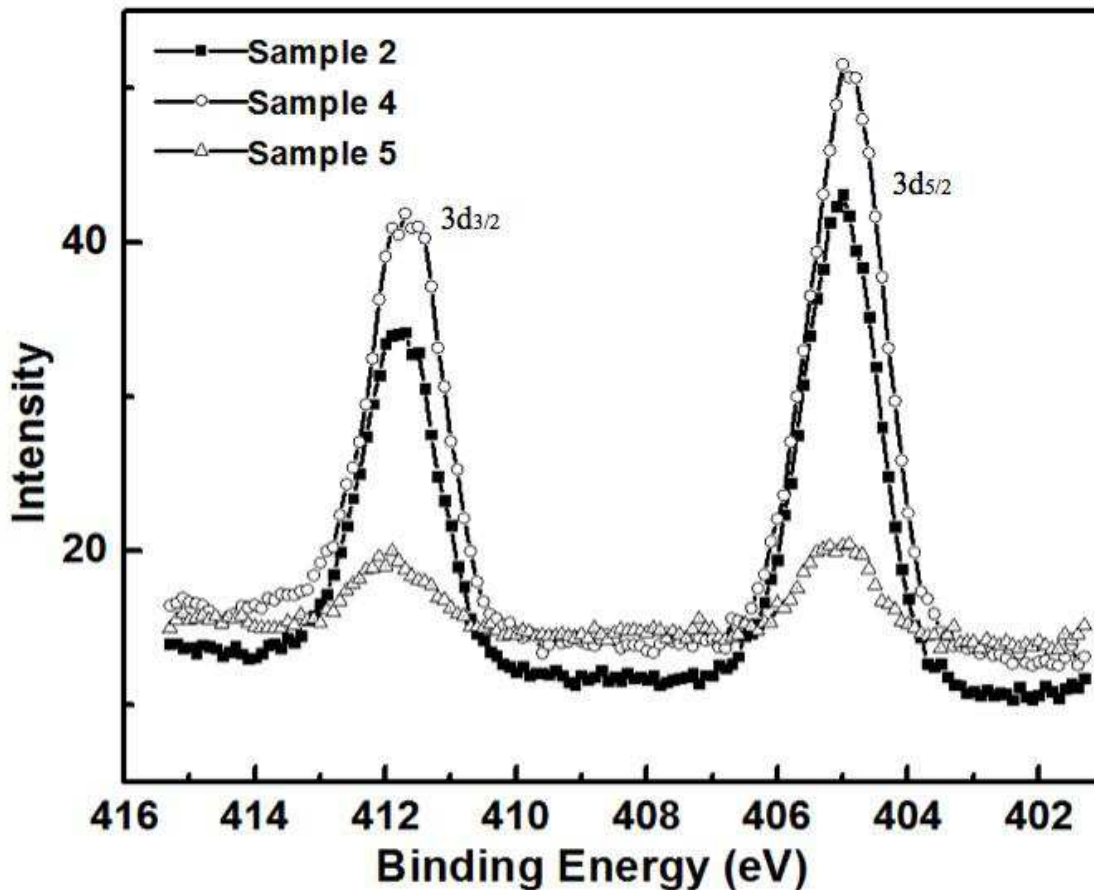
**Figure 2-6.** TEM image of the composite pNIPAm-co-20 % AAc microgel with CdS quantum dots particle

Figure 2-6 shows a part of the composite pNIPAm-co-20 % AAc microgel with CdS quantum dots particle with the scale bar at 20 nm. Most of the small black particles are spherical in shape and the average diameter of the small black particle is about 2.5 nm with uniform particle size. This illustrates monodispersity.

### **2.5.2 Elemental Analysis of Microgel with CdS by XPS (X-ray Photoelectron Spectroscopy)**

Room-temperature XPS experiments were performed at nanoFAB using Kratos Axis spectrometer with monochromatized Al  $K\alpha$  ( $h\nu = 1486.71$  eV). The spectrometer was calibrated by the binding energy (84.0 eV) of Au 4f<sub>7/2</sub> with reference to Fermi level. The pressure of analysis chamber during experiments is better than  $5 \times 10^{-10}$  Torr. A hemispherical electron-energy analyzer working at the pass energy of 20 eV was used to collect core-level spectra while survey spectrum within a range of binding energies from 0 to 1100 eV was collected at analyzer pass energy of 160 eV.

Two comparison samples were prepared here to identify the existence of Cd and S in the composite microgel. Sample 1 is pNIPAm-based microgel while sample 2 is composite microgel with CdS. If Cd and S exist in the sample, the characteristic peaks would show in figure 7.



**Figure 2-7.** Characteristic peaks for Cd by X-ray photoelectron spectroscopy. Sample 2 is composite microgel with CdS, sample 4&5 were prepared in Chapter 3 and will be explained in Chapter 3.

Based on the results from figure 2-7, the characteristic peaks only showed in sample 2, and not in sample 1. The spin-orbit components ( $3d_{3/2}$  and  $3d_{5/2}$ ) of the Cd 3d peak were found at 411.3 and 404.6 eV. The difference between the binding energy of Cd  $3d_{3/2}$  and Cd  $3d_{5/2}$  is 6.7 eV, which corresponding to the presence of the oxidation state +2 of Cd at the surface. Other samples were prepared in Chapter 3 and will be explained in below.

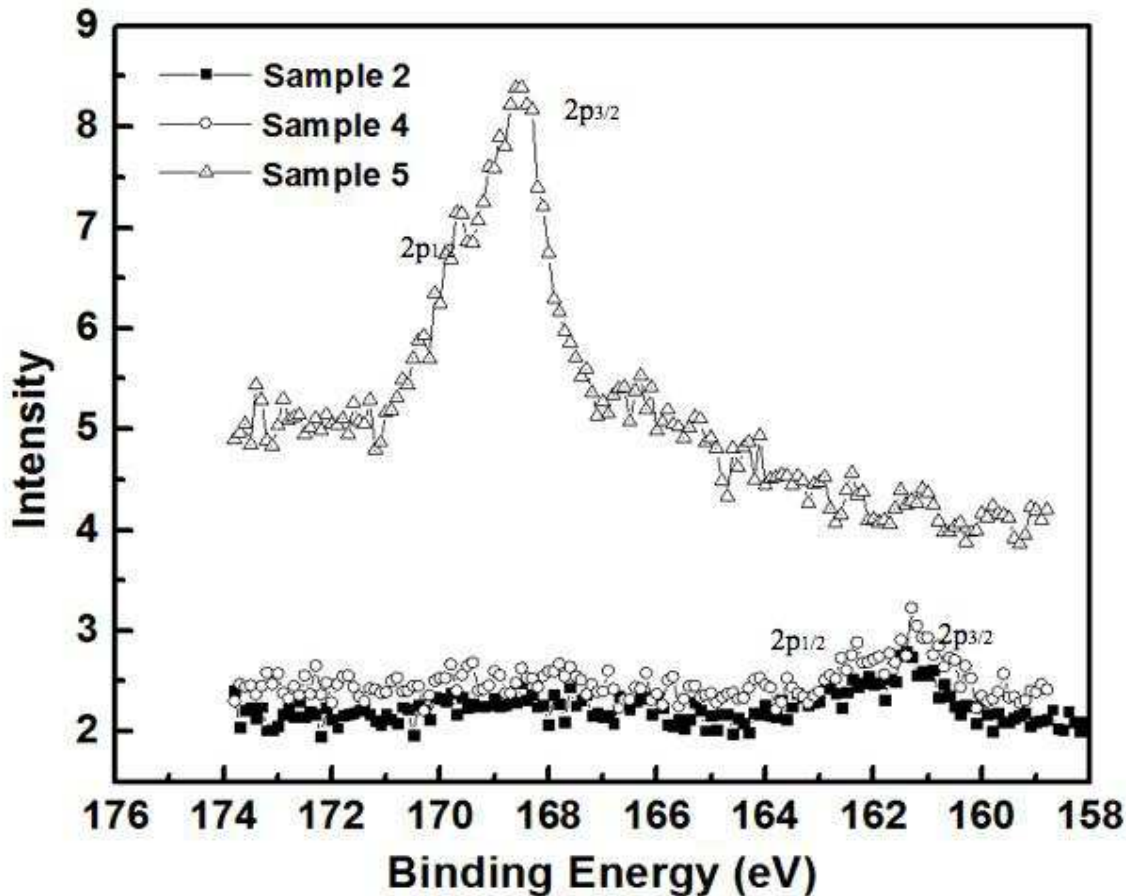


Figure 2-8. Characteristic peaks for S.

The same comparison was made for sample 1 and 2 in regards to S. In sample 2, the S  $2p_{3/2}$  peak was found at 161.8 eV and is attributable to  $S^{2-}$  in CdS. That means both of Cd and S exist in the composite microgel with reasonable valence electrons. Since sample 4 and 5 were prepared for Chapter 3, more analysis will be show in Chapter 3.

## 2.5.3 The Crystallinity of CdS Nanoparticles within pNIPAm-co-20%AAc Microgel

### 2.5.3.1 Raman Spectroscopy

To analyze the molecular structure of the composite microgel with CdS quantum dots especially for CdS quantum dots. The comparison experiments were prepared. For Test 1, the composite microgel with CdS quantum dots was detected while the pNIPAm-co-20%AAc microgel was detected in test 2 by Raman spectroscopy. Both samples were powder and should be lyophilized for 24 hours before using.

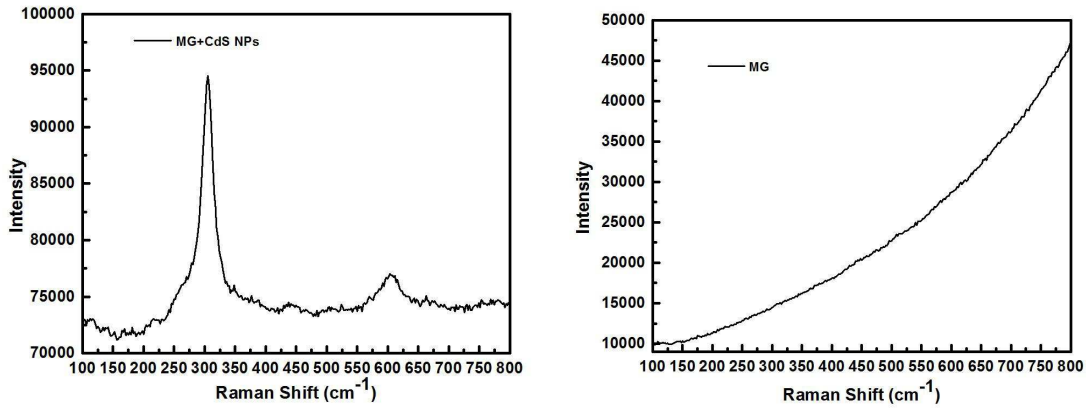


**Figure 2-9.** Raman spectrum of composite pNIPAm-co-20 % AAc microgel (left) and pNIPAm-co-20 % AAc microgel (right) with CdS quantum dots with the excitation by the 514 line of an argon laser

Raman scattering measurements were performed on nanostructured semiconductor CdS. From Figure 2-9 (left), The Raman spectrum of composite pNIPAm-co-20 % AAc microgel with CdS quantum dots clearly exhibit the characteristic first- and second-order longitudinal optical (LO) Raman peaks at 305 cm<sup>-1</sup> and 607cm<sup>-1</sup>, surface phonon peaks, and multiphonon processes when excited with an argon laser of wavelength 514.5 nm at 300K. For the pNIPAm-co-20 % AAc microgel without CdS quantum dots, a large background without any

distinguishing peaks is shown in the Figure 2-9(right). There is no signal for the characteristic peak of CdS molecules.

### 2.5.3.2 X-ray Diffraction

X-ray powder diffraction of the resultant powder sample was performed at room temperature on an Inel diffractometer equipped with a curved position-sensitive detector (CPS 120) and a Cu K $\alpha$ 1 radiation source operated at 40 kV and 20 mA. X-ray Diffraction was used to analyze the crystallinity of the composite pNIPAm-co-20 % AAc microgel with CdS quantum dots. The comparison experiments were prepared. For Test 1, the composite microgel with CdS quantum dots was detected while the pNIPAm-co-20%AAc Microgel was detected in test 2 by X-ray Diffraction. Both samples were powder and should be lyophilized for 24 hours before using.

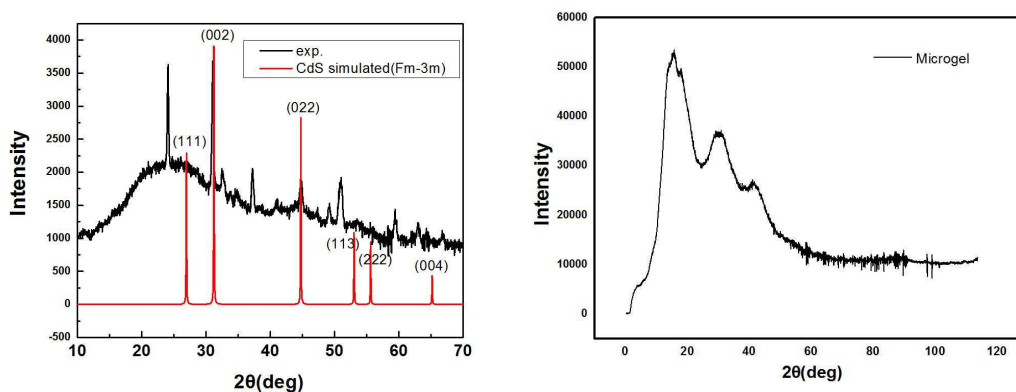


**Figure 2-10.** X-ray Diffraction of composite pNIPAm-co-20 % AAc microgel with CdS quantum dots(left) and pNIPAm-co-20 % AAc microgel(right)

Many sharp peaks are present in the XRD spectrum (Figure 2-10) of composite pNIPAm-co-20 % AAc microgel with CdS quantum dots. The right lineshape shows the one

of the characteristic peaks for CdS. There might be CdS crystalline structure existed with different phases. The XRD results indicate that there are some crystalline structures and the peaks do not fit all but several of the characteristic peaks for CdS very well. During the reaction, there are many impurities that could not be completely removed. That could be the reason of the impurity peaks. At the same time, the quantity of CdS quantum dots is too small compared to the impurities. The other reason is that CdCl<sub>2</sub> and Na<sub>2</sub>S made the composite microgel with CdS in situ. So there might be Na<sub>2</sub>S formed and shows the crystalline signal in Figure 2-10(left). For the pNIPAm-co-20 AAC% microgel without CdS quantum dots, a smooth line shows in Figure 2-10(right). No signal of the characteristic peak for CdS and other.

#### 2.5.3.4 Electron Diffraction

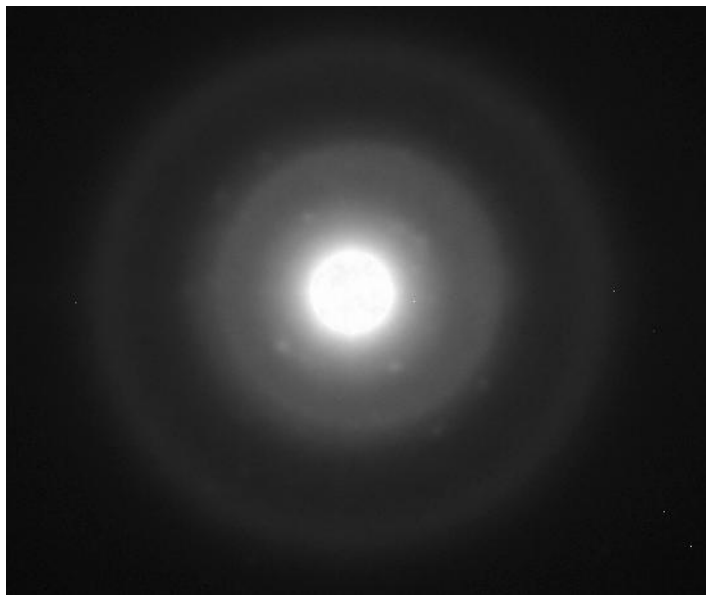


**Figure 2-11.** Electron diffraction pattern of the composite pNIPAm-co-20 % AAc microgel with CdS quantum dots particle

To further measure the crystalline structure of the composite pNIPAm-co-20 % AAc microgel with CdS quantum dots, the electron diffraction pattern was obtained using a HR-TEM. Due to the random orientation of the CdS nanoparticles, the selective area electron diffraction pattern showed a set of rings with spots in Figure 2-11 which exhibit that synthesized particles are polycrystalline in nature. However, the crystalline signal is very weak because of the small size of the CdS quantum dots as shown in Figure 2-8 earlier.

#### **2.5.4 Fluorescence Spectroscopy**

Two milliliter of transparent composite microgel with CdS quantum dots was tested by fluorescence spectroscopy. Then the fluorescent property was tested by fluorescence spectroscopy. The excitation wavelength was 500 nm and the resulting spectrum showed a peak at around 366 nm. However, when we changed the wavelength of exciting light, the peaks shifted correspondingly. That means the peak is either due to artifacts or Raman scattering, rather than fluorescence. This happens mainly due to the content of CdS quantum dots is too low and the influence of pNIPAm-co-20 % AAc microgel.

#### **2.5.5 Summary**

The pNIPAm based microgel with 20% AAc and the pH value at 8.58 are the optimum conditions for the polymerization of composite pNIPAm-co-AAc microgel with CdS quantum dots. The CdS quantum dot has good dispersity within the composite microgel and also shows identifiable peaks from XPS data and Raman spectra. However, the XRD spectrum is not useful due to the impurity and inexact synthetic steps. Also, the signal in

Electron diffraction is very weak because of the too small size there is no fluorescent signal shows.

# Chapter 3 - Remediation Performance

## 3.1 Introduction

Dyes are a class of organic compounds that are used as colorants in textile, cosmetics, food and drug industries.<sup>223</sup> These dyes are directly toxic to both aquatic animals and humans, and they are also be carcinogenic. Therefore, wastewater pollution control is very important. Until now, there are various photocatalysts that have been developed, such as TiO<sub>2</sub>, ZnO, W<sub>2</sub>O<sub>3</sub> and CdS<sup>224-226</sup>. We chose CdS to be the photocatalyst in the wastewater treatment system because CdS is one of the most important II-VI semiconductors with a direct bulk phase band gap (2.42 eV) that corresponds well with the electromagnetic spectrum of solar radiation<sup>226</sup>. Compared to the H<sup>+</sup>/H<sub>2</sub> redox potential, CdS has the advantage of a more negative conduction band edge<sup>236,237</sup>. From Canadian Water Quality Criteria (CWQC, 2014) for the protection of aquatic life, the benchmark for cadmium in freshwater is 0.09 µg/L for long-term exposure and 1.0 µg/L for short-term exposure at 50 mg CaCO<sub>3</sub>/L water hardness.<sup>252</sup> In general, the uses of photocatalysts come from two forms, which are suspensions and hybrids<sup>227</sup>. Although the photocatalytic reaction rate for suspensions is remarkable because of the large surface area and sufficient accessible sites for reaction, there are several inherent disadvantages of suspension catalysts. For example, photocatalysts with nanoparticles tend to aggregate into larger particles and some photocatalysts would be subjected to undesirable photocorrosion. Therefore, the photoreaction efficiency for suspensions will be low and the photocatalytic operation will be hard to process. That is why we used pNIPAm-co-AAc microgel to fabricate the hybrid microgel with CdS quantum dots.

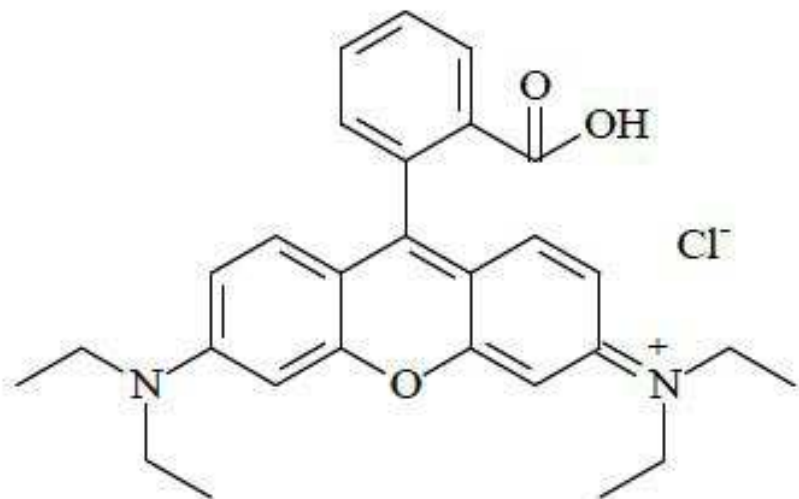
Previously, there are various support materials that are used to encapsulate the inorganic particles, including ceramic<sup>228</sup>, glass<sup>229,230</sup>, montmorillonite<sup>231</sup>, nafion membranes<sup>232</sup>, Fe<sub>3</sub>O<sub>4</sub><sup>233</sup>, active carbon<sup>234</sup>, and polypropylene granules<sup>235</sup>. There are several advantages choosing pNIPAm-co-AAc. The pNIPAm-co-AAc microgels have high specific surface areas and sufficient porous volume for entrapment of CdS particles. The cross-linked structure could help inhibit the aggregation of nanoparticles. Also, the pNIPAm-co-AAc microgels are chemically stable.

The purpose of this chapter is to discuss the performance of the composite pNIPAm-co-AAc microgel with CdS quantum dots and the treatment of wastewater with rhodamine B (RhB). RhB was chosen as the representative dye pollutant because it is usually present in industrial effluents and is resistant to biodegradability<sup>249</sup>. The performance of the composite microgel with CdS quantum dots was monitored by heterogeneous photocatalysis and the change in the overall absorption. In conjunction with heterogeneous photocatalysis, UV-Vis spectroscopy was used to monitor the absorption of dye before and after treatment with the composite microgel with CdS quantum dots.

## **3.2 Materials & Methods**

Rhodamine B (95%) and Sulphur Blue were purchased from Sigma-Aldrich (Oakville, ON). The structure of the RhB molecule is illustrated below. PC-420D hot plate was purchased from Corning. Sir-Kool SK-12 cold plate was obtained from Nano Fab (Department of Chemistry, University of Alberta). Deionized water with a resistivity of 18.2 MΩ·cm was obtained from a Milli-Q Plus system (located in the Biological Laboratory in the

Department of Chemistry, University of Alberta) purchased from Millipore (Billerica, MA), and filtered through a 0.2 m filter prior to use.



Molecular structure of the target pollutant Rhodamine B (RhB)

### 3.2.1 Ultraviolet–visible Spectroscopy (UV-Vis Spectroscopy)

Ultraviolet-visible spectroscopy refers to absorption spectroscopy or reflectance spectroscopy in the ultraviolet-visible spectral region. When a sample is exposed to photons with energies that correspond to electronic transitions within the molecule, the molecule will absorb the photon and the electrons will be excited to a higher energy state. A spectrometer records the degree of absorption by a sample at different wavelengths and the resulting plot of absorbance ( $A$ ) versus wavelength ( $\lambda$ ) is known as a spectrum. The wavelength at which the sample absorbs the maximum amount of light is known as  $\lambda_{\max}$ .<sup>238</sup>

At time intervals, 2mL aliquots were sampled and centrifuged to remove the hybrid microgel particles during the photocatalytic process. The supernatants were analyzed by

recording variations of the absorption band maximum (553nm) in the UV-vis spectra of RhB by using the UV-vis spectrometer<sup>245</sup>.

### **3.2.2 Mass Spectrometry**

In general, mass spectrometry is used to quantify known materials, to identify unknown compounds within a sample and to elucidate the structure and chemical properties of different molecules. It works by ionizing chemical compounds to generate charged molecules or molecule fragments and characterizing their mass to charge ratios (m/z). According to the different mass-to-charge ratio, the ions are separated in the mass spectrometer and are detected in proportion to their abundance. Thus, a mass spectrum of the molecule is produced. The mass spectrometry was used to analyze the production of RhB after the photodegradation test.

## **3.3 Photocatalytic Property of pNIPAm-co-20%AAc Microgel@CdS Tests**

### **3.3.1 Photocatalytic Degradation Mechanism**

For RhB photodegradation by hybrid microgel with CdS, a 350 W ultraviolet lamp was used as the light source and the initial concentration of RhB was set as 10 mg/L. A micropipette was used to transfer 15 mL RhB solution into a Petri dish and magnetically stirred. The temperatures were adjusted by PC-420D hot plate and Sir-Kool SK-12 cold plate. The distance from the Petri dish to the light source was 5 cm. To initiate the

photodegradation, 0.40 g of the hybrid microgel with CdS was introduced into the Petri dish. During the irradiation, about 1 mL of suspensions was continually taken from the reaction mixture at various time intervals (1 hour). After centrifuging, UV-vis spectrophotometer was used to analyze the RhB solutions. The degradation efficiencies of RhB were evaluated by measuring the peak value of the maximum absorption (at the wavelength of 553 nm) in the UV-vis absorption spectra of RhB solution. The photocatalytic activity of the hybrid microgel with CdS was evaluated by comparing different removal efficiency of RhB in the absence and presence of visible light irradiation. In addition, parallel experiments were also processed with other experimental conditions such as changing the temperature, using pNIPAm-co-20%AAC microgel instead of hybrid microgel and so on. The hybrid microgel with CdS was recycled and reused five times to test the recyclability and photocatalytic stability<sup>239</sup>.

Because of the unique optical and electrical properties of metal S semiconductor materials, charge separation occurs on the surface of CdS nanocrystals under visible light irradiation ( $420 < \lambda < 800$  nm). Absorption of light by CdS nanostructures is accompanied by promotion of electrons from the valence band to the conduction band, resulting in the formation of electron (conduction band) and hole (valence band) pair (Eq. (1)). In most previous reports, the separation of electrons and holes was always recognized to be the initial step in the photodegradation mechanism. During the irradiation, the electron/hole pairs and reactive oxygen species (ROS) are the main active species responsible for photocatalytic reactions<sup>240</sup>. Generally, the reactive oxygen species include  $\text{H}_2\text{O}_2$ ,  $\text{O}_2^{\cdot-}$ ,  $\cdot\text{OH}$  and generated during irradiation as shown in Eq. (2), Eq. (3), Eq. (4), Eq. (5), Eq. (6). Since the electrons and holes may recombine and yield no net photocatalysis, it is feasible to study the

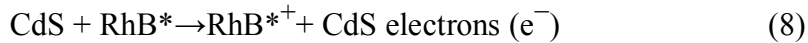
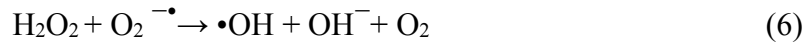
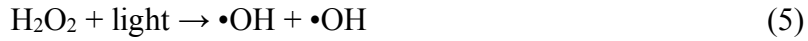
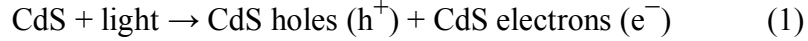
photoreduction/oxidation ability by comparing the energy levels of the standard redox potential ( $E_O$ ) of absorbed substances with valence band ( $E_{VB}$ ) and conduction band ( $E_{CB}$ ). The redox potential for the  $H_2O/\bullet OH$  couple is 2.32 eV ( $E_O(H_2O/\bullet OH)$ , vs NHE) and  $-0.16$  eV ( $E_O(O_2/O_2^{\bullet -})$ , vs NHE) for the dissolved oxygen/superoxide couple<sup>242</sup>. The  $E_{VB}$  and  $E_{CB}$  of metal sulfides are affected by pH in aqueous environment<sup>243</sup>. In our reaction system, the pH value was  $\sim 7.30$  before the photocatalytic reaction. The relevant conduction band edge ( $E_{CB}$ ) and valence band edge ( $E_{VB}$ ) position at pH  $\sim 7.30$  were calculated by<sup>243, 244</sup>:

$$E_{CB, pH7.30} = E_C^O + 0.059 (pH_{ZPC} - pH)$$

$$E_{VB, pH7.30} = E_V^O + 0.059 (pH_{ZPC} - pH)$$

The value of  $E_{CB}^O$  (vs NHE) and  $E_{VB}^O$  (vs NHE) for CdS were found to be  $-0.52$  eV and  $1.88$  eV, the band gap for CdS was found to be  $2.4$  eV when it behaves like a bulk system<sup>244</sup>. The  $pH_{ZPC}$  refers to the point of zero  $\zeta$  potential of the semiconductor. This value was found to be  $2.0$  for CdS. Therefore, the  $E_{CB, pH7.30}$  and  $E_{VB, pH7.30}$  were calculated to be  $-0.84$  eV and  $1.57$  eV (vs NHE), the photogenerated electrons in the CB were then captured by  $O_2$  to form superoxide, and therefore must have a potential less than  $-0.16$  eV. The holes in the VB must have a potential greater than  $2.32$  eV to form hydroxyl radicals. Comparing the redox potential with  $E_{CB, pH7.30}$  and  $E_{VB, pH7.30}$ , the potential in the CB was sufficiently negative to reduce oxygen and generate superoxide anions while holes in the VB was not able to oxidize water to produce hydroxyl radicals, since the potential of VB edge is less than ( $E_O(H_2O/\bullet OH)$ , vs NHE)<sup>240</sup>. Therefore, the production of  $\bullet OH$  in the present system is almost impossible and the generation of  $O_2^{\bullet -}$  plays an important role in the photocatalytic reaction. RhB molecules are then decomposed by superoxide through an oxidation process (Eq. (9)).

It has been reported that the photosensitized process would also work concurrently with the photocatalytic process while the photocatalytic process is the predominant one. Namely, the RhB would first absorb the incident photon flux with the irradiation of UV lamp ( $190 \text{ nm} < \lambda < 400 \text{ nm}$ ) and then transfer the photogenerated electrons to the excited state of the dye owing to the intramolecular  $\pi$ - $\pi^*$  transition. The photoelectrons of the excited state were injected into the CB of CdS immediately. Then, the process was similar as before that the photoelectrons in the CB were captured by  $\text{O}_2$ . In this way, the dyes were also oxidized as shown in Eq. (7), Eq. (8), Eq. (9) <sup>249</sup>.



### 3.3.2 Temperature Influence for the Photocatalytic Efficiency of Rhodamine B

Since the pNIPAm based microgel is temperature responsive and CdS particles were doped in the crosslinked structure, pNIPAm based microgels show the volume phase

transition in the Lower Critical Solution Temperature (LCST) and it might affect the photocatalytic efficiency of RhB. To study the function of temperature, the RhB/hybrid microgel system was observed in different temperatures. For comparison, others conditions were keep constant. The results are summarized as follows:

### **3.3.2.1 Kinetics at Low Temperature**

10 °C was set in the case of low temperature by Sir-Kool SK-12 cold plate. There were four samples made for comparison:

Samples:

a: 0.4g MG@CdS+15mL 10mg/L RhB+UV

b: 0.4g MG@CdS+15mL 10mg/L RhB+Dark

c: no Gel+15mL 10mg/L RhB+UV

d: 0.4g MG no CdS+15mL 10mg/L RhB+UV

For sample a: Firstly, a micropipette was used to transfer 15 mL 10mg/L RhB solution into a petridish reactor (reaction cell). Then, 0.4 g hybrid microgel with CdS was added into the RhB solution. The mixed solution was stirred on the Sir-Kool SK-12 cold plate and the temperature was set at 10 °C. The UV lamp was turned on to irradiate the solution with the distance at 5 cm. During the irradiation, about 5 mL of suspensions were continually taken from the reaction cell at the following time intervals: 0.5h, 1h, 2h, 3h, 4h, 5h for subsequent target dye concentration analysis by UV-vis after centrifuging.

For sample b: Firstly, a micropipette was used to transfer 15 mL 10mg/L RhB solution into a petridish reactor (reaction cell). Then, 0.4 g hybrid microgel with CdS was added into the RhB solution. The mixed solution was stirred on the Sir-Kool SK-12 cold plate and the

temperature was set at 10 °C. The photocatalytic system was wrapped up into a large piece of tin foil to ensure the reaction would proceed in a dark condition without visible light. During the reaction, about 5 mL of suspensions were continually taken from the reaction cell at the following time intervals: 0.5h, 1h, 2h, 3h, 4h, 5h for subsequent target dye concentration analysis by UV-vis after centrifuging.

For sample c: Firstly, a micropipette was used to transfer 15 mL 10mg/L RhB solution into a petridish reactor (reaction cell). Then, the RhB solution was stirred on the Sir-Kool SK-12 cold plate and the temperature was set at 10 °C. The UV lamp was turned on to irradiate the solution with the distance at 5 cm. During the irradiation, about 5 mL of suspensions were continually taken from the reaction cell at the following time intervals: 0.5h, 1h, 2h, 3h, 4h, 5h for subsequent target dye concentration analysis by UV-vis after centrifuging.

For sample d: Firstly, a micropipette was used to transfer 15 mL 10mg/L RhB solution into a petridish reactor (reaction cell). Then, 0.4 g pNIPAm based microgel (without CdS) was added into the RhB solution. The mixed solution was stirred on the Sir-Kool SK-12 cold plate and the temperature was set at 10 °C. The UV lamp was turned on to irradiate the solution with the distance at 5 cm. During the irradiation, about 5 mL of suspensions were continually taken from the reaction cell at the following time intervals: 0.5h, 1h, 2h, 3h, 4h, 5h for subsequent target dye concentration analysis by UV-vis after centrifuging.

The degradation efficiency of RhB by hybrid microgel with CdS was determined in sample a, the three other trials were all comparative. The degradation kinetics of RhB in terms of removal efficiency (percent) at various time intervals (hour) in 10 °C of the four samples was showed in Figure 3-1.

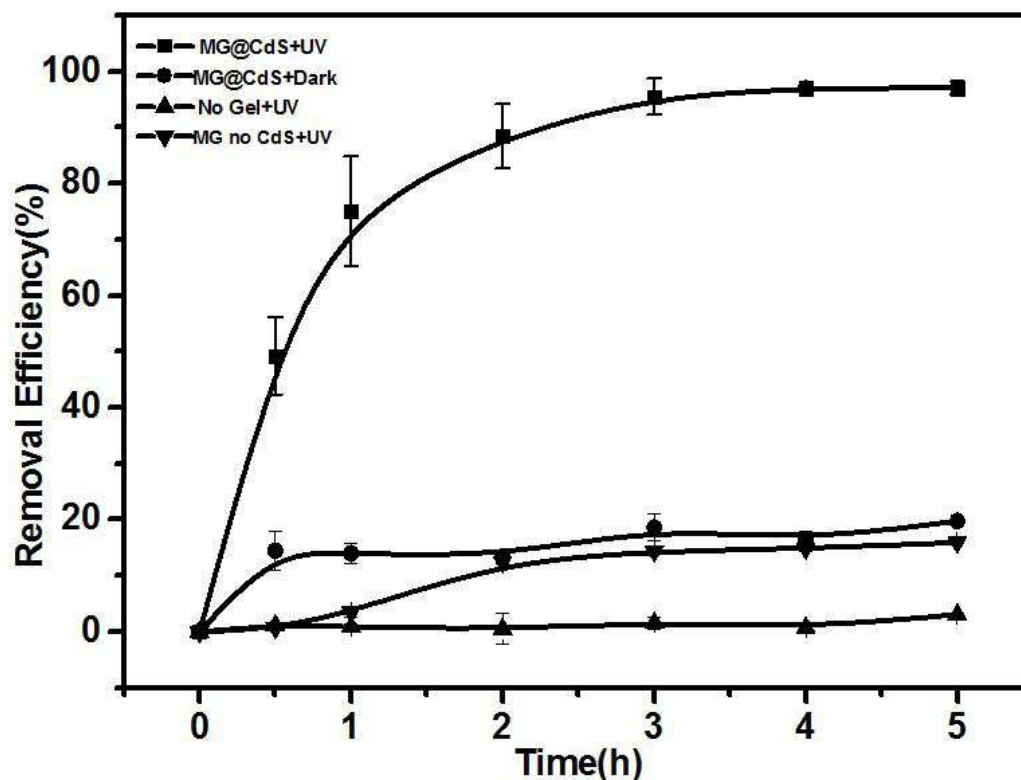


**Figure 3-1.** The degradation kinetics of RhB in terms of removal efficiency (percent) at various time intervals (hour) in 10 °C. MG@CdS+UV: 0.4g MG@CdS+15mL 10mg/L RhB+UV; MG@CdS+Dark : 0.4g MG@CdS+15mL 10mg/L RhB+Dark; No Gel+UV: no Gel+15mL 10mg/L RhB+UV; MG no CdS+UV: 0.4g MG no CdS+15mL 10mg/L RhB+UV

As seen in Figure 3-1, the RhB removal efficiency of hybrid microgels with the irradiation of UV light in equilibrium is much higher than the RhB removal efficiency in b, c and d conditions. From the comparison of sample a and b, UV light irradiation could significantly enhance RhB removal by the existence of hybrid microgel with RhB. However, the removal efficiency of RhB by pNIPAm-based microgel without CdS was lower than 20%

even with the irradiation of UV light. Thus, either hybrid microgel with CdS or UV light was essential for photodegradation.

### 3.3.2.2 Kinetics at High Temperature

45 °C was set in the case of low temperature by PC-420D hot plate. There were four samples made for comparison:

Samples:

a: 0.4g MG@CdS+15mL 10mg/L RhB+UV

b: 0.4g MG@CdS+15mL 10mg/L RhB+Dark

c: no Gel+15mL 10mg/L RhB+UV

d: 0.4g MG no CdS+15mL 10mg/L RhB+UV

For sample a: Firstly, a micropipette was used to transfer 15 mL 10mg/L RhB solution into a Petri dish reactor (reaction cell). Then, 0.4 g hybrid microgel with CdS was added into the RhB solution. The mixed solution was stirred on the PC-420D hot plate and the temperature was set at 45 °C. The UV lamp was turned on to irradiate the solution with the distance at 5 cm. During the irradiation, about 5 mL of suspensions were continually taken from the reaction cell at the following time intervals: 0.5h, 1h, 2h, 3h, 4h, and 5h for subsequent target dye concentration analysis by UV-vis after centrifuging.

For sample b: Firstly, a micropipette was used to transfer 15 mL 10mg/L RhB solution into a Petri dish reactor (reaction cell). Then, 0.4 g hybrid microgel with CdS was added into the RhB solution. The mixed solution was stirred on the PC-420D hot plate and the temperature was set at 45 °C. The photocatalytic system was wrapped up into a large piece of tin foil to ensure the reaction would proceed in a dark condition without visible light. During

the reaction, about 5 mL of suspensions were continually taken from the reaction cell at the following time intervals: 0.5h, 1h, 2h, 3h, 4h, and 5h for subsequent target dye concentration analysis by UV-vis after centrifuging.

For sample c: Firstly, a micropipette was used to transfer 15 mL 10mg/L RhB solution into a Petri dish reactor (reaction cell). Then, the RhB solution was stirred on the PC-420D hot plate and the temperature was set at 45 °C. The UV lamp was turned on to irradiate the solution with the distance at 5 cm. During the irradiation, about 5 mL of suspensions were continually taken from the reaction cell at the following time intervals: 0.5h, 1h, 2h, 3h, 4h, and 5h for subsequent target dye concentration analysis by UV-vis after centrifuging.

For sample d: Firstly, a micropipette was used to transfer 15 mL 10mg/L RhB solution into a Petri dish reactor (reaction cell). Then, 0.4 g pNIPAm based microgel (without CdS) was added into the RhB solution. The mixed solution was stirred on the PC-420D hot plate and the temperature was set at 45 °C. The UV lamp was turned on to irradiate the solution with the distance at 5 cm. During the irradiation, about 5 mL of suspensions were continually taken from the reaction cell at the following time intervals: 0.5h, 1h, 2h, 3h, 4h, 5h for subsequent target dye concentration analysis by UV-vis after centrifuging.

The degradation efficiency of RhB by hybrid microgel with CdS was determined in sample a, and the other three trials are all for comparison. The degradation kinetics of RhB in terms of removal efficiency (percent) at various time intervals (hour) in 45 °C of the four samples was showed in Figure 3-2.

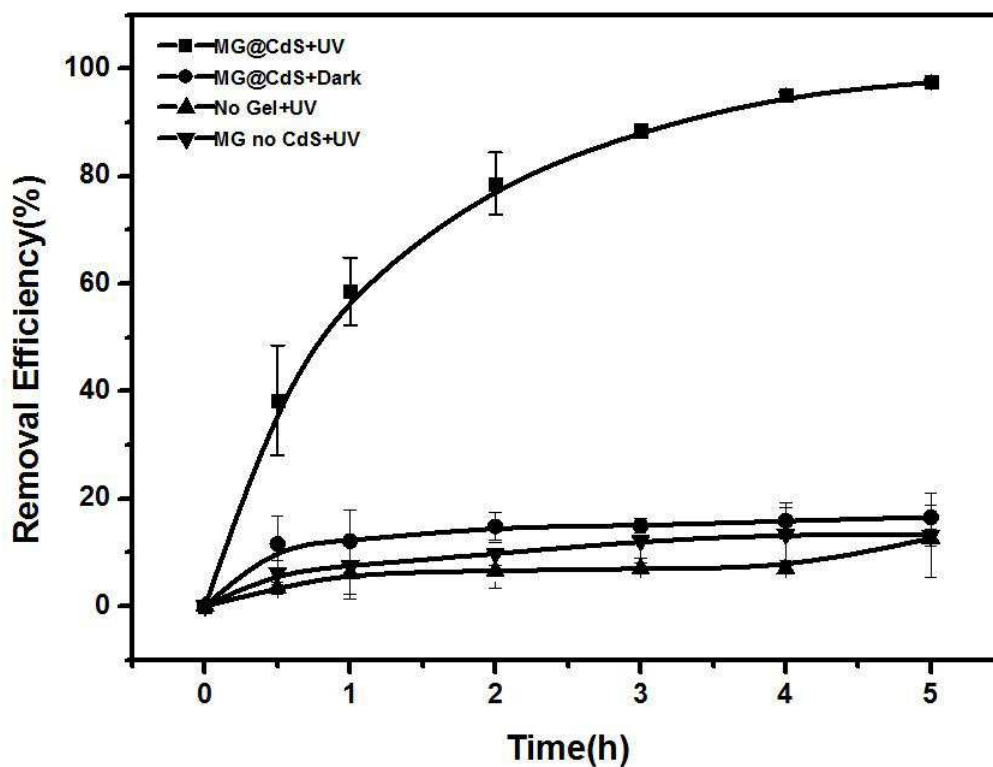


**Figure 3-2.** The degradation kinetics of RhB in terms of removal efficiency (percent) at various time intervals (hour) in 45 °C. MG@CdS+UV: 0.4g MG@CdS+15mL 10mg/L RhB+UV; MG@CdS+Dark : 0.4g MG@CdS+15mL 10mg/L RhB+Dark; No Gel+UV: no Gel+15mL 10mg/L RhB+UV; MG no CdS+UV: 0.4g MG no CdS+15mL 10mg/L RhB+UV

As seen in Figure 3-2, the RhB removal efficiency of hybrid microgel with the irradiation of UV light in equilibrium is much higher than the RhB removal efficiency in b, c and d conditions.

### 3.3.2.3 The Comparison of Photocatalytic Efficiency of Hybrid Microgel at Different Temperatures

The comparison of the photocatalytic efficiency of hybrid microgel at different temperatures was shown as Figure 3-3.

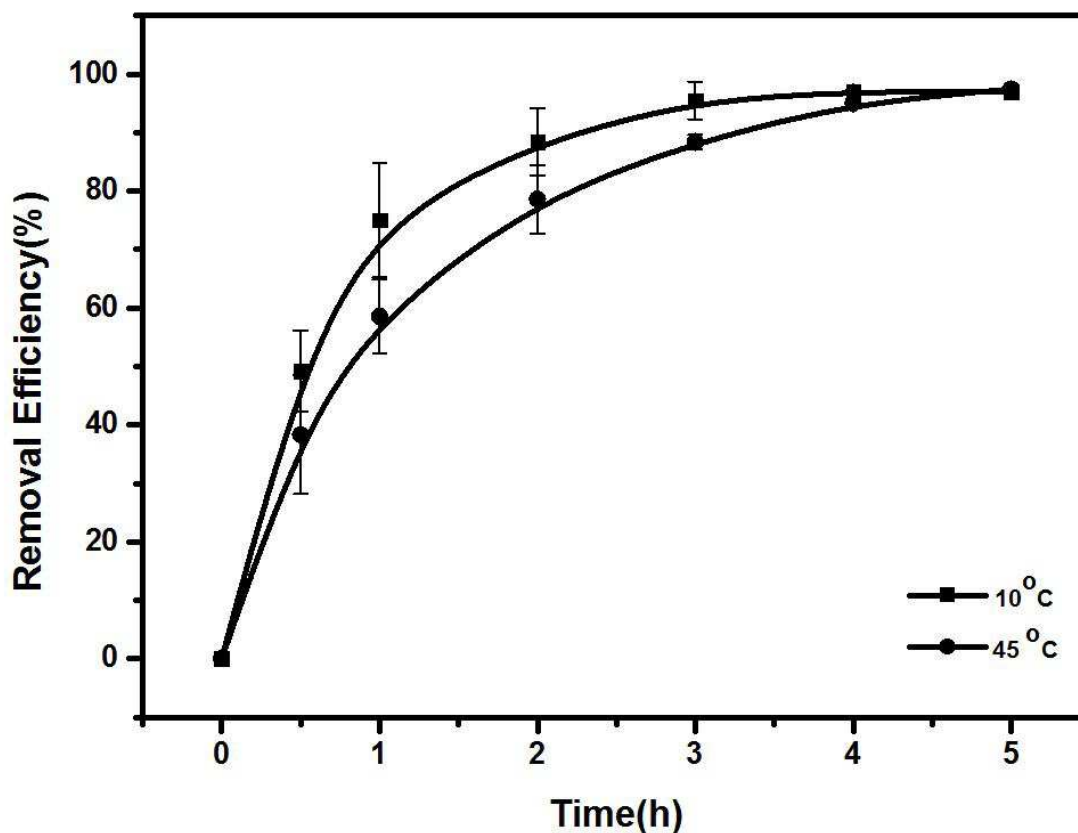


**Figure 3-3.** The comparison of degradation kinetics of RhB at different temperatures at: 0.4g MG@CdS+15mL 10mg/L RhB+UV

Theoretically, the volume and size of pNIPAm-based microgels can be adjusted by changing the temperature which could alter the photocatalytic effect. When the volume and size of pNIPAm-based microgel is larger, the specific area for CdS increases, which increases the efficiency of the photocatalytic reaction. The comparison of the degradation

kinetics of RhB in both 10 °C and 45 °C for sample a shows in Figure 3-3. After 0.5 hour, the removal efficiency in 10 °C was 49.5% and 11% faster than the removal efficiency in 45 °C, which was 38.5%. Thus, over 95% RhB were removed from the mixed solution within 5 hours in both temperatures. The photocatalytic efficiency is higher at temperature lower than LCST of pNIPAm based microgel.

### **3.3.3 Photocatalytic Data for Various Amount of pNIPAm-co-20%AAc Microgel@CdS**

Based on the removal efficiency in 10 °C was higher than the removal efficiency in 45 °C, 10 °C was set to measure the degradation kinetics of RhB in terms of removal efficiency (percent) at various time intervals (hour) with adding different amount of hybrid microgel.

Three samples were made a, b, c:

a: 0.2g MG@CdS+15mL 10mg/L RhB+UV

b: 0.4g MG@CdS+15mL 10mg/L RhB+UV

c: 0.6g MG@CdS+15mL 10mg/L RhB+UV

The photocatalytic system was also observed under the same conditions except for the amount of hybrid microgel with CdS added.

For sample a: Firstly, a micropipette was used to transfer 15 mL 10mg/L RhB solution into a petridish reactor (reaction cell). Then, 0.2 g hybrid microgel with CdS was added into the RhB solution. The mixed solution was stirred on the Sir-Kool SK-12 cold plate and the temperature was set at 10 °C. The UV lamp was turned on to irradiate the solution with the distance at 5 cm. During the irradiation, about 5 mL of suspensions were continually taken from the reaction cell at the following time intervals: 0.5h, 1h, 2h, 3h, 4h, 5h for subsequent target dye concentration analysis by UV-vis after centrifuging.

For sample b: The conditions and processes were the same as in sample a except for adding 0.4 g hybrid microgel with CdS into the RhB solution.

For sample c: The conditions and processes were the same as in sample a except for adding 0.6 g hybrid microgel with CdS into the RhB solution.

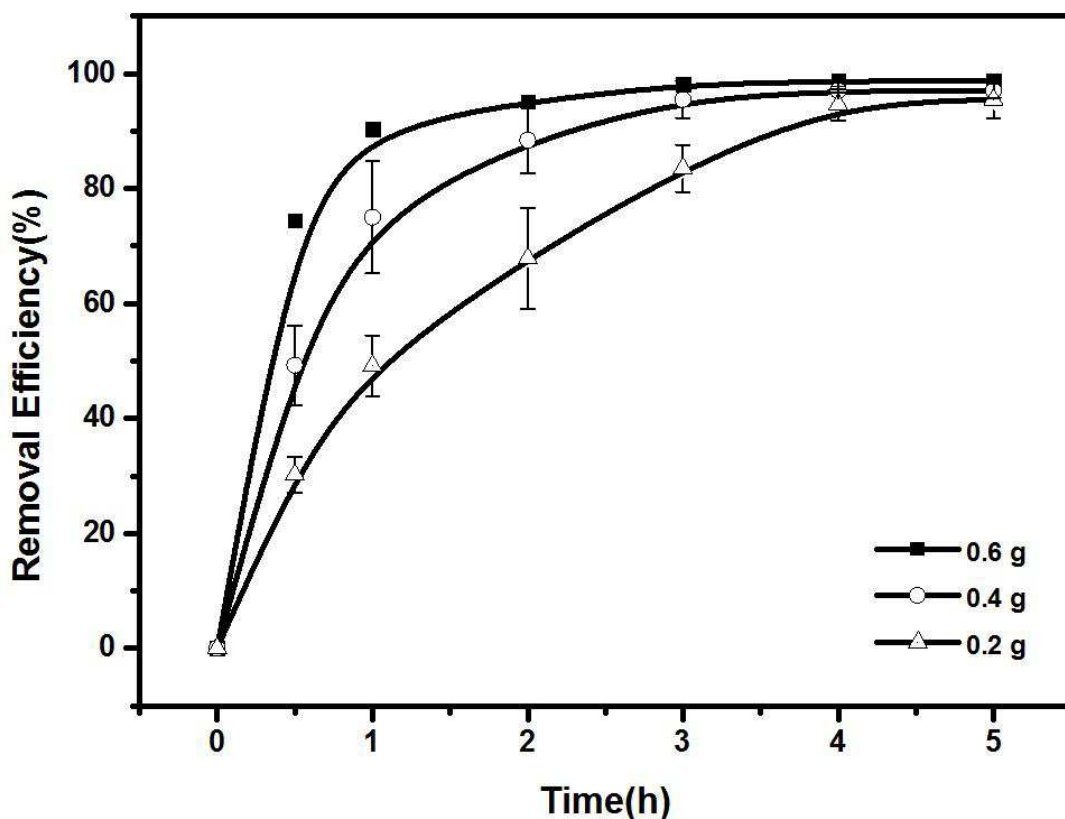


**Figure 3-4.** The comparison of degradation kinetics of RhB at different amount (0.6g, 0.4g, 0.2g) of hybrid microgel with CdS.

On the basis of the above results (Figure 3-4), the removal efficiency of RhB in sample c was observed higher than in sample b and higher than in sample a. Thus, as we increase the amount of microgel with CdS, we increase the removal efficiency of RhB. Regardless of how much (0.2, 0.4, 0.6) hybrid microgel with CdS was added, over 95% RhB

was removed after 5 hours. Note that even 0.2 g hybrid microgel can remove the vast majority of RhB. The recyclability of hybrid microgel with CdS was examined under UV light irradiation as in 3.3.3.

### **3.3.4 Photocatalytic Data For Using pNIPAm-co-20%AAc Microgel@CdS Recyclable**

10 °C was also set to study the recyclability of hybrid microgel with CdS. Firstly, a micropipette was used to transfer 15 mL 10mg/L RhB solution into a petridish reactor (reaction cell). Then, 0.6 g hybrid microgel with CdS was added into the RhB solution. The mixed solution was stirred on the Sir-Kool SK-12 cold plate and the temperature was set at 10 °C. The UV lamp was turned on to irradiate the solution with the distance at 5 cm. During the irradiation, about 5 mL of suspensions were continually taken from the reaction cell at the following time intervals: 0.5h, 1h, 2h, 3h, 4h, and 5h for subsequent target dye concentration analysis by UV-vis after centrifuging.

For the cyclic operation, 0.6 g hybrid microgel with CdS was used in the photocatalytic reaction for 4 more times. Namely, after the first photocatalytic reaction and UV-vis testing, the mixed solution was collected to get the recyclable hybrid microgel by centrifuging. Next, 15 mL of new 10mg/L RhB solution was transferred into the petridish reactor (reaction cell), and then the recyclable hybrid microgel was added into the RhB solution. The same process was repeated for 5 times.

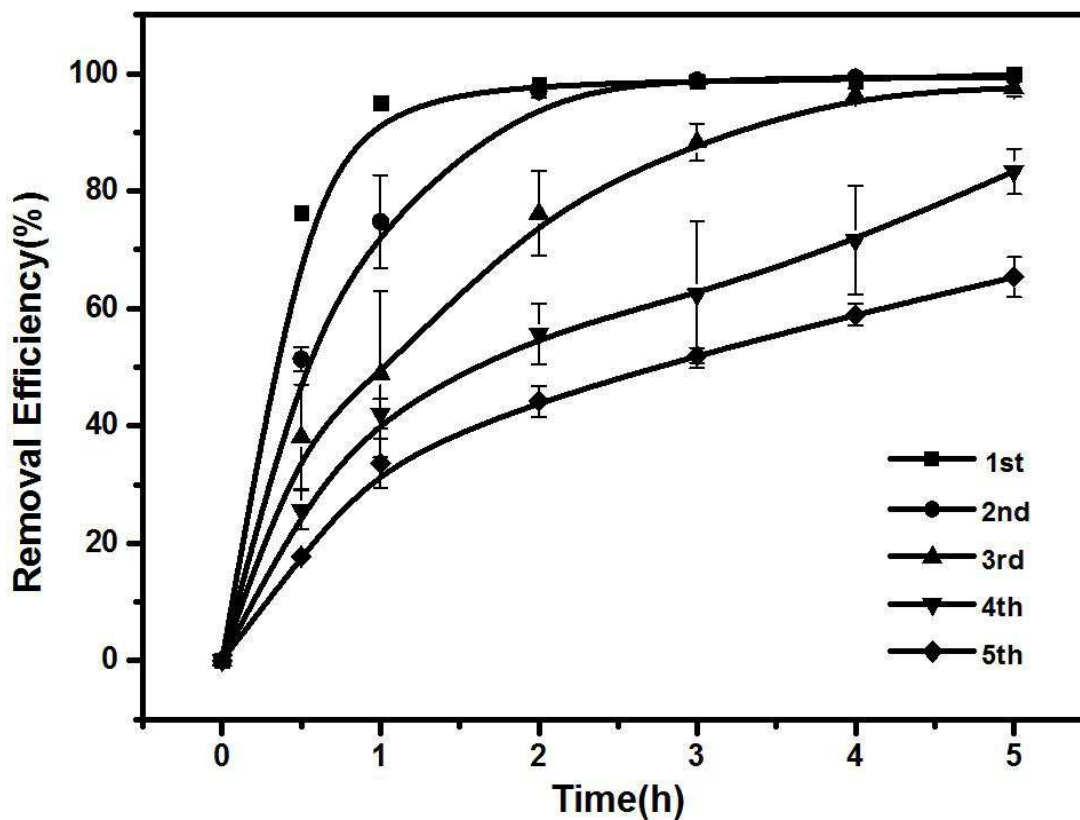


**Figure 3-5.** The degradation kinetics of RhB in terms of removal efficiency (percent) at various time intervals (hour) in 45 °C

Although the rate of photocatalytic degradation decreased as the number of the cycles was increased, the removal efficiency was 63.5% after 5 hours of irradiation. If the photocatalytic reaction was allowed to continue under the irradiation of UV light for a longer time, over 95% RhB was removed even in the fifth cyclic operation.

### 3.3.5 The XPS Data of Atomic Concentration for Cd and S Before and After Photocatalytic Operation

During the photocatalytic reaction, there is leaking of Cd and S, which increases the toxicity of the wastewater with RhB. Also, the leaking of Cd and S indicates that some part of the hybrid microgel structure was destroyed with the irradiation of UV light. To investigate the effect of the irradiation process on the stability of CdS immobilized on the pNIPAm based microgel, five samples were made by adding a drop of liquid sample on a silicon substrate and dried on the PC-420D hot plate:

Sample 1. pNIPAm based microgel

Sample 2. Hybrid microgel with CdS

Sample 3. RhB solution

Sample 4. Mixed solution of hybrid microgel with RhB before photocatalytic operation

Sample 5. Supernatant of sample 4 after photocatalytic operation

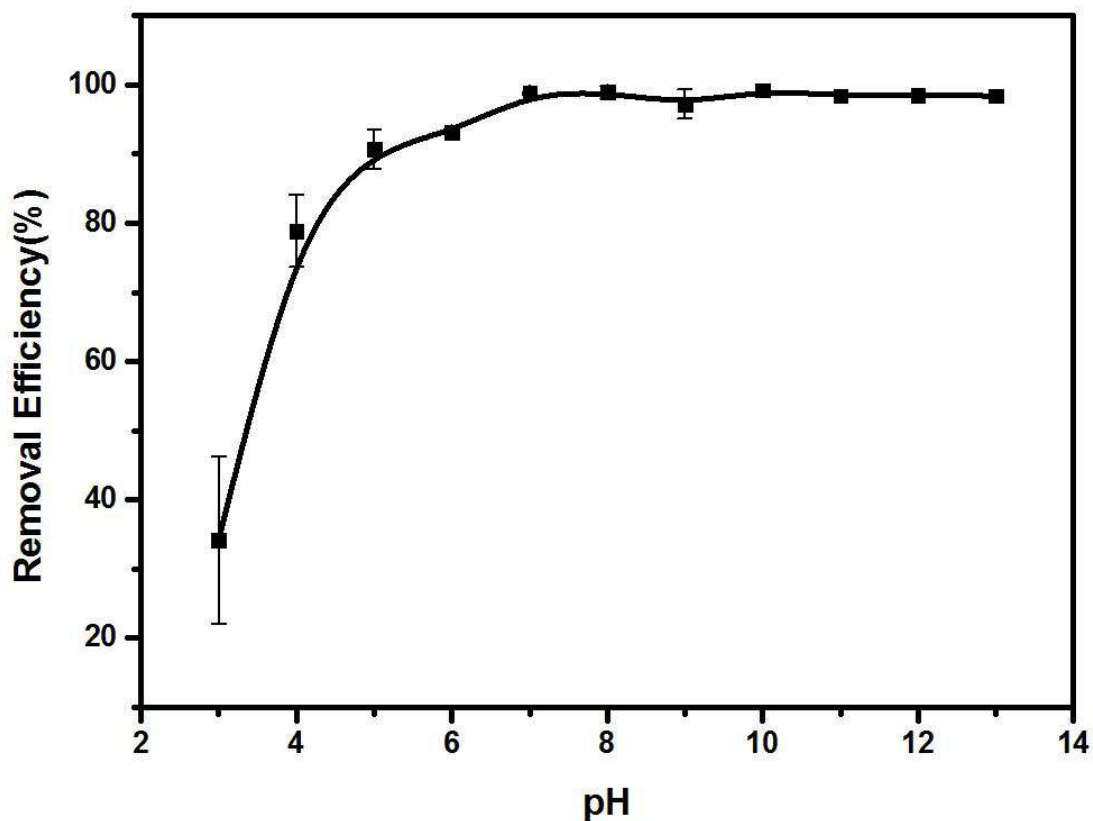
<b>SAMPLE</b>	<b>Atomic Conc% of Cd</b>	<b>Atomic Conc% of S</b>
<b>1 microgel</b>	<b>0</b>	<b>0</b>
<b>2 microgel@CdS</b>	<b>1.09(+2)</b>	<b>0.14(-2)</b>
<b>3 RhB</b>	<b>0</b>	<b>0</b>
<b>4 Rhb+Microgel@CdS before photocatalytic</b>	<b>1.01(+2)</b>	<b>0.13(-2)</b>
<b>5 supernatant after photocatalytic</b>	<b>0.10(+2)</b>	<b>1.16(+6)</b>

**Figure 3-6.** The XPS data of atomic concentration for Cd and S (red marks are the valence states detailed before in chapter 2)

On the basis of the above results (Figure 3-6), the ratio of Cd to S was 1.09: 0.14 in the hybrid microgel with CdS. After photocatalytic operation, the ratio of Cd to S in sample 5 (the supernatant of sample 4 after centrifuging) was 0.10: 1.16. As the data showed in Chapter 2 (Figure 2-8 & Figure 2-9) by XPS, the characteristic peaks for Cd were unchanged at +2 but the characteristic peaks for S shifted in sample 5. The peak observed at 167.5 eV is due to the presence of sulphate. It shows the presence of other oxidation states. This means S was oxidized during the irradiation and the valence state for S changed from -2 to +6. Since the valence state was changed, the chemical bond between Cd and S was broken, resulting in the leaking of S into the mixed solution during irradiation. Thus, the atomic concentration for S is a lot higher than Cd. It can be assumed that all S from sample 2 was oxidized and leaked into the mixed solution during the irradiation. Namely, the proportion of S from sample 2 (0.14%) occupied 1.16% in the supernatant after photocatalytic operation. The proportion increased for S because most other elements were centrifuged after irradiation. Since the valence state for Cd was still +2, the bond between carboxylic group and Cd were not broken, resulting in less leaking of Cd compared with S. On the basis of the ratio from sample 5, 0.10% Cd in the supernatant implies occupied 0.012% would leak into the solution for sample 2. Namely, if the initial atomic concentration of Cd to total elements is 1.09%, then 0.012% would leak into the mixed solutions. So the leaking percentage was:  $0.012\%/1.09\%=0.011\%$ . In summary, 0.011% of Cd was leaked into mixed solution during the photocatalytic operation.

### **3.3.6 Data of Working pH Range for pNIPAm-co-20%AAc Microgel@CdS**

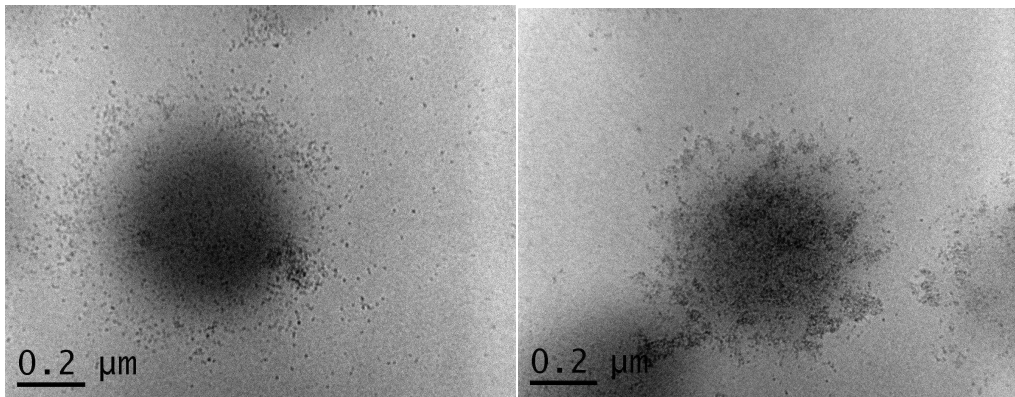
The effect of solution pH on the stability of CdS that were immobilized on the pNIPAm based microgel is investigated. 10 °C was also set to study the working pH range of hybrid microgel with CdS. Eleven photocatalytic systems were made with the only difference being the pH. Firstly, a micropipette was used to transfer 15 mL 10mg/L RhB solutions into each petridish reactors (reaction cells). Then, 0.4 g hybrid microgels with CdS were added into the RhB solutions. The pH values were adjusted of the mixed solutions from ~3 to ~13. After that, the mixed solutions were stirred on the Sir-Kool SK-12 cold plates and the temperatures were set at 10 °C. The UV lamp was turned on to irradiate the solution with the distance at 5 cm. About 5 mL of suspensions were taken from the reaction cells in 5 hours for subsequent target dye concentrations analysis by UV-vis after centrifugation.



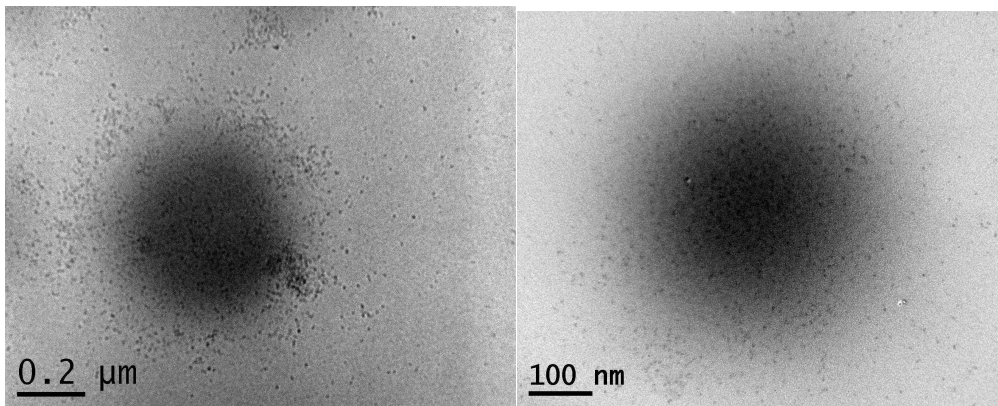
**Figure 3-6.** Working pH range for the hybrid microgel with CdS

Figure 3-7 describes the removal efficiency of RhB by hybrid microgel with CdS at different pH values. It is reasonable that higher acidity corresponds to lesser removal of RhB because at high pH, there is lower CdS stability and increased dissolution. If the concentration of  $H^+$  was increased, the negatively charged carboxylic groups would bond to  $H^+$  resulting in the dissolution of CdS nanoparticles. In general, CdS nanoparticles immobilized on pNIPAm based microgel seemed stable and functional in the studied pH ranges (>4.5).

### 3.3.7 Stability of Hybrid Microgel with CdS Nanoparticles



**Figure 3-7.** TEM of hybrid microgel before (left) and after (right) photocatalytic operations



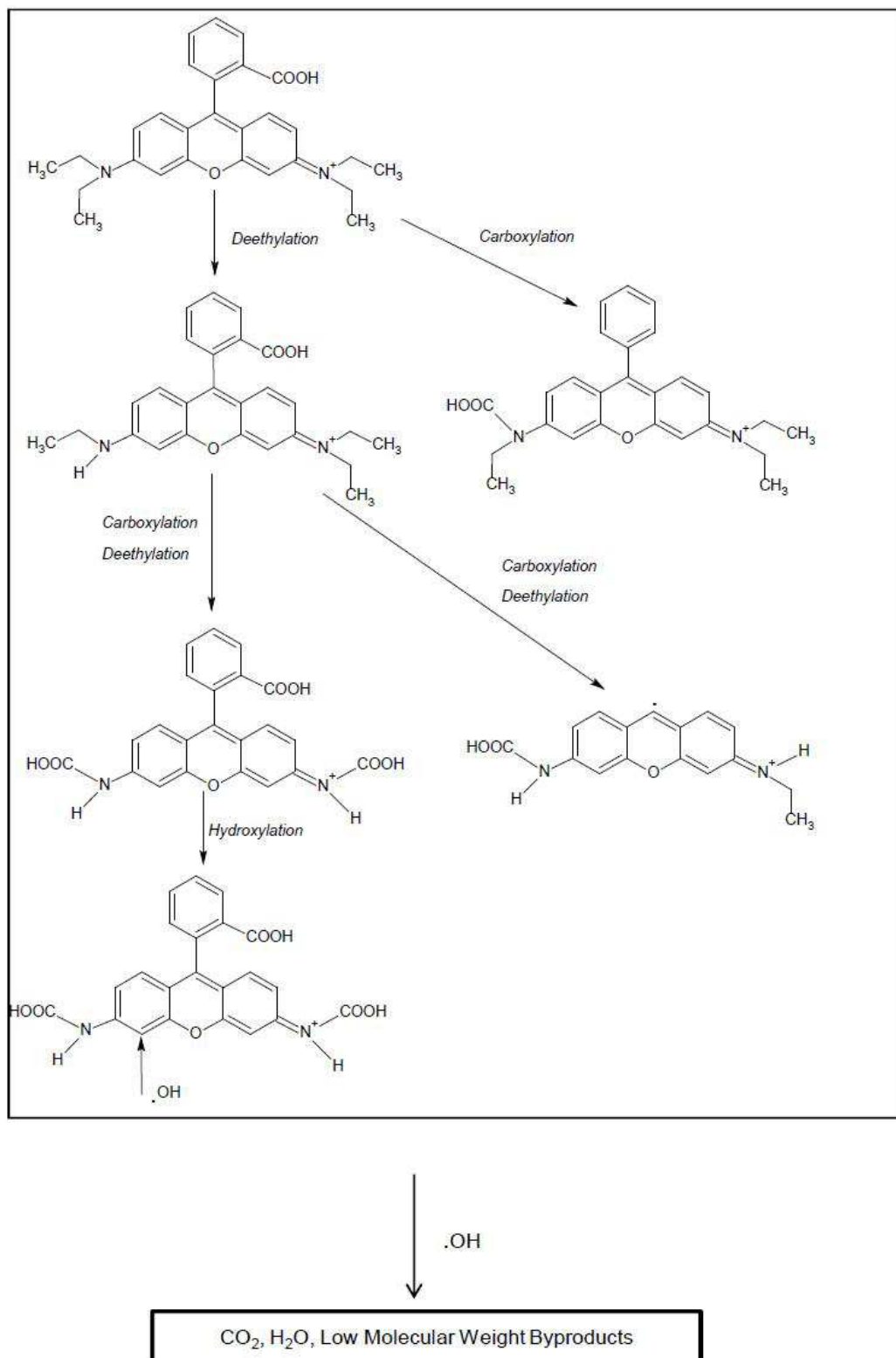
**Figure 3-8.** TEM of hybrid microgel before (left) and after (right) half a year

Figure 3-8 shows the structure of the hybrid microgel with CdS before (left) and after (right) photocatalytic operations. Figure 3-9 describes the structure of the hybrid microgel with CdS before (left) and after (right) half a year. On the basis of the results above, part of the CdS nanoparticles (black spots) were aggregated after photocatalytic operations but most the CdS nanoparticles (black spots) were still coated in the pNIPAm-based microgel. The

results also indicated that the stability of the hybrid microgel is very high due to the desired structure of CdS nanoparticles (black spots) immobilized on the polymeric host.

### **3.3.8 Analyzing the Product of RhB After Photocatalytic Operation by Mass Spectroscopy.**

According to some previous investigations, one possible explanation for the degradation of RhB is composed by many deethylations and carboxylations of the dye and the intermediates (Figure 3-10)<sup>246, 247</sup>. Finally, the compound is mineralized to CO<sub>2</sub> and H<sub>2</sub>O.



**Figure 3-9.** Possible degradation intrmediates of RhB during the photocatalytic process.

To analyze the product of RhB after photocatalytic operation, mass spectroscopy was used and the data are shown as in Figure 3-11.

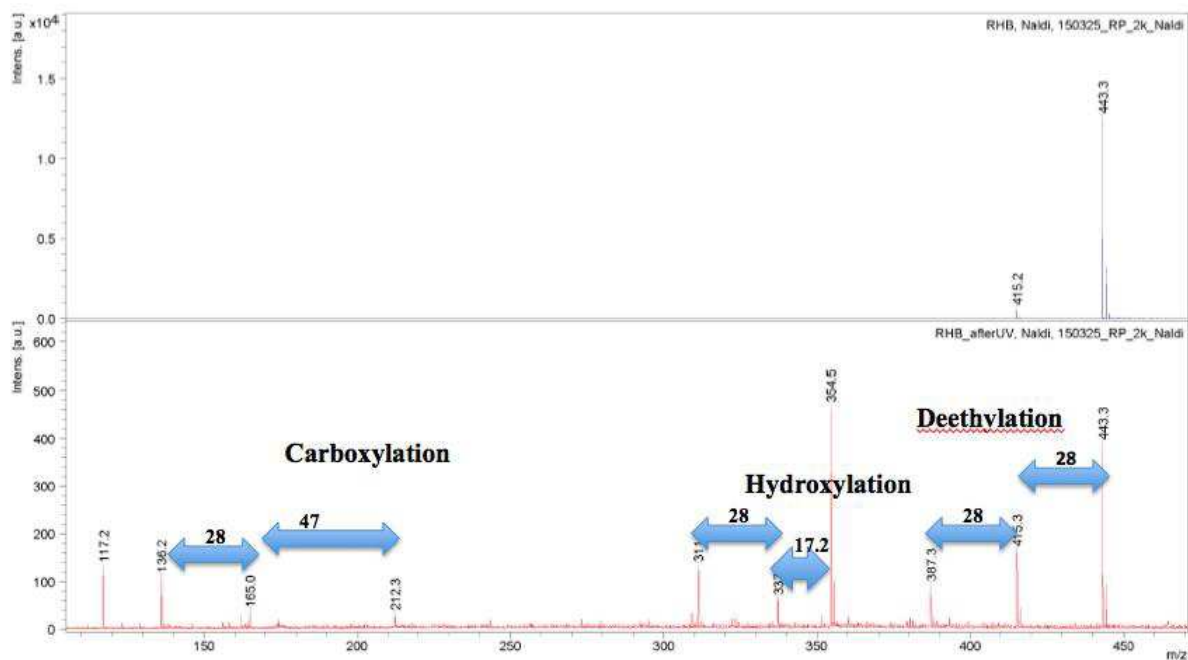


**Figure 3-10.** Mass spectra of RhB before irradiation (blue) and after 5 h irradiation (red).

The figure above (blue) shows the mass spectra for RhB solution before irradiation and the red spectrum shows the mass spectra of supernatant after irradiation. As expected, the RhB solution gives a well defined spectrum for cation  $C_{28}H_{31}N_2O_3$  while the supernatant gives a more complex spectrum with many additional peaks. Except for 443.3 m/z, which is the peak for RhB, the primary peaks are at 415.3 m/z, 387.3 m/z, and 354.5 m/z. It's not hard to find that the difference value between 443.3 m/z and 415.3 m/z is  $\sim 28$ , between 415.3 m/z and 387.3 m/z is  $\sim 28$ , between 387.3 m/z and 354.5 m/z is  $\sim 32$ , it could be the loss of  $CH_2CH_2$  or CO. Furthermore, the maximum value of molecular weight is 443.3 m/z. According to the structure of RhB, it is easy to break the carbon bond connected with

CH<sub>2</sub>CH<sub>2</sub>. Based on the analysis above, the degradation products of RhB are CO<sub>2</sub>, H<sub>2</sub>O and some low molecular weight byproducts.

### 3.3.9 Photocatalytic Data of Other Organic Dye (Sulphur Blue).



Sulphur blue was also used to be the pollutants in the photocatalytic system besides RhB. The conditions of photocatalytic degradation of sulphur blue were the same as in the photocatalytic system of RhB. The initial color of the sulphur blue dye is blue, the color faded to colorless within 1 hour as showed above. Furthermore, the removal efficiency of sulphur blue was analyzed by UV-vis and shows that over 95% dye were removed.

## 3.4 Summary

The CdS nanoparticles would be steadily immobilized on pNIPAm-based microgel. In the photocatalytic system, the hybrid microgel is effective for efficient degradation of RhB and also for repeated use the catalysts. Furthermore, the photocorrosion of other organic dyes could also be performed by the hybrid microgel with CdS.

## Conclusions

Chapter 1 provided a general concept of polymer/nanocrystal systems for wastewater treatment and introduced stimuli-responsive polymers and quantum dots. The chapter showed the importance of wastewater treatment and the properties and applications of stimuli-responsive polymers and quantum dots. The chapter introduced the polymeric nanocomposite photocatalyst nanocrystal/pNIPAm that could deal with organic contaminants in photocatalytic oxidation wastewater treatment.

Chapter 2 showed polymerization and modification of pNIPAm/CdS composite microgel. To find the best condition in synthesizing composite microgel, we tested the amount of AAC in microgels and the different pH values of the microgels to see how they affected the structure of composite microgel. We determined that 20% AAC and the pH value at 8.58 are the optimum conditions for the polymerization of composite pNIPAm-co-AAC microgel with CdS quantum dots. We fabricated a hybrid catalyst pNIPAm/CdS by encapsulating CdS nanoparticles within a porous cation exchanger.

In Chapter 3, RhB was chosen as the representative dye pollutant during the photocatalytic oxidation wastewater system, the polymeric nanocomposite photocatalyst would be steadily immobilized within the outer surface of the spherical beads, which is dominant for efficient degradation of RhB and for repeated use the catalysts. Furthermore, photocorrosion of CdS is effectively inhibited through hybridation, as demonstrated by the constant performance of continuous photodegradation runs<sup>26</sup>.

Since the materials generated here have been able to perform at a high level for many photodegradation cycles,<sup>26</sup> and they are low cost, the results reported in this thesis may be of considerable value for real-world applications and can be used by various companies in

Canada such as BioRefinex Canada Inc.<sup>249</sup>, EnviroSim Associates Ltd.<sup>250</sup> and Natural Environmental Systems, LLC.<sup>251</sup>

## Future Work

As discussed in Chapter 2, X-ray photoelectron spectroscopy (XPS) was used to confirm the existence of CdS quantum dots doped in pNIPAm-based microgels. However, the content of CdS quantum dots was low. This work can be further modified by further increasing the concentrations of AAC present in the microgels and perform more detailed analysis of how pH, concentration of CdCl<sub>2</sub> and Na<sub>2</sub>S can affect the content of CdS.

During the synthesis of hybrid microgels, the dense-structure of pNIPAm-based microgels may affect the percentage of CdS nanoparticles in the microgels, and may affect the photodegradation efficiency. Therefore, more investigations should be done to analyze the effect of crosslinker concentration and method of addition on the photodegradation efficiency.

In Chapter 3, results from XPS were discussed. It was established the leaking of CdS in wastewater during photocatalytic operation. New contaminant was imported in the wastewater. Further experiments can be performed on these systems using a more suitable equipment to avoid the leaking of CdS. Also, the production of RhB after photocatalytic operation was established. Several other equipments and treatment methods can be performed more detailed analysis of the production of RhB after photocatalytic operation. The photocatalytic operation should also be carried for longer time to see if all the RhB could be degraded into H<sub>2</sub>O and CO<sub>2</sub> to certify the possible explanation from previous report.

More comparison experiments should also be completed. For example, the photocatalytic efficiency of CdS nanoparticles on their own, at various temperatures, should be evaluated and compared to the doped microgels.

Furthermore, more work should be done to determine if the CdS is capable of degrading the microgels. This can be done by exposing the CdS-loaded microgels to UV light and evaluating the degradation products by mass spectrometry.

## References

1. D. D. Mara, *Public health*, 2003, **117**, 452-456.
2. D. M. Johnson, D. R. Hokanson, Q. Zhang, K. D. Czupinski and J. Tang, *Journal of environmental management*, 2008, **88**, 416-427.
3. J. Theron and T. Cloete, *Critical reviews in microbiology*, 2002, **28**, 1-26.
4. P. Leonard, S. Hearty, J. Brennan, L. Dunne, J. Quinn, T. Chakraborty and R. O'Kennedy, *Enzyme and Microbial Technology*, 2003, **32**, 3-13.
5. N. J. Ashbolt, *Toxicology*, 2004, **198**, 229-238.
6. P. ON, 2013.
7. L. Snider, *Social & Legal Studies*, 2004, **13**, 265-289.
8. C. L. Moe and R. D. Rheingans, *Journal of water and health*, 2006, **4**, 41.
9. Y. Yu, K. Hubacek, K. Feng and D. Guan, *Ecological Economics*, 2010, **69**, 1140-1147.
10. K. Brown, *Science*, 2002, **297**, 926-927.
11. N. R. Mizyed, *Environmental science & policy*, 2013, **25**, 186-195.
12. C. Brasquet and P. Le Cloirec, *Carbon*, 1997, **35**, 1307-1313.
13. P. Le Cloirec, C. Brasquet and E. Subrenat, *Energy & Fuels*, 1997, **11**, 331-336.
14. S. Wang, M. Soudi, L. Li and Z. Zhu, *Journal of Hazardous Materials*, 2006, **133**, 243-251.
15. D. Sun, X. Zhang, Y. Wu and X. Liu, *Journal of hazardous materials*, 2010, **181**, 335-342.
16. F. Bingling, *INDUSTRIAL WATER TREATMENT*, 1998, **4**.
17. J. Wu, M. A. Eiteman and S. E. Law, *Journal of environmental engineering*, 1998.

18. J. Su, Q. Yang, J. F. Teo and T.-S. Chung, *Journal of membrane science*, 2010, **355**, 36-44.
19. W. Chen, Y. Su, J. Peng, X. Zhao, Z. Jiang, Y. Dong, Y. Zhang, Y. Liang and J. Liu, *Environmental science & technology*, 2011, **45**, 6545-6552.
20. H. Fenton, *Journal of the Chemical Society, Transactions*, 1894, **65**, 899-910.
21. G. V. Buxton, C. L. Greenstock, W. P. Helman and A. B. Ross, *Journal of physical and chemical reference data*, 1988, **17**, 513-886.
22. E. Neyens and J. Baeyens, *Journal of Hazardous materials*, 2003, **98**, 33-50.
23. J. J. Pignatello, E. Oliveros and A. MacKay, *Critical reviews in environmental science and technology*, 2006, **36**, 1-84.
24. J. Ma, W. Ma, W. Song, C. Chen, Y. Tang, J. Zhao, Y. Huang, Y. Xu and L. Zang, *Environmental science & technology*, 2006, **40**, 618-624.
25. A. Mills, R. H. Davies and D. Worsley, *Chem. Soc. Rev.*, 1993, **22**, 417-425.
26. M. A. Fox and M. T. Dulay, *Chemical reviews*, 1993, **93**, 341-357.
27. B. Ohtani and S. Nishimoto, *The Journal of Physical Chemistry*, 1993, **97**, 920-926.
28. Z. Baolong, C. Baishun, S. Keyu, H. Shangjin, L. Xiaodong, D. Zongjie and Y. Kelian, *Applied Catalysis B: Environmental*, 2003, **40**, 253-258.
29. C. A. Martinez-Huitle and S. Ferro, *Chemical Society Reviews*, 2006, **35**, 1324-1340.
30. K. Rajeshwar and J. G. Ibanez, *Environmental electrochemistry: Fundamentals and applications in pollution sensors and abatement*, Academic press, 1997.
31. M. Oturan, *Journal of Applied Electrochemistry*, 2000, **30**, 475-482.
32. Z. Ting-xi, *Fine Chemicals*, 2006, **11**, 016.
33. L. Dong-lian, *Henan Chemical Industry*, 2004, **12**, 001.

34. R. Asahi, T. Morikawa, T. Ohwaki, K. Aoki and Y. Taga, *science*, 2001, **293**, 269-271.
35. A. Mills and S. Le Hunte, *Journal of photochemistry and photobiology A: Chemistry*, 1997, **108**, 1-35.
36. R. J. Davis, J. L. Gainer, G. O'Neal and I.-W. Wu, *Water Environment Research*, 1994, **66**, 50-53.
37. V. Colvin, M. Schlamp and A. Alivisatos, *Nature*, 1994, **370**, 354-357.
38. H. Zhang, C. Wang, M. Li, J. Zhang, G. Lu and B. Yang, *Advanced Materials*, 2005, **17**, 853-857.
39. H. Zhang, C. Wang, M. Li, X. Ji, J. Zhang and B. Yang, *Chemistry of materials*, 2005, **17**, 4783-4788.
40. K. C. Weng, C. O. Noble, B. Papahadjopoulos-Sternberg, F. F. Chen, D. C. Drummond, D. B. Kirpotin, D. Wang, Y. K. Hom, B. Hann and J. W. Park, *Nano letters*, 2008, **8**, 2851-2857.
41. B. I. Lemon and R. M. Crooks, *Journal of the American Chemical Society*, 2000, **122**, 12886-12887.
42. C. C. Wang, A. L. Chen and I. H. Chen, *Polymers for advanced technologies*, 2006, **17**, 598-603.
43. R. K. Capek, M. Weber and A. Eychmüller, *Chemistry of Materials*, 2010, **22**, 4912-4918.
44. J. Zhang, S. Xu and E. Kumacheva, *Journal of the American Chemical Society*, 2004, **126**, 7908-7914.
45. A. Nelson, *Nature materials*, 2008, **7**, 523-525.

46. M. A. C. Stuart, W. T. Huck, J. Genzer, M. Müller, C. Ober, M. Stamm, G. B. Sukhorukov, I. Szleifer, V. V. Tsukruk and M. Urban, *Nature materials*, 2010, **9**, 101-113.
47. F. Liu and M. W. Urban, *Progress in Polymer Science*, 2010, **35**, 3-23.
48. B. Jeong and A. Gutowska, *Trends in biotechnology*, 2002, **20**, 305-311.
49. S. Dai, P. Ravi and K. C. Tam, *Soft Matter*, 2009, **5**, 2513-2533.
50. R. Pelton, *Advances in colloid and interface science*, 2000, **85**, 1-33.
51. H. G. Schild, *Progress in polymer science*, 1992, **17**, 163-249.
52. C. de las Heras Alarcón, S. Pennadam and C. Alexander, *Chemical Society Reviews*, 2005, **34**, 276-285.
53. P. Schattling, F. D. Jochum and P. Theato, *Chemical Communications*, 2011, **47**, 8859-8861.
54. J. Zhuang, M. R. Gordon, J. Ventura, L. Li and S. Thayumanavan, *Chemical Society Reviews*, 2013, **42**, 7421-7435.
55. Y. Yu, M. Nakano and T. Ikeda, *Nature*, 2003, **425**, 145-145.
56. Y.-L. Zhao and J. F. Stoddart, *Langmuir*, 2009, **25**, 8442-8446.
57. Y. Yu and T. Ikeda, *Angewandte Chemie International Edition*, 2006, **45**, 5416-5418.
58. M. A. Ward and T. K. Georgiou, *Polymers*, 2011, **3**, 1215-1242.
59. D. Roy, W. L. Brooks and B. S. Sumerlin, *Chemical Society Reviews*, 2013, **42**, 7214-7243.
60. S. Nayak, S. B. Debord and L. A. Lyon, *Langmuir*, 2003, **19**, 7374-7379.
61. V. Bharti, *Electroresponsive polymers and their applications*, Materials Research Society, 2006.

62. C. Katsuno, A. Konda, K. Urayama, T. Takigawa, M. Kidowaki and K. Ito, *Advanced Materials*, 2013, **25**, 4636-4640.
63. J. Bünsow, J. Erath, P. M. Biesheuvel, A. Fery and W. T. Huck, *Angewandte Chemie*, 2011, **123**, 9803-9806.
64. D. Schmaljohann, *Advanced drug delivery reviews*, 2006, **58**, 1655-1670.
65. S. Dai, P. Ravi and K. C. Tam, *Soft Matter*, 2008, **4**, 435-449.
66. A. Kawamura and T. Miyata, *Encyclopedia of Polymeric Nanomaterials*, 2015, 1619-1626.
67. C. Geraths, E. H. Christen and W. Weber, *Macromolecular rapid communications*, 2012, **33**, 2103-2108.
68. D. Cohn, A. Sosnik and A. Levy, *Biomaterials*, 2003, **24**, 3707-3714.
69. J. Zhang and N. A. Peppas, *Macromolecules*, 2000, **33**, 102-107.
70. M. Heskins and J. E. Guillet, *Journal of Macromolecular Science—Chemistry*, 1968, **2**, 1441-1455.
71. Y. Okada and F. Tanaka, *Macromolecules*, 2005, **38**, 4465-4471.
72. W. Agut, A. Brûlet, C. Schatz, D. Taton and S. Lecommandoux, *Langmuir*, 2010, **26**, 10546-10554.
73. V. San Miguel, A. Limer, D. M. Haddleton, F. Catalina and C. Peinado, *European Polymer Journal*, 2008, **44**, 3853-3863.
74. N. Takeda, E. Nakamura, M. Yokoyama and T. Okano, *Journal of controlled release*, 2004, **95**, 343-355.
75. M. A. Ward and T. K. Georgiou, *Journal of Polymer Science Part A: Polymer Chemistry*, 2010, **48**, 775-783.

76. V. Bütün, S. Armes and N. Billingham, *Polymer*, 2001, **42**, 5993-6008.
77. W. Deng, H. Yamaguchi, Y. Takashima and A. Harada, *Angewandte Chemie*, 2007, **119**, 5236-5239.
78. M. Nakahata, Y. Takashima, H. Yamaguchi and A. Harada, *Nature communications*, 2011, **2**, 511.
79. N. Ma, Y. Li, H. Xu, Z. Wang and X. Zhang, *Journal of the American Chemical Society*, 2009, **132**, 442-443.
80. A. Rajput, W. Gibb, X. Zhong, K. Shannak, S. Kish, L. Chang and O. Hornykiewicz, *Annals of neurology*, 1994, **35**, 396-402.
81. M. Toyoshima, A. Oka, Y. Egi, T. Yamamoto, M. Onozuka, K. Nosaka, E. Naito and K. Yamada, *Pediatric neurology*, 2005, **33**, 98-104.
82. J. Pu, I. Chronis, D. Ahn and B. C. Dickinson, *Journal of the American Chemical Society*, 2015.
83. A. Schlossbauer, J. Kecht and T. Bein, *Angewandte Chemie*, 2009, **121**, 3138-3141.
84. D. Liu, H. Liu and N. Hu, *The Journal of Physical Chemistry B*, 2012, **116**, 1700-1708.
85. S. Hackelbusch, T. Rossow, H. Becker and S. Seiffert, *Macromolecules*, 2014, **47**, 4028-4036.
86. Q. Zhao, J. W. Dunlop, X. Qiu, F. Huang, Z. Zhang, J. Heyda, J. Dzubiella, M. Antonietti and J. Yuan, *Nature communications*, 2014, **5**.
87. C. Boyer and R. Hoogenboom, *European Polymer Journal*, 2015, **69**, 438-440.
88. M. STUDENOVSKÝ, O. SEDLÁČEK, M. HRUBÝ, J. PÁNEK and K. Ulbrich, *Anticancer research*, 2015, **35**, 753-757.

89. P. Schattling, F. D. Jochum and P. Theato, *Polymer Chemistry*, 2014, **5**, 25-36.
90. Y. Li, C. Zhang, Y. Zhou, Y. Dong and W. Chen, *European Polymer Journal*, 2015.
91. F. A. Plamper, A. Schmalz, M. Ballauff and A. H. Müller, *Journal of the American Chemical Society*, 2007, **129**, 14538-14539.
92. J. Seuring and S. Agarwal, *Macromolecular rapid communications*, 2012, **33**, 1898-1920.
93. K. Pagonis and G. Bokias, *Polymer*, 2004, **45**, 2149-2153.
94. H. Yamauchi and Y. Maeda, *The Journal of Physical Chemistry B*, 2007, **111**, 12964-12968.
95. N. Higashida, J. Kressler and T. Inoue, *Polymer*, 1995, **36**, 2761-2764.
96. N. T. Southall, K. A. Dill and A. Haymet, *The Journal of Physical Chemistry B*, 2002, **106**, 521-533.
97. I. Bischofberger, D. Calzolari, P. De Los Rios, I. Jelezarov and V. Trappe, *Scientific reports*, 2014, **4**.
98. D. Crespy and R. M. Rossi, *Polymer International*, 2007, **56**, 1461-1468.
99. K. Jain, R. Vedarajan, M. Watanabe, M. Ishikiriyama and N. Matsumi, *Polymer Chemistry*, 2015, **6**, 6819-6825.
100. H. Vihola, A. Laukkanen, L. Valtola, H. Tenhu and J. Hirvonen, *Biomaterials*, 2005, **26**, 3055-3064.
101. V. Boyko, A. Pich, Y. Lu, S. Richter, K.-F. Arndt and H.-J. P. Adler, *Polymer*, 2003, **44**, 7821-7827.
102. J. Ramos, A. Imaz and J. Forcada, *Polymer Chemistry*, 2012, **3**, 852-856.
103. X. Han, X. Zhang, H. Zhu, Q. Yin, H. Liu and Y. Hu, *Langmuir*, 2013, **29**, 1024-1034.

104. S. Furyk, Y. Zhang, D. Ortiz-Acosta, P. S. Cremer and D. E. Bergbreiter, *Journal of Polymer Science Part A: Polymer Chemistry*, 2006, **44**, 1492-1501.
105. J. Ruths, F. Essler, G. Decher and H. Riegler, *Langmuir*, 2000, **16**, 8871-8878.
106. A. M. Caminade, C. O. Turrin, R. Laurent, C. Rebout and J. P. Majoral, *Polymer international*, 2006, **55**, 1155-1160.
107. J. M. Knipe, F. Chen and N. A. Peppas, *Journal of Applied Polymer Science*, 2014, **131**.
108. J. V. Weaver and D. J. Adams, *Soft Matter*, 2010, **6**, 2575-2582.
109. S. Y. Park and Y. H. Bae, *Macromolecular rapid communications*, 1999, **20**, 269-273.
110. Y. Nagasaki, L. Luo, T. Tsuruta and K. Kataoka, *Macromolecular Rapid Communications*, 2001, **22**, 1124-1127.
111. J. E. Elliott, M. Macdonald, J. Nie and C. N. Bowman, *Polymer*, 2004, **45**, 1503-1510.
112. L. Ying, P. Wang, E. Kang and K. Neoh, *Macromolecules*, 2002, **35**, 673-679.
113. D. Garcia, J. Escobar, N. Bada, J. Casquero, E. Hernáez and I. Katime, *European polymer journal*, 2004, **40**, 1637-1643.
114. S. Zhou and B. Chu, *The Journal of Physical Chemistry B*, 1998, **102**, 1364-1371.
115. Z. Song, K. Wang, C. Gao, S. Wang and W. Zhang, *Macromolecules*, 2015.
116. D. Mazia, G. Schatten and W. Sale, *The Journal of cell biology*, 1975, **66**, 198-200.
117. J. Wiseman, C. Goddard, D. McLelland and W. Colledge, *Gene therapy*, 2003, **10**, 1654-1662.
118. M. N. R. Kumar, *Reactive and functional polymers*, 2000, **46**, 1-27.
119. M. Rinaudo, *Progress in polymer science*, 2006, **31**, 603-632.
120. S. V. Madhally and H. W. Matthew, *Biomaterials*, 1999, **20**, 1133-1142.

121. G. S. Kumar and D. Neckers, *Chemical Reviews*, 1989, **89**, 1915-1925.
122. A. Lendlein, H. Jiang, O. Jünger and R. Langer, *Nature*, 2005, **434**, 879-882.
123. H. S. Blair and C. B. McArdle, *Polymer*, 1984, **25**, 999-1005.
124. M. Irie, *Macromolecules*, 1986, **19**, 2890-2892.
125. C. M. Soukoulis, *Photonic crystals and light localization in the 21st century*, Springer Science & Business Media, 2012.
126. P. V. Braun and P. Wiltzius, *Nature*, 1999, **402**, 603-604.
127. C. J. Barrett, J.-i. Mamiya, K. G. Yager and T. Ikeda, *Soft Matter*, 2007, **3**, 1249-1261.
128. A. C. Arsenault, D. P. Puzzo, I. Manners and G. A. Ozin, *Nature Photonics*, 2007, **1**, 468-472.
129. R. Hayward, D. Saville and I. Aksay, *Nature*, 2000, **404**, 56-59.
130. X. Zhao and M. Wang, *European polymer journal*, 2006, **42**, 247-253.
131. M. Irie and D. Kunwatchakun, *Macromolecules*, 1986, **19**, 2476-2480.
132. C. Bird and A. Kuhn, *Chem. Soc. Rev.*, 1981, **10**, 49-82.
133. J. E. Ghadiali and M. M. Stevens, *Advanced Materials*, 2008, **20**, 4359-4363.
134. M. E. Hahn and N. C. Gianneschi, *Chem. Commun.*, 2011, **47**, 11814-11821.
135. R. V. Ulijn, *Journal of Materials Chemistry*, 2006, **16**, 2217-2225.
136. J. Hu, G. Zhang and S. Liu, *Chemical Society Reviews*, 2012, **41**, 5933-5949.
137. H. Yi, L.-Q. Wu, W. E. Bentley, R. Ghodssi, G. W. Rubloff, J. N. Culver and G. F. Payne, *Biomacromolecules*, 2005, **6**, 2881-2894.
138. J. Hyun, J. Kim, S. L. Craig and A. Chilkoti, *Journal of the American Chemical Society*, 2004, **126**, 4770-4771.

139. Z. Yang, H. Gu, D. Fu, P. Gao, J. K. Lam and B. Xu, *Advanced materials*, 2004, **16**, 1440-1444.
140. P. D. Thornton, R. J. Mart and R. V. Ulijn, *Advanced materials*, 2007, **19**, 1252-1256.
141. M. Zelzer and R. V. Ulijn, *Chemical Society Reviews*, 2010, **39**, 3351-3357.
142. P. D. Thornton, R. J. Mart, S. J. Webb and R. V. Ulijn, *Soft Matter*, 2008, **4**, 821-827.
143. M. Zelzer, S. J. Todd, A. R. Hirst, T. O. McDonald and R. V. Ulijn, *Biomaterials Science*, 2013, **1**, 11-39.
144. A. S. Hoffman, *Advanced drug delivery reviews*, 2012, **64**, 18-23.
145. T. Miyata, M. Jige, T. Nakaminami and T. Urugami, *Proceedings of the National Academy of Sciences of the United States of America*, 2006, **103**, 1190-1193.
146. W. Hennink and C. F. Van Nostrum, *Advanced drug delivery reviews*, 2012, **64**, 223-236.
147. K. Yeomans, *Chemistry Review*, 2000, **10**, 2-5.
148. K. Y. Lee and D. J. Mooney, *Chemical reviews*, 2001, **101**, 1869-1880.
149. T. Miyata, N. Asami and T. Urugami, *Nature*, 1999, **399**, 766-769.
150. Y. Tamai, H. Tanaka and K. Nakanishi, *Macromolecules*, 1996, **29**, 6761-6769.
151. A. E. English, S. Mafé, J. A. Manzanares, X. Yu, A. Y. Grosberg and T. Tanaka, *The Journal of chemical physics*, 1996, **104**, 8713-8720.
152. Q. Yan and A. S. Hoffman, *Polymer*, 1995, **36**, 887-889.
153. T. Tanaka, I. Nishio, S.-T. Sun and S. Ueno-Nishio, *Science*, 1982, **218**, 467-469.
154. T. Hoare and R. Pelton, *Macromolecules*, 2004, **37**, 2544-2550.
155. K. Tam, S. Ragaram and R. Pelton, *Langmuir*, 1994, **10**, 418-422.
156. H. Senff and W. Richtering, *The Journal of chemical physics*, 1999, **111**, 1705-1711.

157. M. J. Serpe, K. A. Yarmey, C. M. Nolan and L. A. Lyon, *Biomacromolecules*, 2005, **6**, 408-413.
158. C. D. Jones and L. A. Lyon, *Macromolecules*, 2000, **33**, 8301-8306.
159. L. A. Lyon, Z. Meng, N. Singh, C. D. Sorrell and A. S. John, *Chemical Society Reviews*, 2009, **38**, 865-874.
160. Y. Guan and Y. Zhang, *Soft Matter*, 2011, **7**, 6375-6384.
161. P. Liu, Q. Luo, Y. Guan and Y. Zhang, *Polymer*, 2010, **51**, 2668-2675.
162. Y. Gao, G. P. Zago, Z. Jia and M. J. Serpe, *ACS applied materials & interfaces*, 2013, **5**, 9803-9808.
163. H. Tobita, M. Kumagai and N. Aoyagi, *Polymer*, 2000, **41**, 481-487.
164. A. Pich and W. Richtering, in *Chemical Design of Responsive Microgels*, Springer, 2010, pp. 1-37.
165. A. Proust, B. Matt, R. Villanneau, G. Guillemot, P. Gouzerh and G. Izzet, *Chemical Society Reviews*, 2012, **41**, 7605-7622.
166. D. A. LaVan, D. M. Lynn and R. Langer, *Nature Reviews Drug Discovery*, 2002, **1**, 77-84.
167. N. Murthy, M. Xu, S. Schuck, J. Kunisawa, N. Shastri and J. M. Fréchet, *Proceedings of the National Academy of Sciences*, 2003, **100**, 4995-5000.
168. M. Das, S. Mardyani, W. C. Chan and E. Kumacheva, *Advanced Materials*, 2006, **18**, 80-83.
169. H. Zhang, S. Mardyani, W. C. Chan and E. Kumacheva, *Biomacromolecules*, 2006, **7**, 1568-1572.

170. T. Hoare, B. P. Timko, J. Santamaria, G. F. Goya, S. Irusta, S. Lau, C. F. Stefanescu, D. Lin, R. Langer and D. S. Kohane, *Nano letters*, 2011, **11**, 1395-1400.
171. D. Sivakumaran, D. Maitland and T. Hoare, *Biomacromolecules*, 2011, **12**, 4112-4120.
172. J. D. Debord, S. Eustis, S. Byul Debord, M. T. Lofye and L. A. Lyon, *Advanced Materials*, 2002, **14**, 658-662.
173. S. Xu, J. Zhang, C. Paquet, Y. Lin and E. Kumacheva, *Advanced Functional Materials*, 2003, **13**, 468-472.
174. L. E. Brus, *The Journal of chemical physics*, 1984, **80**, 4403-4409.
175. A. P. Alivisatos, *The Journal of Physical Chemistry*, 1996, **100**, 13226-13239.
176. B. Dubertret, P. Skourides, D. J. Norris, V. Noireaux, A. H. Brivanlou and A. Libchaber, *Science*, 2002, **298**, 1759-1762.
177. W. U. Huynh, J. J. Dittmer and A. P. Alivisatos, *science*, 2002, **295**, 2425-2427.
178. J. S. Steckel, S. Coe-Sullivan, V. Bulović and M. G. Bawendi, *Advanced Materials*, 2003, **15**, 1862-1866.
179. A. Y. Nazzal, L. Qu, X. Peng and M. Xiao, *Nano letters*, 2003, **3**, 819-822.
180. A. Eychmüller, *The Journal of Physical Chemistry B*, 2000, **104**, 6514-6528.
181. J. Aldana, Y. A. Wang and X. Peng, *Journal of the American Chemical Society*, 2001, **123**, 8844-8850.
182. S. Ogawa, K. Hu, F.-R. F. Fan and A. J. Bard, *The Journal of Physical Chemistry B*, 1997, **101**, 5707-5711.
183. M. Reed, J. Randall, R. Aggarwal, R. Matyi, T. Moore and A. Wetsel, *Physical Review Letters*, 1988, **60**, 535.

184. A. Ekimov and A. Onushchenko, *Soviet Physics Semiconductors-Ussr*, 1982, **16**, 775-778.
185. A. Ekimov, A. L. Efros and A. Onushchenko, *Solid State Communications*, 1985, **56**, 921-924.
186. A. Leheny, R. Rossetti and L. E. Brus, *The Journal of Physical Chemistry*, 1985, **89**, 211-213.
187. A. M. Smith and S. Nie, *Accounts of chemical research*, 2009, **43**, 190-200.
188. L. Brus, *The Journal of chemical physics*, 1983, **79**, 5566-5571.
189. C. B. Murray, C. Kagan and M. Bawendi, *Annual Review of Materials Science*, 2000, **30**, 545-610.
190. V. Singh and P. Chauhan, *Journal of Physics and Chemistry of Solids*, 2009, **70**, 1074-1079.
191. N. Shanmugam, S. Cholan, N. Kannadasan, K. Sathishkumar and G. Viruthagiri, *Journal of Nanomaterials*, 2013, **2013**, 1.
192. C. Murray, D. J. Norris and M. G. Bawendi, *Journal of the American Chemical Society*, 1993, **115**, 8706-8715.
193. S. Chen, M. Ahmadiantehrani, N. G. Publicover, K. W. Hunter and X. Zhu, *RSC advances*, 2015, **5**, 60612-60620.
194. Y. K. Jung, J. I. Kim and J.-K. Lee, *Journal of the American Chemical Society*, 2009, **132**, 178-184.
195. J.-H. Zhan, X.-G. Yang, D.-W. Wang, S. Li, Y. Xie, Y. Xia and Y. Qian, *Advanced Materials*, 2000, **12**, 1348-1351.
196. X. Wang, J. Zhuang, Q. Peng and Y. Li, *Nature*, 2005, **437**, 121-124.

197. X. Wang, Q. Peng and Y. Li, *Accounts of chemical research*, 2007, **40**, 635-643.
198. M. Bruchez, M. Moronne, P. Gin, S. Weiss and A. P. Alivisatos, *science*, 1998, **281**, 2013-2016.
199. W. K. Leutwyler, S. L. Bürgi and H. Burgl, *Science*, 1996, **271**, 933-937.
200. P. Alivisatos, *Nature biotechnology*, 2004, **22**, 47-52.
201. M. R. Hoffmann, S. T. Martin, W. Choi and D. W. Bahnemann, *Chemical reviews*, 1995, **95**, 69-96.
202. W. C. Chan and S. Nie, *Science*, 1998, **281**, 2016-2018.
203. K. Krishnamoorthy, R. Mohan and S.-J. Kim, *Applied Physics Letters*, 2011, **98**, 244101.
204. L. E. Brus, *The Journal of chemical physics*, 1984, **80**, 4403-4409.
205. A. P. Alivisatos, *The Journal of Physical Chemistry*, 1996, **100**, 13226-13239.
206. B.-R. Hyun, H. Chen, D. A. Rey, F. W. Wise and C. A. Batt, *The Journal of Physical Chemistry B*, 2007, **111**, 5726-5730.
207. Z. Hens, D. Tallapin, H. Weller and D. Vanmaekelbergh, *Applied physics letters*, 2002, **81**, 4245-4247.
208. J. S. Owen, J. Park, P.-E. Trudeau and A. P. Alivisatos, *Journal of the American Chemical Society*, 2008, **130**, 12279-12281.
209. A. Dong, X. Ye, J. Chen, Y. Kang, T. Gordon, J. M. Kikkawa and C. B. Murray, *Journal of the American Chemical Society*, 2010, **133**, 998-1006.
210. V. Colvin, M. Schlamp and A. Alivisatos, *Nature*, 1994, **370**, 354-357.
211. N. C. Greenham, X. Peng and A. P. Alivisatos, *Physical review B*, 1996, **54**, 17628.

212. J. Liu, T. Tanaka, K. Sivula, A. P. Alivisatos and J. M. Fréchet, *Journal of the American Chemical Society*, 2004, **126**, 6550-6551.
213. J. Zhang, S. Xu and E. Kumacheva, *Journal of the American Chemical Society*, 2004, **126**, 7908-7914.
214. M. Artemyev, V. Sperling and U. Woggon, *Journal of applied physics*, 1997, **81**, 6975-6977.
215. D. Fogg, L. Radzilowski, R. Blanski, R. Schrock and E. Thomas, *Macromolecules*, 1997, **30**, 417-426.
216. D. Fogg, L. Radzilowski, B. Dabbousi, R. Schrock, E. Thomas and M. Bawendi, *Macromolecules*, 1997, **30**, 8433-8439.
217. B. Dabbousi, M. Bawendi, O. Onitsuka and M. Rubner, *Applied Physics Letters*, 1995, **66**, 1316-1318.
218. C. Kagan, C. Murray and M. Bawendi, *Physical Review B*, 1996, **54**, 8633.
219. D. Palioura, S. Armes, S. Anastasiadis and M. Vamvakaki, *Langmuir*, 2007, **23**, 5761-5768.
220. V. Lesnyak, N. Gaponik and A. Eychmüller, *Chemical Society Reviews*, 2013, **42**, 2905-2929.
221. Y. Yang, J. Huang, S. Liu and J. Shen, *J. Mater. Chem.*, 1997, **7**, 131-133.
222. I. Bischofberger, D. Calzolari, P. De Los Rios, I. Jelezarov and V. Trappe, *Scientific reports*, 2014, **4**.
223. Parasuraman, D.; Serpe, M J.; *ACS Appl. Mater. Interfaces* 2011, **3**, 2732-2737

224. Huang BC, Yang Y, Chen XS, Ye DQ. Preparation and characterization of CdS–TiO<sub>2</sub> nanoparticles supported on multi-walled carbon nanotubes. *Catal Commun*, 2010, 11: 844–847
225. Hirai T, Okubo H, Komasaawa I. Incorporation of CdS nanoparticles formed in reverse micelles into silica matrices via a sol-gel process: preparation of nano-CdS containing silica colloids and silica glass. *J Mater Chem*, 2000, 10: 2592–2596
226. Linsebigler AL, Lu G, Yates Jr JT. Photocatalysis on TiO<sub>2</sub> surfaces: Principles, mechanisms, and selected results. *Chem Rev*, 1995, 95(3): 735–758
227. Tasbihi M, Ngah CR, Aziz N, Mansor A, Abdullah AZ, Teong LK, Mohamed AR. Lifetime and regeneration studies of various supported TiO<sub>2</sub> photocatalysts for the degradation of phenol under UV-C light in a batch reactor. *Ind Eng Chem Res*, 2007, 46(26): 9006–9014
228. Xie TH, Lin J. Origin of photocatalytic deactivation of TiO<sub>2</sub> film coated on ceramic substrate. *J Phys Chem C*, 2007, 111(27): 9968–9974
229. Raja P, Bandara J, Giordano P, Kiwi J. Innovative supported composite photocatalyst for the oxidation of phenolic waters in reactor processes. *Ind Eng Chem Res*, 2005, 44(24): 8959–8967
230. Benmami M, Chhor K, Kanaev AV. Supported nanometric titanium oxide sols as a new efficient photocatalyst. *J Phys Chem B*, 2005, 109(42): 19766–19771
231. Wu TS, Wang KX, Li GD, Sun SY, Sun J, Chen JS. Montmorillonite- supported Ag/TiO<sub>2</sub> nanoparticles: an efficient visible-light bacteria photodegradation material. *ACS Appl Mater Interface*, 2010, 2(2): 544–550

232. Wang SM, Liu P, Wang XX, Fu XZ. Homogeneously distributed CdS nanoparticles in nafion membranes: Preparation, characterization, and photocatalytic properties. *Langmuir*, 2005, 21(25): 11969–11973
233. Liu XW, Fang Z, Zhang XJ, Zhang W, Wei XW, Geng BY. Preparation and characterization of Fe<sub>3</sub>O<sub>4</sub>/CdS nanocomposites and their use as recyclable photocatalysts. *Cryst Growth Des*, 2009, 9(1): 197–202
234. Lee JJ, Suh JK, Hong JS, Lee JM, Lee YS, Park JW. The synthesis of spherical activated carbons containing zinc and their photochemical activity. *Carbon*, 2008, 46: 1648–1655
235. Han H, Bai R. Buoyant photocatalyst with greatly enhanced visible-light activity prepared through a low temperature hydrothermal method. *Ind Eng Chem Res*, 2009, 48(6): 2891–2898
236. J. Ma, G.A. Tai, W.L. Guo, Ultrasound-assisted microwave preparation of Ag-doped CdS nanoparticles, *Ultrason. Sonochem.* 17 (2010) 534–540.
237. P.S. Lunawat, S. Senapati, R. Kumar, N.M. Gupta, Visible light-induced splitting of water using CdS nanocrystallites immobilized over water-repellant polymeric surface, *Int. J. Hydrogen Energy* 32 (2007) 2784–2790
238. <http://pharmaxchange.info/press/2011/12/ultraviolet-visible-uv-vis-spectroscopy-principle/>
239. Xie YM, Lv L, Li MH, Pan BC, Chen Q, Zhang WM, Zhang QX, Development of cation exchanger-based nano-CdS hybrid catalyst for visible-light photodegradation of rhodamine B from water. *SCIENCE CHINA Chemistry*, 2011, 10.1007/s11426-011-4416-6

240. Jia HM, He WW, Wayne G, Wamer, Han XN, Zhang BB, Zhang S, Zheng Z, Xiang Y, Yin JJ, Generation of Reactive Oxygen Species, Electrons/Holes, and Photocatalytic Degradation of Rhodamine B by Photoexcited CdS and Ag<sub>2</sub>S Micro-Nano Structures. *Physical Chemistry*, 2014, 118, 21447-21456
241. Turchia, C. S.; Ollis, D. F. Photocatalytic Degradation of Organic Water Contaminants: Mechanisms Involving Hydroxyl Radical Attack. *J. Catal.* 1990, 122, 178–192.
242. Wood, P. M. The Potential Diagram for Oxygen at Ph 7. *Biochem. J.* 1988, 253, 287–289.
243. Li, Y.; Zhang, W.; Niu, J. F.; Chen, Y. S. Mechanism of Photogenerated Reactive Oxygen Species and Correlation with the Antibacterial Properties of Engineered Metal-Oxide Nanoparticles. *ACS Nano* 2012, 6, 5164–5173.
244. Xu, Y.; Schoonen, M. A. A. The Absolute Energy Positions of Conduction and Valence Bands of Selected Semiconducting Minerals. *Am. Mineral.* 2000, 85, 543–556.
245. Fu HB, Pan CS, Yao WQ, Zhu YF. Visible-light-induced degradation of Rhodamine B by nanosized Bi<sub>2</sub>WO<sub>6</sub>. *J Phys Chem B*, 2005, 109(47): 22432–22439
246. Cotto-Maldonado MC. Heterogeneous Catalysis Applied To Advanced Oxidation Processes (AOPs) For Degradation of Organic Pollutants, Dissertation, Universidad del Turabo; 2012.
247. Sun M, Li D, Chen Y, Chen W, Li W, He Y, Fu X. Synthesis and Photocatalytic Activity of Calcium Antimony Oxide Hydroxide for the Degradation of Dyes in Water. *J Phys Chem C.* 2009;113(31):13825-13831.

248. Xie YM, LV L, LI MH, PAN BC, CHEN Q, ZHANG WM&ZHANG QX. Development of cation exchanger-based nano-CdS hybrid catalyst for visible-light photodegradation of rhodamine B from water. SCIENCE CHINA chemistry. 2012; 10.1007/s11426-011-4416-6
249. <http://www.environmental-expert.com/companies/biorefinex-canada-inc-39802>
250. <http://www.environmental-expert.com/companies/envirosim-associates-ltd-3796>
251. <http://www.environmental-expert.com/companies/natural-environmental-systems-llc-26535>
252. [eqg-rcqe.ccme.ca/download/en/148](http://eqg-rcqe.ccme.ca/download/en/148)

# Appendix

**Table2-1.** pNIPAm-co- 10%AAc Microgel

	%	mmole	M (g/mol)	Mass (g)
NIPAm	85	11.951	113.16	1.3524
BIS	5	0.703	154.17	0.1084
AAC	10	1.406	72.06	96.4 (μL)
APS	0.046g			

**Table2-2.** pNIPAm-co-15%AAc Microgel

	%	mmole	M(g/mol)	Mass(g)
NIPAm	80	11.248	113.16	1.2728
BIS	5	0.703	154.17	0.1084
AAC	15	2.109	72.06	144.6(μL)
APS	0.046g			

**Table2-3.** pNIPAm-co-20%AAc Microgel

	%	mmole	M(g/mol)	Mass(g)
NIPAm	75	10.545	113.16	1.1933
BIS	5	0.703	154.17	0.1084
AAC	20	2.812	72.06	192.8(μL)

APS	0.046g
-----	--------

**Table2-4.** pNIPAm-co-30%AAc Microgel

	%	mmole	M(g/mol)	Mass(g)
NIPAm	65	9.139	113.16	1.034
BIS	5	0.703	154.17	0.1084
AAC	30	4.218	72.06	289.2( $\mu$ L)
APS	0.046g			

**Table2-5.** pNIPAm-co-40%AAc Microgel

	%	mmole	M(g/mol)	Mass(g)
NIPAm	55	7.733	113.16	0.875
BIS	5	0.703	154.17	0.1084
AAC	40	5.624	72.06	385.6( $\mu$ L)
APS	0.046g			

**Table2-6.** pNIPAm-co-50%AAc Microgel

	%	mmole	M(g/mol)	Mass(g)
NIPAm	45	6.327	113.16	0.71598
BIS	5	0.703	154.17	0.1084
AAC	50	7.03	72.06	482( $\mu$ L)
APS	0.046g			

